Resurrecting the Alternative Splicing Landscape of Archaic Hominins using Machine Learning

Colin M. Brand[1,2], Laura L. Colbran[3], and John A. Capra[1,2,*]

[1]Bakar Computational Health Sciences Institute, University of California, San Francisco, CA, USA
[2]Department of Epidemiology and Biostatistics, University of California, San Francisco, CA, USA
[2]Department of Genetics, Perelman School of Medicine, University of Pennsylvania, Philadelphia, PA, USA

[*]*Correspondence to* tony@capralab.org

Abstract

Alternative splicing contributes to adaptation and divergence in many species. However, it has not been possible to directly compare splicing between modern and archaic hominins. Here, we unmask the recent evolution of this previously unobservable regulatory mechanism by applying SpliceAI, a machine-learning algorithm that identifies splice altering variants (SAVs), to high-coverage genomes from three Neanderthals and a Denisovan. We discover 5,950 putative archaic SAVs, of which 2,343 are archaic-specific and 3,607 also occur in modern humans via introgression (237) or shared ancestry (3,370). Archaic-specific SAVs are enriched in genes that contribute to many traits potentially relevant to hominin phenotypic divergence, such as perspiration, platelet volume, and spinal rigidity. Compared to shared SAVs, archaic-specific SAVs occur in sites under weaker selection and are more common in genes with tissue-specific expression. Further underscoring the importance of negative selection on SAVs, Neanderthal lineages with low effective population sizes are enriched for SAVs compared to Denisovan and shared SAVs. Finally, we find that nearly all introgressed SAVs in humans were shared across Neanderthals, suggesting that older SAVs were more tolerated in modern human genomes. Our results reveal the splicing landscape of archaic hominins and identify potential contributions of splicing to phenotypic differences among hominins.

1 Introduction

While the paleontological and archaeological records provide evidence about some phenotypes of extinct hominins, most ancient tissues have not survived to the present. The discovery and successful sequencing of DNA genome-wide from a Denisovan (Meyer et al., 2012) and multiple Neanderthal genomes (Prüfer et al., 2014; Prüfer et al., 2017; Mafessoni et al., 2020) enabled direct comparisons of the genotypes of these archaic hominins to one another and anatomically modern humans. These data also enable the potential for indirect phenotypic comparisons by predicting archaic phenotypes from their genomes (Brand et al., 2022). Diverse molecular mechanisms collectively shape the similarities and differences between archaic hominins and modern humans. Given that the biology linking genotype to organism-level phenotype is complex and that the mapping may not generalize across human populations (Martin et al., 2019), predicting "low-level" molecular phenotypes from genetic information is a promising alternative. Recent work has successfully explored such differences in protein-coding sequence (Castellano et al., 2014) and differences relevant to gene expression, such as divergent gene regulation (Colbran et al., 2019), differential methylation (Gokhman et al., 2019), and divergent 3D genome contacts (McArthur et al., 2022).

Variation in gene splicing could also underlie phenotypic differences between archaic hominins and modern humans, but archaic splicing patterns have not been comprehensively quantified. Alternative splicing enables the production of multiple protein isoforms from a single gene (Lopez, 1998; Graveley, 2001; Black, 2003). The resulting proteomic diversity is essential for many processes, including development and establishing tissue identity (Baralle and Giudice, 2017). Defects in splicing underlie many human diseases (e.g., Cáceres and Kornblihtt, 2002; Faustino and Cooper, 2003; Nissim-Rafinia and Kerem, 2002; Krawczak et al., 1992; Wang and Cooper, 2007; Li et al., 2016; Scotti and Swanson, 2016; Li et al., 2017), and variation in splicing contributes to differences in traits in non-human species (see Verta and Jacobs, 2022, Table 1). Further, alternative splicing can evolve rapidly and respond to environmental factors—suggesting it often contributes to adaptation (Singh and Ahi, 2022; Verta and Jacobs, 2022; Wright et al., 2022) and species differences (Blekhman et al., 2010; Barbosa-Morais et al., 2012; Merkin et al., 2012).

Splicing patterns are directly influenced by the nucleotide sequences surrounding splice sites (Sibley et al., 2016). This has enabled the development of many algorithms to predict alternative splicing from RNA-seq data (Jenkinson et al., 2020; Zhang et al., 2018; Mertes et al., 2021), RNA sequence, or DNA sequence (Cheng et al., 2019; Jagadeesh et al., 2019; Jaganathan et al., 2019; Danis et al., 2021; Zeng and Li, 2022). Beyond human clinical applications, methods that require only DNA sequence can be leveraged to understand alternative splicing in extant species for which acquiring RNA-seq data may be difficult to impossible or in extinct taxa, such as archaic hominins.

Here, we resurrect the genome-wide alternative splicing landscape of archaic hominins using SpliceAI, a pre-trained algorithm that predicts splicing patterns from sequence alone (Jaganathan et al., 2019). First, we assess the distribution of splice-altering variants (SAVs) among all four archaic individuals, identify which genes are affected, and describe how the transcripts are modified. Second, we quantify which SAVs are also present in modern humans due to shared ancestry or introgression. Third, we quantify SAV enrichment among gene sets that underlie modern human phenotypes. Fourth, we explore how selection shaped alternative

splicing in archaics. Fifth, we evaluate the expression and function of archaic SAVs that are also present in modern humans. Finally, we highlight a handful of archaic SAVs with potential evolutionary significance.

2 Results

We examined the alternative splicing landscape in archaic hominins using all four currently available high-coverage archaic genomes, representing three Neanderthals (Mafessoni et al., 2020; Prüfer et al., 2014; Prüfer et al., 2017) and a Denisovan (Meyer et al., 2012). We applied the SpliceAI classifier to sites with high-quality genotype calls where at least one archaic individual exhibited at least one allele different from the human reference (hg19/GRCh37) using the built-in GENCODE, Human Release 24, annotations to identify variants in gene bodies (**Figure 1A**). SpliceAI estimates Δ, the splice-altering probability (SAP), for each variant of: 1) an acceptor gain, 2) an acceptor loss, 3) a donor gain, and 4) a donor loss (**Figure 1A**). SpliceAI also indicates the positions changed for each of these four effects in basepairs.

Alternative splicing occurs across nearly all eukaryotes and its molecular mechanisms are deeply conserved (Collins and Penny, 2005). We therefore anticipated that the sequence patterns learned by SpliceAI in humans would generalize to archaics. To confirm this, we searched for archaic variants in the 246 genes associated with the major spliceosome complex (Tweedie et al., 2021) that were absent from individuals sequenced by the 1000 Genomes Project (1KG) (Lowy-Gallego et al., 2019), i.e., "archaic-specific" variants (**File S1**). We annotated these variants using the Ensembl Variant Effect Predictor (McLaren et al., 2016). We found only two missense variants that were scored as likely to disrupt protein function by both PolyPhen and SIFT, neither of which were fixed in all four archaics (**File S1**). Thus, there is near complete conservation of the proteins involved in splicing between archaic hominins and modern humans.

2.1 Thousands of splice altering variants (SAVs) are present in archaic hominins.

We identified 1,567,894 autosomal positions with $\geq$ 1 non-reference allele in the archaic individuals. Among these, 1,049 variants had high splice altering probability (SAP; SpliceAI $\Delta \geq 0.5$) out of 1,607,350 archaic variants we analyzed. 5,950 archaic variants had moderate SAP ($\Delta \geq 0.2$). Hereafter, we refer to these variants as high-confidence splice altering variants (SAVs) and SAVs, respectively, and to maximize sensitivity, we focus on the SAVs in the main text.

The number of SAVs was similar among the four archaics, ranging from 3,482 (Chagyrskaya) to 3,705 (Altai) (**Table S1**). These values fell within the range of SAVs observed in individual modern humans, estimated from one randomly sampled individual per 1KG population (**Table S2**). SAVs were most commonly shared among all four archaic individuals (**Figure 1B**; **Figure S1**). As expected from the known phylogeny, the Denisovan exhibited the most unique SAVs, followed by all Neanderthals, and each individual Neanderthal (**Figure 1B**; **Figure S1**).

A total of 4,242 genes have at least one archaic SAV. 3,111 genes have only one SAV; however, 1,131 had multiple SAVs (**Table S3**). Among the genes with the largest number of archaic SAVs are: *WWOX* (N = 9), which is involved in bone growth development (Aqeilan et al., 2008), *HLA-DPA1* (N = 7) and *HLA-DPB1* (N = 10), essential components of the immune

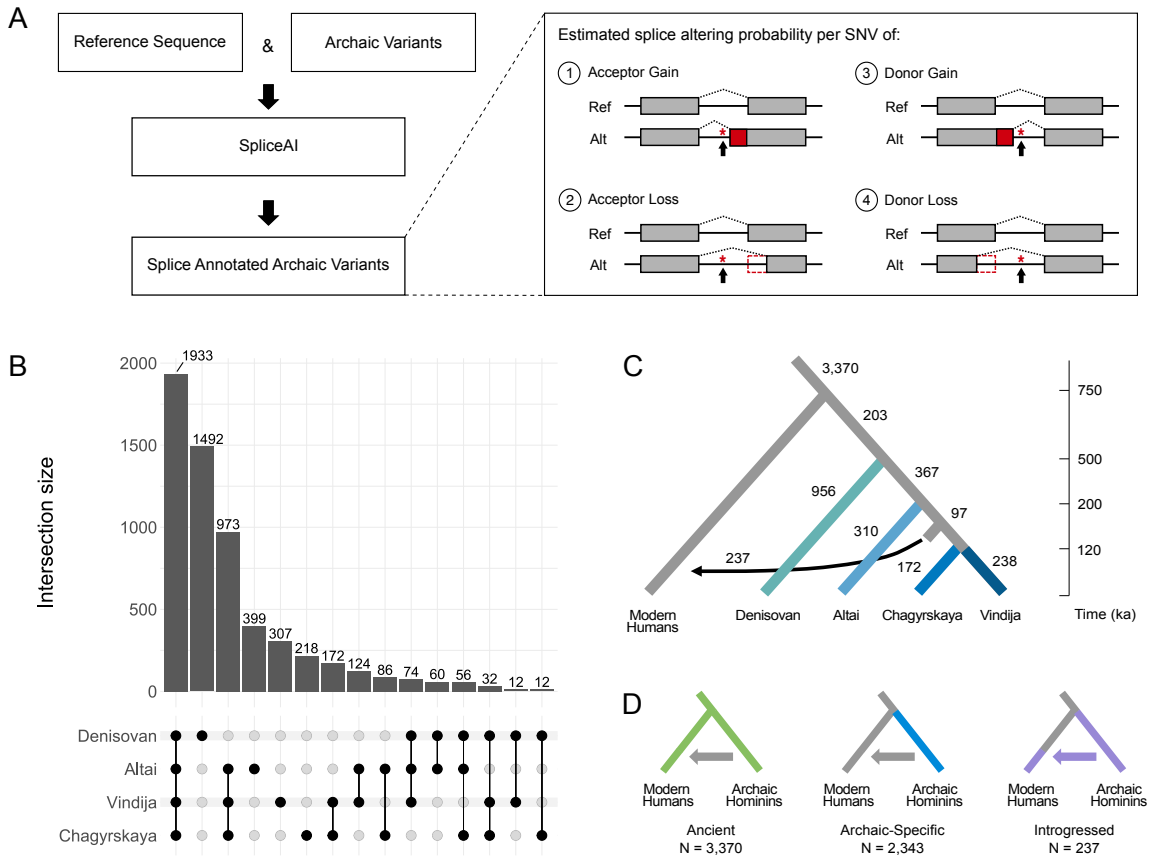

Figure 1: The identification, distribution, and origin of archaic SAVs.
(A) We used SpliceAI to identify putative splice altering variants in archaic hominin genomes. We analyzed autosomal SNVs from four archaic hominins compared to the reference sequence (hg19/GRCh37). SpliceAI annotates each variant with splice altering probabilities (Δ scores) and position changes for each class of splicing alteration: 1) acceptor gain, 2) acceptor loss, 3) donor gain, or 4) donor loss. **(B)** The distribution of the presence of archaic SAVs at $\Delta \geq 0.2$ across archaic individuals. The dots indicate which lineage(s) have the associated SAVs. **(C)** The evolutionary origins of the archaic SAVs. From the distribution of SAVs across archaic and modern individuals, we inferred their origins using parsimony. We also identified introgressed archaic SAVs using two Neanderthal ancestry sets: Vernot et al., 2016 (shown here) and Browning et al., 2018. The divergence times and placement of the introgression arrow reflect recent estimates from Mafessoni et al., 2020 and Rogers et al., 2020. **(D)** We consider three main categories of archaic SAVs based on their origin and presence across populations. "Ancient" are archaic SAVs present in both modern and archaic hominin individuals and are inferred to have origins before the last common ancestor of these groups. "Archaic-Specific" are archaic SAVs that are present in archaic hominins, but not modern humans. "Introgressed" are archaic SAVs that were introgressed into Eurasian populations due to archaic admixture.

system (Shiina et al., 2009), and *CNTNAP2* (N = 11), a nervous system protein associated with neurodevelopmental disorders that is also one of the longest genes in the human genome (Rodenas-Cuadrado et al., 2014).

Many SAVs (47.8%) have a high SAP for only one of the four classes splicing change (acceptor gain, acceptor loss, donor gain, and donor loss), and as expected, the overall association between the probabilities of different change types was negative (ρ = -0.34 – -0.14) for variants with at least one SAP greater than 0 (**Figure S2**). Donor gains were the most frequent result of splice altering variants for both thresholds (29.5% and 35.1% of variant effects, respectively **Figure S3**). While this may reflect the true distribution, we cannot rule out that the classifier has greater power to recognize donor gains compared to acceptor gains, acceptor losses, and donor losses.

2.2 39% of archaic SAVs are archaic-specific.

We inferred the origin of archaic variants based on parsimony. We identified 2,343 SAVs that are not present in modern humans in 1KG nor present in GTEx sQTL data (**Figure 1C**). We refer to this 39% of archaic SAVs as "archaic-specific".

The remaining 61% archaic SAVs are present in modern humans. Archaic hominins and modern humans last shared a common ancestor approximately 570–752 ka (Rogers et al., 2020). SAVs present in both archaic and modern humans may be the result of either introgression, shared ancestry, or independent occurrence. To identify SAVs present in 1KG due to introgression, we used two datasets on archaic introgression into modern humans (Vernot et al., 2016; Browning et al., 2018). While modern human genomes retain Denisovan and Neanderthal ancestry, most 1KG samples have minimal ($<$ 1%) Denisovan ancestry (Browning et al., 2018; Vernot et al., 2016). Therefore, we focused on Neanderthal introgression and classified 237 SAVs identified by Vernot et al., 2016 in 232 genes (**Figure 1D**; **Figure S4**) and 377 SAVs identified by Browning et al., 2018 in 353 genes as "introgressed" (**Figure S4**). Despite only modest overlap between the two introgression datasets (**Figure S5**), we observed few qualitative differences in downstream analyses. Hereafter, we present results using the Vernot et al., 2016 introgressed variants in the main text and include results using the Browning et al., 2018 set in the supplemental text.

Non-introgressed variants present in both archaic and modern humans likely evolved prior to our most recent common ancestor. We refer to these SAVs as "ancient", and we consider the archaic SAVs with an allele frequency $\geq$ 0.05 in at least two 1KG superpopulations "high-confidence ancient". This decreases the probability of independent occurrence or misclassification of introgressed alleles. Hereafter, "ancient" refers to these high-confidence ancient variants unless otherwise specified. We identified 2,252 such variants based on Vernot et al., 2016 among 1,896 genes (**Figure 1D**; **Figure S4**) and 2,195 variants based on Browning et al., 2018 among 1,856 genes (**Figure S4**).

2.3 Archaic-specific SAVs are enriched in genes with diverse phenotypes.

To identify the potential phenotypic consequences of archaic-specific SAVs, we tested for enrichment of functional annotations among genes with SAVs. Following McArthur et al., 2022, we considered links between genes and phenotypes from two sources: GWAS Catalog 2019

(Buniello et al., 2019) and the Human Phenotype Ontology (Köhler et al., 2021), that capture common and rare disease annotations, respectively. Structural properties of genes, such as the number of exons, influence the probability that they have SAVs (**Table S4**; **Figure S6**). To account for these different probabilities, we generated a permutation-based empirical null distribution (Methods) and used it to estimate enrichment for each phenotype and control the false-discovery rate (FDR).

Given that we cannot directly observe archaic individuals, functions associated with genes with archaic-specific SAVs are of particular interest. We found enrichment for many phenotypes among the 2,012 genes with archaic-specific SAVs (**Figure 2**; **File S2**). The common phenotype enrichments were dominated by immune (e.g., malaria resistance and ulcerative colitis) and metabolic (e.g., blood metabolite levels) traits. There were substantially more phenotypes enriched among genes associated with rare phenotypes (**Figure 2B**), and these included traits that are known to differentiate archaic hominins and modern humans, including skeletal traits such as lumbar hyperlordosis and several cranial features. At least one significantly enriched trait occurred in every system across the GWAS Catalog and Human Phenotype Ontology, except for the endocrine system.

Next, we sought to characterize similarities and differences among the archaic hominin individuals. We assessed phenotype enrichment among genes that contained shared, Neanderthal-specific, and lineage-specific SAVs (**File S2**). We found minimal enrichment among the 152 genes with shared SAVs (bronchitis and progranulin levels) (**Figure S7**). However, there was considerable enrichment across various systems for Neanderthal- and lineage-specific SAVs (**Figure S8**, **Figure S9**, **Figure S10**, **Figure S11**, **Figure S12**). For example, all Neanderthals were enriched for SAVs in genes underlying skin conditions including abnormal skin blistering and fragile skin (**Figure S11**). The Denisovan exhibited enrichment for SAVs in genes associated with many skeletal and skeletal muscle system traits including skull defects, spinal rigidity, abnormal skeletal muscle fiber size, increased muscle fiber diameter variation, and type 1 muscle fiber predominance (**Figure S10**). Only two traits were enriched in multiple different sets of lineage-specific SAVs at FDR-adjusted significance levels: 1) blood metabolite levels in the Altai and Vindija Neanderthal and 2) generalized amyotrophy in the Chagyrskaya Neanderthal and Denisovan.

2.4 Site-level evolutionary conservation varies across SAV origin.

Genes vary in their tolerance to mutation and SAVs often disrupt gene function and contribute to disease (Li et al., 2016; Scotti and Swanson, 2016; Li et al., 2017). To evaluate if the presence of archaic SAVs is associated with evolutionary constraint on genes, we compared the per gene tolerance to missense and loss-of-function variants from gnomAD (Karczewski et al., 2020) among ancient, archaic-specific, introgressed, and non-splice altered genes. In addition to constraint at the gene level, evolutionary constraint can be quantified at nucleotide level by methods like phyloP that quantify deviations from the expected neutral substitution rate at the site-level between species (Pollard et al., 2010). Thus, to explore the constraint on splicing altering variant sites themselves, we also compared their phyloP scores.

While we found a significant difference in the observed/expected number of missense variants per transcript among genes with different classes of SAV (Kruskal-Wallis, $H = 18.886$, $P = 0.0003$), the effect size was minimal (**Figure S13A**). Furthermore, genes with SAVs of different

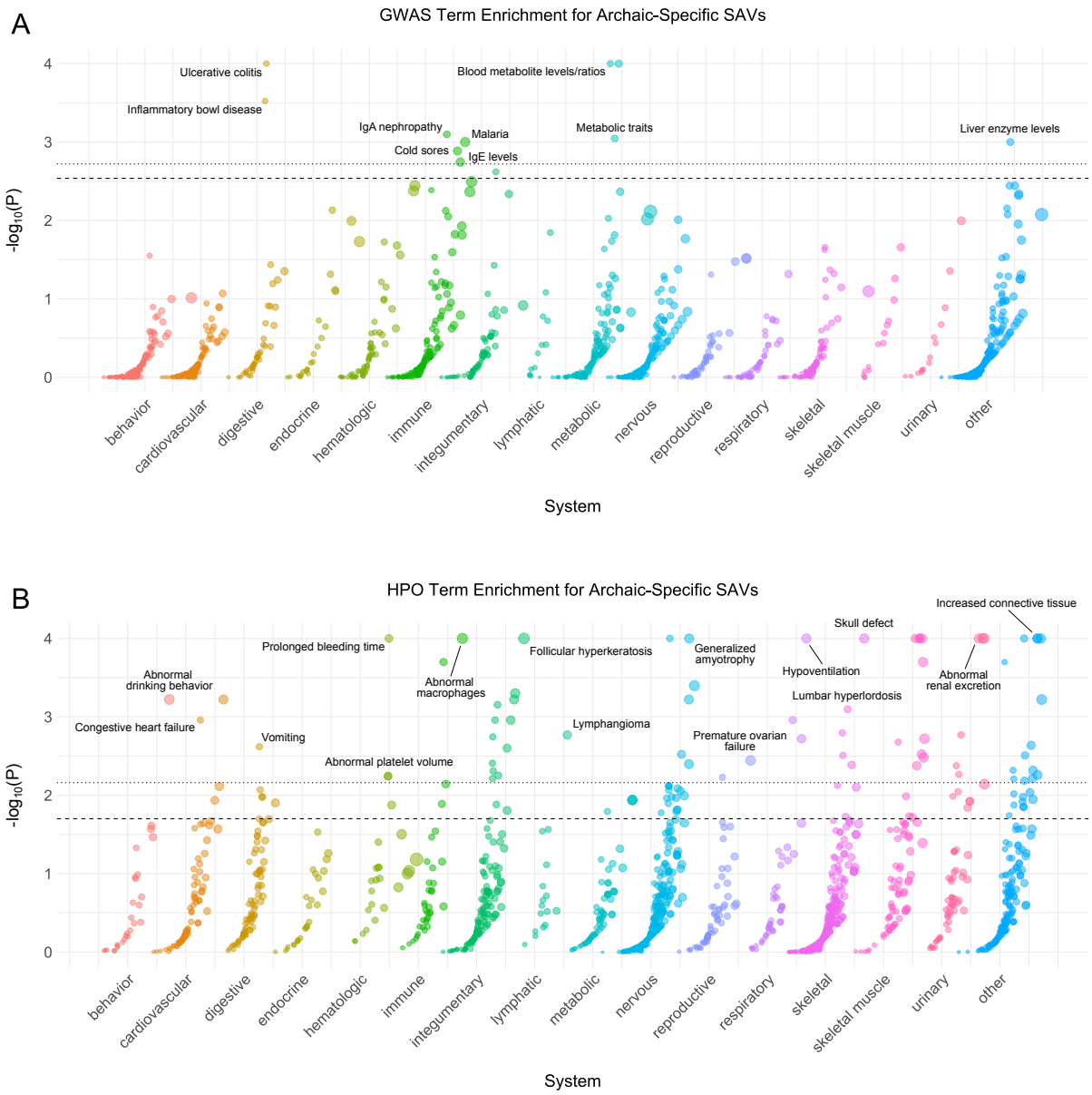

Figure 2: Genes with archaic-specific SAVs are enriched for roles in many phenotypes. **(A)** Phenotype associations enriched among genes with archaic-specific SAVs based on annotations the from GWAS Catalog. Phenotypes are ordered by increasing enrichment within manually curated systems. Circle size indicates enrichment magnitude. Enrichment and p-values were calculated from an empirical null distribution generated from 10,000 shuffles of maximum Δ across the entire dataset (Methods). Dotted and dashed lines represent false discovery rate (FDR) corrected p-value thresholds at FDR = 0.05 and 0.1, respectively. At least one example phenotype with a p-value $\leq$ the stricter FDR threshold (0.05) is annotated per system. **(B)** Phenotypes enriched among genes with archaic-specific SAVs based on annotations from the Human Phenotype Ontology (HPO). Data were generated and visualized as in **A**. See **File S2** for all phenotype enrichment results.

origins did not significantly differ in the observed/expected number of loss-of-function variants per transcript (Kruskal-Wallis, H = 1.697, P = 0.638) (**Figure S13B**). Variants classified per Browning et al., 2018 exhibited the same pattern (**Figure S13C**; **Figure S13D**). These results suggest that genes with alternative splicing in archaics are similar in their gene-level constraint to other genes.

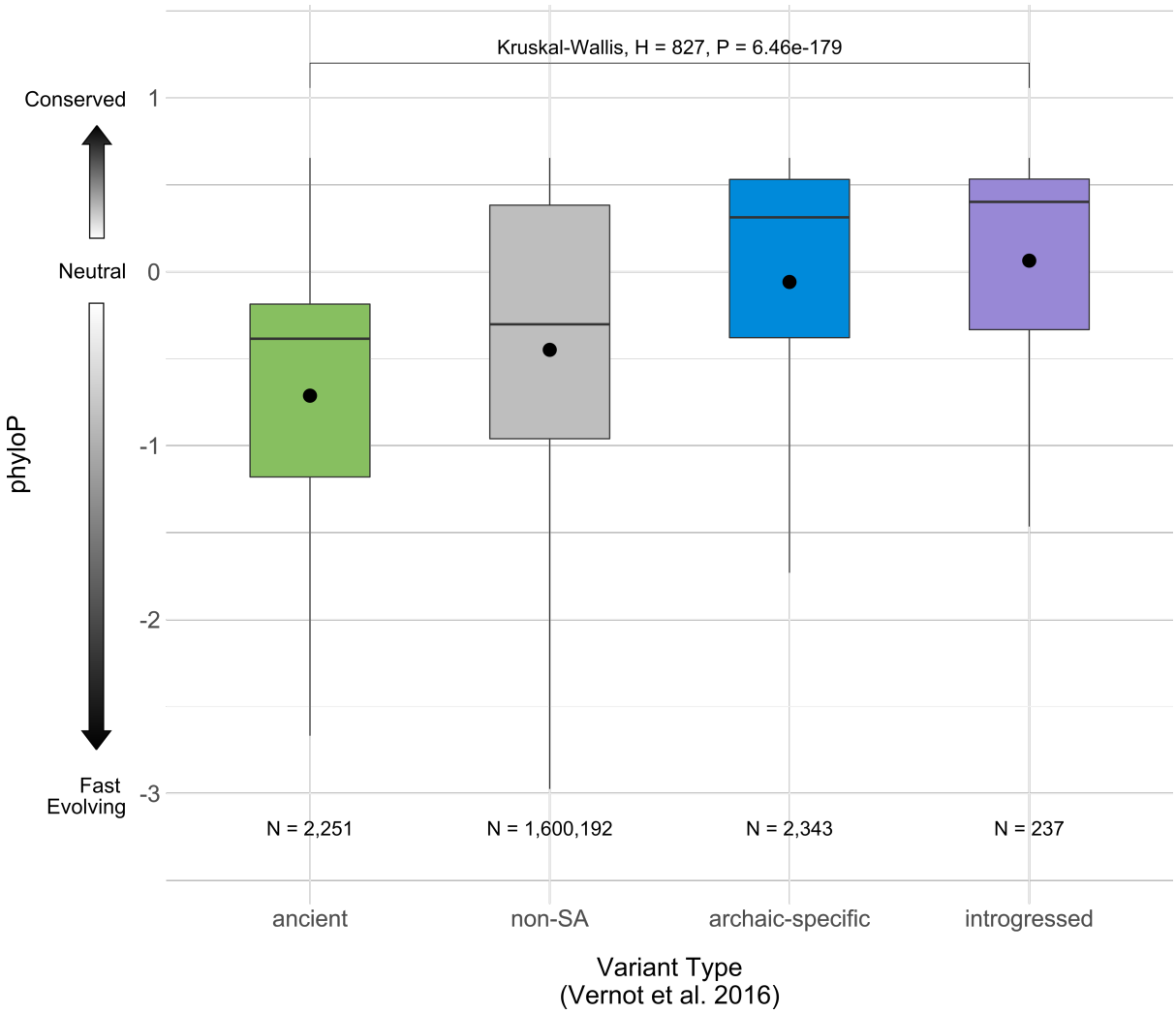

Figure 3: Site-level evolutionary conservation varies across SAVs with different origins. phyloP evolutionary conservation score distributions for archaic SAVs of different origins and non-SAVs. Positive scores indicate substitution rates slower than expected under neutral evolution (conservation), while negative scores indicate higher substitution rates than expected (fast evolution). The boxplots give the first quantile, median, and third quantile of the distributions, and the mean is noted by the black point. Ns are the number of variants per set. SAV classifications were based on Vernot et al., 2016 introgression calls.

In contrast, phyloP scores were significantly different between ancient SAVs, archaic-specific SAVs, introgressed SAVs, and non-SAVs (Kruskal-Wallis, H = 826.862, P = 6.463×10^{-179}) (**Figure 3**). All of the variant sets exhibited a wide range of phyloP scores, indicating diverse pressures on SAVs of each type. However, ancient SAVs and non-SAVs exhibited largely negative phyloP scores suggesting substitution rates faster than expected under neutral evolution. In contrast, archaic-specific and introgressed SAVs had higher median phyloP scores suggesting that more of these loci experienced negative constraint. However, they were mostly in the range consistent with neutral evolution. Variants classified per Browning et al., 2018 exhibited similar patterns (**Figure S14**); however, archaic-specific, rather than introgressed, variants had

a larger mean phyloP score.

2.5 The prevalence of SAVs across lineages is consistent with purifying selection on most SAVs.

Variants that disrupt splicing and/or produce new isoforms are expected to be under strong negative selection (e.g., Kriventseva et al., 2003). However, given differences in ages of archaic SAVs and the effective population sizes (N_e) of the lineages in which they arose, different SAVs were likely exposed to different strengths of selection for different periods. Thus, we hypothesized that the probability a given SAV would survive to the present would vary based on its origin. For example, SAVs that arose in the ancestor all archaic lineages were likely subject to purifying selection over a longer time scale than lineage-specific SAVs, especially those that arose in lineages with low N_e.

Shared archaic variants are depleted for SAVs compared to lineage-specific variants, and this depletion increased with higher splice altering probability thresholds (**Figure 4A**, **Figure 4B**, **Table S5**). This result is consistent with the hypothesis that most splicing variants are deleterious and that the longer exposure to negative selection for older variants results in a smaller fraction of remaining SAVs. It is also with concordant with the site-level constraint results.

Given that the population histories for each archaic lineage were likely different, we also compared within lineages. Neanderthals are thought to have lived in smaller groups and exhibited a lower N_e than Denisovans (Mafessoni et al., 2020). We tested this hypothesis by repeating the SAV enrichment test for variants specific to each individual archaic lineage (**Figure 4A**). All three Neanderthals were significantly enriched for unique SAVs compared to shared archaic variants after Bonferroni correction (OR = 1.205-1.447, **Figure 4C**, **Table S6**). In contrast, variants on the longer and higher N_e Denisovan lineage were not significantly enriched for SAVs (OR = 1.075). At the stricter high-confidence SAV threshold, both the Altai and Vindija Neanderthals remained significantly enriched with increased odds ratios (**Figure S15**).

2.6 Introgressed SAVs found in modern humans were present across archaics.

We hypothesized that the evolutionary history of SAVs might also influence their prevalence in modern human populations. For example, introgressed variants experienced strong negative selection in the generations immediately after interbreeding (Petr et al., 2019), so archaic SAVs that survived stronger and longer-term selection would be more likely to survive in modern humans. To test this, we first considered the distribution of remaining introgressed variants among the archaics. Most introgressed SAVs were present in all Neanderthals (N = 141) or present in all archaics (N = 66; **Table S7**). No SAVs private to Vindija or Chagyrskaya nor shared between both late Neanderthals were identified as introgressed, even though Neanderthal ancestry in most modern humans is most closely related to Vindija and Chagyrskaya (Prüfer et al., 2017; Mafessoni et al., 2020). This is consistent with weaker selection on lineage-specific SAVs and previous work suggesting that older introgressed archaic variants were more tolerated in humans (Telis et al., 2020; McArthur et al., 2021).

To further test this, we compared the expected origin distribution for introgressed SAVs (based on the distribution of archaic-specific SAVs) to the observed distribution for introgressed SAVs. Fewer Altai-specific SAVs occur among introgressed variants whereas shared Nean-

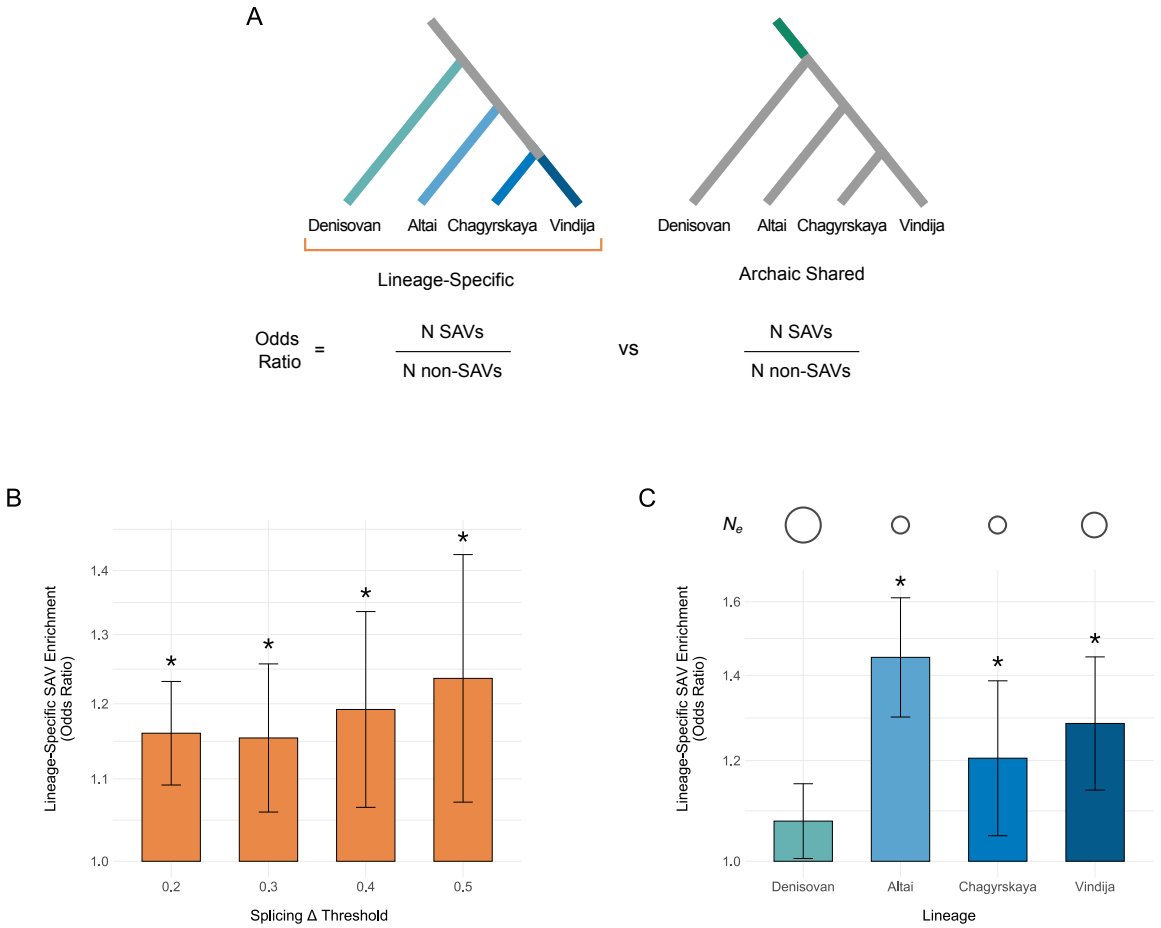

Figure 4: Lineage-specific archaic variants are enriched for SAVs compared to shared archaic variants.
(A) We hypothesized that lineage-specific archaic variants would be enriched for SAVs compared to variants shared across the four archaic individuals, due to less exposure to strong negative selection. To test this, we computed the odds ratio for being an SAV over all variants unique to each lineage (turquoise and blue edges) compared to variants shared among all four lineages (dark green edge). We also hypothesized that lineage-specific archaic variants would vary in their SAV enrichment compared to shared variants, based on the different effective population sizes and lengths of each branch. To test this, we computed the odds ratio for being an SAV over variants unique to each lineage individually compared to variants shared among all four lineages. **(B)** Archaic variants with origins in specific archaic lineages are enriched for SAVs compared to variants shared among all four archaic lineages. The enrichment increases at increasing splice altering probability (Δ) thresholds. Note the y-axis is $\log_{10}$ transformed. **(C)** Lineage-specific archaic variants vary in their enrichment for SAVs. The Neanderthal lineage-specific variants have stronger SAV enrichment than Denisovan-specific variants. Estimated N_e per lineage is denoted by a circle above each lineage, with increasing size reflecting larger N_e. N_e estimates are from Mafessoni et al., 2020. In all panels, asterisks reflect significance of Fisher's exact tests using a Bonferroni corrected α (0.0125). Error bars denote the 95% CI. The number of variants used in each enrichment test are listed in **Table S5** and **Table S6**. Note the y-axis is $\log_{10}$ transformed.

derthal SAVs are more prevalent than expected (**Figure 5A**). This pattern remains for high-confidence and Browning et al., 2018 SAVs (**Figure S16**). These patterns suggest that older SAVs, either those that evolved prior to the Neanderthal common ancestor or prior to the Denisovan and Neanderthal common ancestor were the most tolerated after introgression.

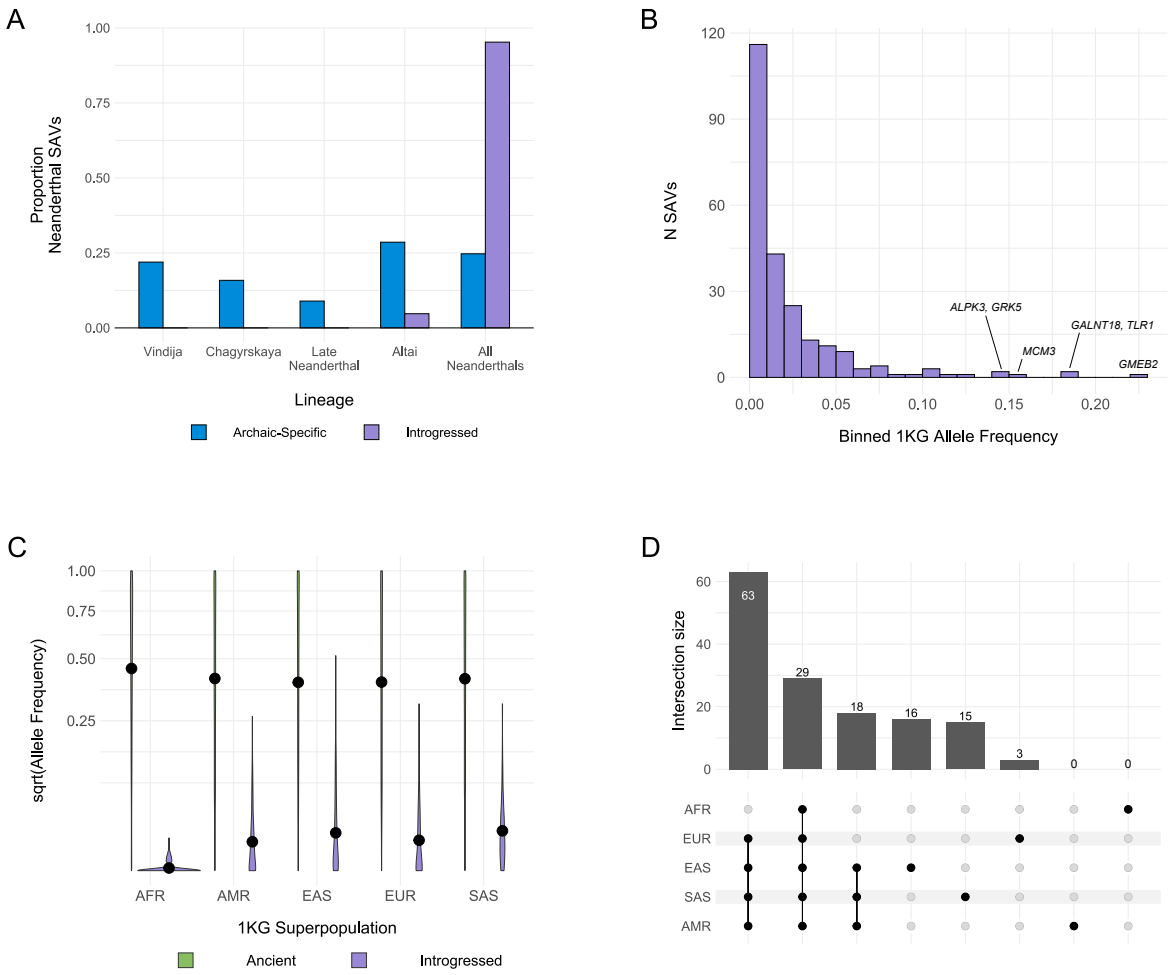

Figure 5: Introgressed SAVs present in modern humans were shared across archaic individuals.
(A) Histograms comparing distributions of the presence of all Neanderthal SAVs (blue) and introgressed SAVs (purple), as defined by Vernot et al., 2016, in different sets of Neanderthal individuals. Introgressed SAVs are significantly older than expected from all Neanderthal SAVs. We focused on Neanderthal lineages because of low power to detect introgressed Denisovan SAVs. All data are presented in **Table S7**. **(B)** Allele frequency distribution for introgressed SAVs per Vernot et al., 2016 with $\Delta \geq 0.2$. Allele frequencies represent the mean from the AFR, AMR, EAS, EUR, SAS frequencies from the Vernot et al., 2016 metadata. **(C)** Allele frequency distributions for SAVs present in both archaic and modern individuals stratified by 1KG superpopulation and origin (ancient vs. introgressed). The black dot represents the mean allele frequency for each set. The y-axis is square root transformed. **(D)** The number of introgressed SAVs with a minimum allele frequency of at least 0.01 in each modern human population. We display all individual populations, the non-African set, and Asian/American set here. See **Figure S21** for all sets.

Consistent with known introgression patterns, introgressed SAVs occurred at lower overall frequencies (**Figure 5B**). However, a small number of introgressed SAVs occur at modest to high frequencies among genes including *GMEB2*, *GALNT18*, and *TLR1* (**Figure 5B**). The latter occurs in an adaptively introgressed locus spanning three toll-like receptors—key components of the innate immune system (Dannemann et al., 2016). In contrast, ancient SAVs occur at

high frequencies in all five 1KG superpopulations, and their frequencies are significantly higher among Africans (μ = 0.522) than non-Africans (μ = 0.476) (Mann-Whitney U, U = 10,963,956, P = 2.66×10^{-09}) (**Figure 5C**, **Figure S17**). Furthermore, most ancient SAVs are present at $\geq$ 0.05 frequency in all five 1KG superpopulations **Figure S18**, **Figure S19**). Introgressed SAVs have significantly lower frequencies in all superpopulations (**Figure 5B**) and are less likely to be shared among multiple populations (**Figure 5C**, **Figure S20**, **Figure S21**).

It is possible these patterns reflect the general attributes of introgressed variants, rather than splicing effects of SAVs. We therefore examined the relationship between allele frequency in 1KG and splice altering probability (Δ max) for introgressed SAVs. 1KG populations did not generally differ in Δ max for either ancient or introgressed SAVs, although introgressed SAVs had a higher Δ max (**Figure S22**). We anticipated, however, SAVs that were more likely to be splice altering would occur at lower frequencies. Indeed, we found a significant negative association between allele frequency and Δ max for $\Delta \geq 0.2$ (Spearman, ρ = -0.2362, P = 0.0002) (**Figure S23**).

2.7 Introgressed SAVs have limited functional associations.

We tested whether any functional annotations were enriched among the 353 genes with Browning et al., 2018 introgressed SAVs and 232 genes with Vernot et al., 2016 introgressed SAVs (**File S2**). We found little enrichment among any GWAS or HPO terms (**Figure S24**, **Figure S25**). Only two terms were significantly enriched among genes with Vernot et al., 2016 introgressed SAVs: adverse response to breast cancer chemotherapy (GWAS) and Oligohydramnios (HPO) (**Figure S24**). Only one HPO term, abnormal hip-girdle musculature, was enriched among genes with Browning et al., 2018 introgressed SAVs (**Figure S25A**). However, four GWAS terms met our FDR-corrected significance threshold: asthma and hay fever, diabetes in response to drug treatment, *H. pylori* serologic status, and systemic sclerosis (**Figure S25B**). Overall, these results suggest that most SAVs surviving in modern human populations are unlikely to have large phenotypic or fitness effects.

We further considered the potential functional effects of introgressed SAVs by intersecting the with Neanderthal variants exhibiting allele-specific expression (ASE) in modern humans (McCoy et al., 2017). We identified 16 SAVs out of 1,236 ASE variants, including variants in *GSDMC*, *HSPG2*, and *RARS* (**Table S8**). We also note that a handful of the McCoy et al., 2017 variants fell just under our SAV threshold, including a variant (rs950169) in *ADAMTSL3* highlighted in the ASE study with correctly predicted acceptor loss (Δ = 0.19) (McCoy et al., 2017).

2.8 Introgressed SAVs are more tissue-specific than ancient SAVs.

Given their different histories of selective pressures, we hypothesized that introgressed SAVs would be more tissue-specific than ancient SAVs in their effects. To explore this, we identified 1,381 archaic SAVs with sQTL data from GTEx across 49 tissues.

Introgressed sQTL SAVs were significantly associated with tissue specific gene expression compared to ancient sQTL SAVs (Mann-Whitney U, U = 33,629.5, P = 0.035) (**Figure 6A**). On average, introgressed SAVs influenced splicing in 4.72 fewer tissues than ancient SAVs. Further, all sQTL SAVs with broad effects ($>$ 40 tissues) were ancient (107 high-confidence and

5 low-confidence). 74 of these were shared among all four archaics (**Table S9**), suggesting that core sQTL SAVs were more likely to evolve in the deep past. These patterns were also observed among the Browning et al., 2018 variants (**Figure S26**). Collectively, 30% of sQTL SAVs (N = 427) were associated with tissue specific effects on splicing (1 or 2 tissues) (**Figure S27**). Consistent with known gene expression patterns, testis had the most unique sQTL among SAVs, followed by skeletal muscle and thyroid.

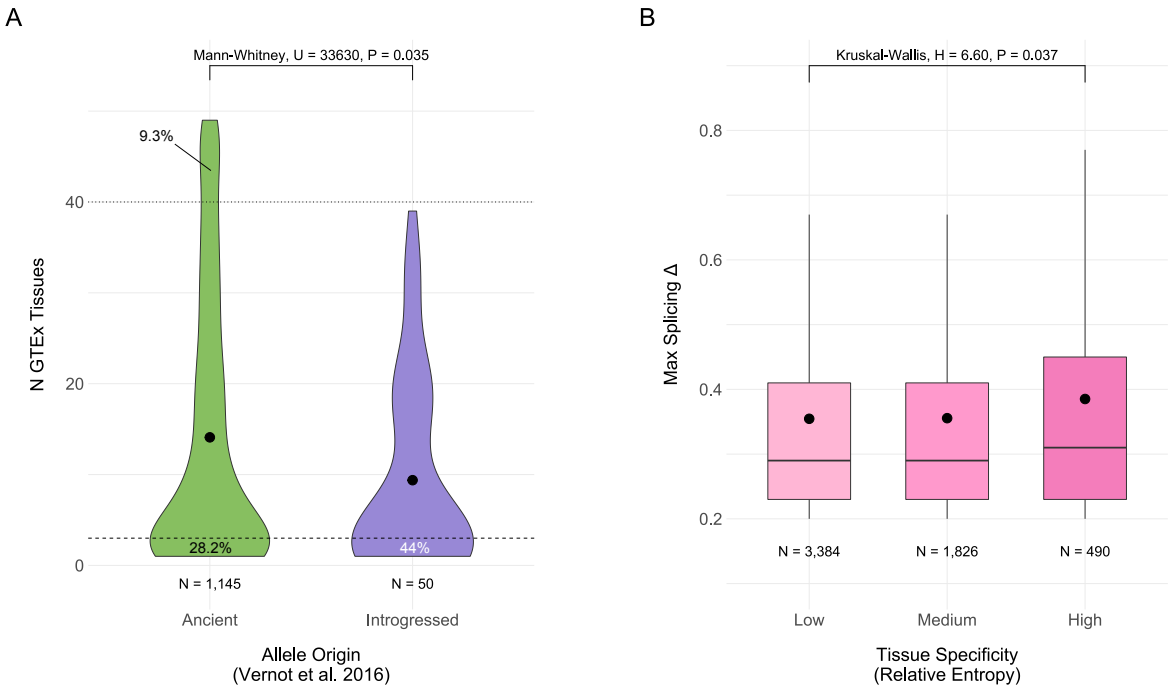

Figure 6: Increased tissue-specificity is associated with introgressed SAVs and with increased probability of alternative splicing.
(A) The distribution of the number of GTEx tissues in which an ancient or introgressed SAV (per Vernot et al., 2016) was identified as an sQTL. Introgressed variants are significantly more tissue-specific (Mann-Whitney U 33630; P = 0.035). We defined "tissue-specific" variants as those occurring in 1 or 2 tissues and "core" sQTLs as those occurring in > 40 of the 49 tissues. The dashed and dotted lines represent these definitions, respectively. The proportion of SAVs below and above these thresholds are annotated for each SAV group. **(B)** The distributions of maximum splice altering probability (Δ) for SAVs in 4,061 genes binned by tissue-specificity of expression. We quantified the tissue-specificity of each gene as the relative entropy of expression levels across 34 tissues from GTEx compared to genes overall. Low tissue specificity reflects relative entropy ≤ 0.1, medium tissue specificity reflects relative entropy > 0.1 and ≤ 0.5, and high tissue specificity reflects relative entropy > 0.5 (**Figure S28**).

Variation in gene expression among tissues may also influence the efficacy of negative selection to remove deleterious SAVs. For example, Saudemont et al., 2017 demonstrated that more ubiquitously expressed genes in *Paramecium tetraurelia* exhibited less alternative splicing compared to genes with more tissue-specific expression due to the differences in the efficacy of negative selection. We predicted that tissue-specificity of expression would be associated with the number of SAVs per gene or maximum Δ. We quantified tissue-specificity of expression using the relative entropy of the TPM count for each gene across tissues compared to the expression distribution across tissues for all genes in GTEx. This metric ranges from 0 to 1, with higher values reflecting greater tissue specificity. Most genes exhibited broad expression (**Figure S28**), so we divided genes into low, medium, and high tissue-specificity based on the relative entropy.

Genes with the most tissue-specific expression had significantly higher median maximum splice altering probability (Δ) than genes with broader expression patterns (**Figure 6B**; Kruskal-Wallis, H = 6.599, P = 0.037). This could indicate greater selection against SAVs likely to influence expression across many tissues; however, we note that the effect was small in magnitude. The distribution of the number of archaic SAVs per gene did not differ significantly between entropy classes (Kruskal-Wallis, H = 1.89, P = 0.388) (**Figure S29**); all had a median of 1 SAV.

2.9 Archaic SAVs with potential evolutionary significance.

Many archaic SAVs influence genes with known or previously hypothesized significance to the evolutionary divergence between archaic hominins and modern humans. For example, the 2'-5' oligoadenylate synthetase *OAS* locus harbors an adaptively introgressed splice altering variant at chr12:113,357,193 (G $>$ A) that disrupts an acceptor site and results in multiple isoforms and leads to reduced activity of the antiviral enzyme (Mendez et al., 2012; Sams et al., 2016). This ancestral variant was reintroduced in to modern Eurasian populations by Neanderthal introgression (Rinker et al., 2020). SpliceAI correctly predicted the acceptor loss at this site (Δ = 0.89). This locus harbors 92 additional archaic variants (N = 92). We found one additional SAV at chr12:113,355,275 in *OAS1* that potentially results in an acceptor gain (Δ = 0.26). This allele was unique to the Denisovan, is derived, and was present in only one of 2,054 1KG samples as a heterozygote. This suggests potential further splice variant evolution of this locus, with possible Denisovan-specific effects.

We also identified several variants at other well-studied loci. Variation in human populations at the *EPAS1* locus includes a Denisovan-introgressed haplotype thought to contribute to adaptation to living at high altitude among Tibetans (Huerta-Sánchez et al., 2014). Of 184 archaic variants occurring at this locus, we identified two as candidate SAVs. One variant (chr2: 46,584,859; rs372272284) is fixed in the Denisovan whereas all Neanderthals have the human reference allele (**Figure 7A**). The variant is introgressed and present at low frequency in East Asians in 1KG, and is also the lead variant in an observed association of the introgressed haplotype with decreased hemoglobin levels in Tibetans (Jeong et al., 2018). This SAV, rs372272284, strengthens a canonical 5' splice site (CAA|GT to CAG|GT) (Sibley et al., 2016), resulting in a donor gain (Δ = 0.37) (**Figure 7A**). If used, this splice site would introduce multiple stop codons, resulting in nonsense mediated decay (NMD) of the mRNA. This would result in the same molecular effect (decreased circulating *EPAS1* RNA) that is thought to contribute to hypoxia adaptation (Peng et al., 2017). The other candidate SAV (chr2: 46,610,904) is absent from 1KG and occurs as a heterozygyote in the Altai Neanderthal, and is near the end of the last intron of the gene, making it much less likely to fundamentally alter the mRNA product.

We also identified three archaic SAVs within *ERAP2*, a gene subject to strong and consistent balancing selection in different human populations (Andrés et al., 2010). SpliceAI correctly identified a previously characterized human variant (rs2248374), which causes a donor loss (Δ = 0.51) and results in a truncated protein and subsequent NMD of the mRNA. However, we identified an additional Neanderthal SAV, which is also introgressed and occurs at low frequencies among Americans (5%), Europeans (6%), and South Asians (2%) in 1KG (**Figure 7B**). This SAV, rs17486481, is a donor gain (Δ = 0.53) that introduces a canonical 5' splice site (AT|GTAAT to AT|GTAAG) and would similarly result in NMD (**Figure 7B**). However this al-

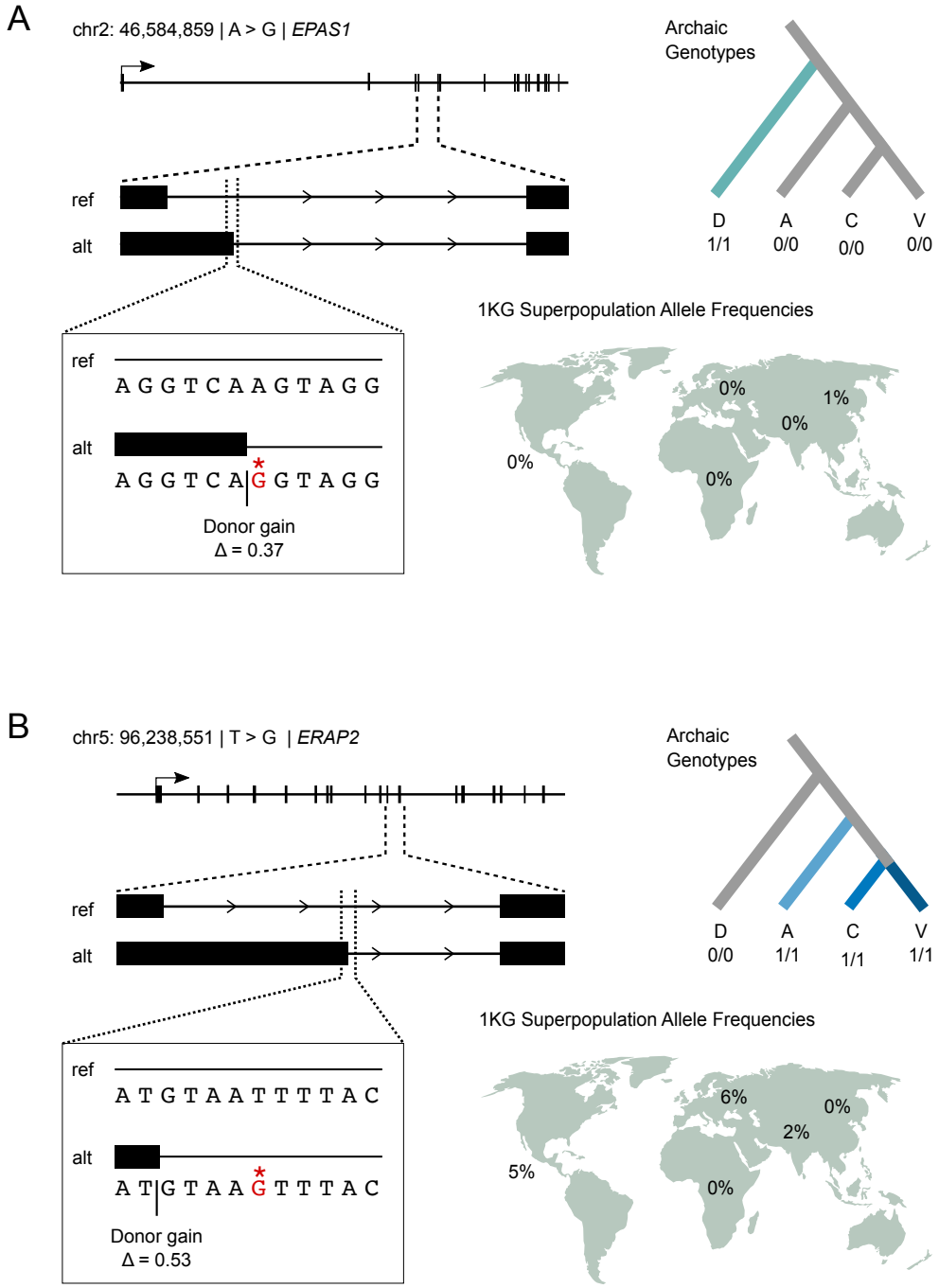

Figure 7: Example archaic SAVs leading to nonsense mediated decay in loci with evidence of recent adaptive evolution.
(A) A Denisovan-specific homozygous SAV results in a donor gain in *EPAS1*, hypoxia-inducible factor-2alpha, between the fourth and fifth exon. The transcript resulting from the SAV introduces at least one stop codon, which likely results in the elimination of the transcript via nonsense mediated decay. This SAV potentially contributes to the effects of the introgressed haplotype in Tibetan adaptation to living at high altitude. This variant is present as a heterozygote in 12 individuals from 1KG: 8 from the East Asian superpopulation and 4 from the South Asian superpopulation. **(B)** Three archaic SAVs, including a Neanderthal-specific variant, occur in *ERAP2*, a MHC presentation gene with evidence of strong balancing selection in human populations. Consistent with this, the SNV occurs at low frequency in three of the five 1KG superpopulations. As in the *EPAS1* example, this variant results in a donor gain between the 11th and 12th exons, which introduces at least one stop codon.

lele always occurs with the non-truncated version of rs2248374 (while being much rarer), and the need to maintain the non-truncated allele is most likely why it remains uncommon. The third variant (chr5: 96,248,413) was archaic-specific—occurring as a heterozygote in the Altai Neanderthal—and results in an acceptor gain (Δ = 0.24).

3 Discussion

Alternative splicing plays a critical role in organismal biology, particularly during development and establishing tissue identity (Baralle and Giudice, 2017). Thus, alternative splicing often contributes to adaptation and phenotypic differences between closely related species (Blekhman et al., 2010; Barbosa-Morais et al., 2012; Merkin et al., 2012; Singh and Ahi, 2022; Verta and Jacobs, 2022; Wright et al., 2022). The development of machine learning algorithms that can predict alternative splicing from sequence alone now enables analysis of alternative splicing in populations for which transcriptomic data are difficult or impossible to generate, including archaic hominins. Here, we use SpliceAI to uncover the previously unobservable genome-wide alternative splicing landscape of archaic hominins.

We identify thousands of putative splice altering variants from the high-coverage genomes of three Neanderthals and a Denisovan. We find that many of these variants do not occur in modern humans, and we propose that they are implicated in specific phenotypic differences between archaic hominins and modern humans. Additionally, many SAVs are shared with modern humans and are ancient, evolving before the common ancestor of archaic hominins and modern humans. Furthermore, a few hundred SAVs are present in human populations due to introgression, and these surviving introgressed SAVs are almost entirely shared across Neanderthals. We also observe multiple lines of evidence supporting the role of negative selection in shaping SAV patterns.

Given that introgressed and ancient SAVs are present in modern humans, their splicing patterns have the potential to be directly studied to further understanding of their phenotypic effects. We found that 35% of archaic SAVs were identified in modern humans in GTEx as sQTLs. There are several reasons why archaic SAVs might not have been detected as sQTL. Splicing is influenced by sequence, but is also a somewhat stochastic process influenced by other cellular dynamics, such as polymerase pausing (Sibley et al., 2016). This, coupled with the limited power in many GTEx tissues, particularly for SAVs at low frequency in Europeans, means that all splice-altering variants would not necessarily be detected. Indeed, we observe higher fractions of SAVs as sQTL when focusing on high frequency variants (**Figure S30**). Nonetheless, the degree to which SAV tissue-specificity in modern humans reflects specificity in archaic hominins is unknown without further experimental study. However, such studies are challenging because the genomic and archaic cellular context cannot be perfectly replicated (i.e., a Neanderthal genome in a Neanderthal tissue).

Our results offer new insight into an essential molecular mechanism and previously unstudied attributes of archaic hominins; however, we note some limitations of our approach. First, we did not include structural variants (InDels) or variants from the sex chromosomes in this analysis, both of which warrant further study. For example, the X chromosome exhibits high levels of alternative splicing (Karlebach et al., 2020) and splicing can occur in a sex-specific manner (Blekhman et al., 2010; Rogers et al., 2021). Future development and application of models

with sex-specific transcriptomic data may offer additional phenotypic insights but, for now, we are left we high-coverage sequences from only females. Second, the modern humans used in this analysis have considerable genetic diversity, but some additional variants classified as "archaic-specific" could occur in modern humans not included here. Even so, they would be rare and a significant number of archaic-specific variants would remain. Third, the tag SNPs and modern human samples used in this analysis are best suited to identifying Neanderthal rather than Denisovan introgression (Browning et al., 2018; Vernot et al., 2016). Our conservative approach means that the number of introgressed SAVs reported here is an underestimate and does not include Denisovan-derived SAVs. Multiple modern human populations contain considerable Denisovan ancestry, therefore, future work should consider these variants.

In summary, our approach of combining machine learning with ancient DNA and modern population genetic data identifies thousands of archaic variants that potentially alter splicing, including many that appear to be specific to archaic hominins. Genes affected by archaic SAVs are enriched for roles in a variety of phenotypes and several influence loci with known relevance to recent human evolution. For example, two archaic SAVs that we highlight likely cause in NMD of the resulting *EPAS1* and *ERAP2* transcripts. Downregulation of *EPAS1* is thought to underlie high-altitude adaptation in Tibetans (Peng et al., 2017). In *ERAP2*, another variant in human populations that induces NMD has experienced strong balancing selection (Andrés et al., 2010). These examples underscore that phenotypic effects from alternative splicing are not limited to expanded proteomic diversity, but also downregulation of gene expression via NMD (Ge and Porse, 2014; Smith and Baker, 2015). Further work is needed to understand the functional effects of these and other archaic SAVs. Nonetheless, our results suggest that alternative splicing played a role in hominin divergence and offers specific molecular hypotheses for testing. We also anticipate that our sequence-based approach will enable study of alternative splicing in other extinct or difficult to sample taxa.

4 Methods

4.1 Archaic Genomic Data

We retrieved four high-coverage publicly available archaic hominin genomes representing three Neanderthals (Mafessoni et al., 2020; Prüfer et al., 2014; Prüfer et al., 2017) and a Denisovan (Meyer et al., 2012).

We excluded sites that were invariant among the archaic individuals ("ALT $=$.") and variants with low site quality ("QUAL $<$ 30"). Further, low quality genotypes were set to missing based on read depth ("FMT/DP $<$ 10") and genotype quality ("FMT/GQ $<$ 30"). We also normalized InDels and split multi-allelic records into separate entries for positions with multiple variants ("norm -m -"). All filtering was completed using bcftools, version 1.13 (Li, 2011).

All genomic coordinates presented in the manuscript and supplementary material refer to hg19/GRCh37.

4.2 Variant Annotation

We annotated variants for putative alternative splicing using SpliceAI, version 1.3.1 (Jaganathan et al., 2019). Briefly, SpliceAI uses a deep residual neural network to estimate the splice alter-

ing probability and position change of each variant from DNA sequence alone making it ideal for studying archaic hominins, for which we cannot obtain transcript-level data. The model considers 5 kbp flanking the variant in both directions. The output includes four splice altering probabilities (Δs) for 1) acceptor gain (AG), 2) acceptor loss (AL), 3) donor gain (DG), and 4) donor loss (DL) as well as the position changes for each of the four deltas. Δs range from 0 to 1 and represent the likelihood a variant is splice altering for one or more of the four categories. We implemented SpliceAI in a Conda package using keras, version 2.3.1 (Chollet et al., 2015) and tensorflow, version 1.15.0 (Abadi et al., 2015).

After filtering, we ran SpliceAI on sets of 5×10^3 variants using the hg19 reference genome using the GENCODE, Human Release 24, annotations (Harrow et al., 2012) included with the package. We concatenated all results and further split variants with multiple annotations. Among all variants, 32,105 exhibited multiple annotations with different effects on splicing (**Table S11**). While we included InDels and variants on the X chromosome in this scan, we restricted all downstream analyses to autosomal SNVs (Discussion).

4.3 Defining SAVs

For each variant, we identified the maximum SAP (Δ) among all four classes: AG, AL, DG, and DL. We then defined SAVs using two Δ thresholds: Δ max $\geq$ 0.2 and 0.5, "SAVs" and "high-confidence SAVs", respectively.

We determined whether the number of SAVs identified in each archaic individual was different than expected by randomly selecting a sample from 24 1KG populations. We annotated all variants present among these individuals using SpliceAI and the hg38 annotations included with the package. We then analyzed the variants as for the archaics (i.e., splitting multi-allelic sites and variants with multiple GENCODE annotations). We filtered for variants with a Δ max $\geq$ 0.2 and summed the number of variants per 1KG sample that had at least one alternate allele present.

4.4 Archaic Variants in Modern Humans

We noted the distribution of each variant among the archaics using eight classes: 1) Altai, 2) Chagyrskaya, 3) Denisovan, 4) Vindija, 5) Late Neanderthal (Chagyrskaya and Vindija), 6) Neanderthal (Altai, Chagyrskaya, and Vindija), 7) Shared (all four archaics) and 8) Other (all remaining possible subsets). The assignment was based on the presence of at least one allele with an effect.

We assessed whether any variants present among the archaics are also present in modern humans using biallelic SNVs and InDels from 1KG, Phase 3 (Lowy-Gallego et al., 2019). We used LiftOver (Hinrichs et al., 2006) to convert variants from hg19 to hg38. We then normalized the 1KG variants ("norm -m - -f hg38.fa") and subset variants to those within gene bodies ("view -R genes.bed"). We queried these variants for allele count, allele number, and allele frequencies ("query -f"). Allele frequencies included the overall allele frequency and an allele frequency per 1KG superpopulation: Africa (AFR), Americas (AMR), East Asia (EAS), Europe (EUR), and South Asia (SAS). These precomputed values had been rounded to two decimal places in the VCFs. Normalization, filtering, and querying was done using bcftools (Li, 2011). After using LiftOver to convert back to hg19 coordinates, we merged the 1KG variants with the

archaic variants ensuring the archaic and 1KG reference and alternate alleles matched. We recalculated the allele frequency for Africans as the annotated frequency included samples from an admixed African population: African ancestry in SW USA (ASW). We subset samples from Esan (ESN), Mandinka (GWD), Luhya (LWK), Mende (MSL), and Yoruban (YRI) and calculated allele frequency as allele count divided by allele number per site.

We used two datasets to identify introgressed variants: Vernot et al., 2016 and Browning et al., 2018. These datasets differ in their approach to recognizing introgressed sequences and partly overlap the archaic variants considered in this study. Vernot et al., 2016 used the S* statistic to classify human sequences as introgressed. S* leverages high linkage-disequilibrium among variants in an admixed target population that are absent in an unadmixed reference population (Plagnol and Wall, 2006; Vernot and Akey, 2014). Introgressed haplotypes are then identified by maximizing the sum of scores among all SNP subsets at a particular locus (Plagnol and Wall, 2006; Vernot and Akey, 2014). Tag SNPs are those variants that match an archaic allele and occur with at least two other tag SNPs in a 50 Kb window. Haplotypes were defined as regions encompossing $\geq$ 5 tag SNPs in LD within a given human population ($R^2 \geq 0.8$). We collated tag SNPs from all four populations: East Asian (ASN), European (EUR), Melanesian (PNG), and South Asian (SAS). We retained all metadata from Vernot et al., 2016. A handful of tag SNPs encompass multiple haplotypes that reflect differences in haplotype size between modern human populations; we retained the first record per variant. Browning et al., 2018 developed a modified S* statistic, Sprime, which employs a scoring method that adjusts the score based on the local mutation and recombination rates, allows for low frequency introgression in the unadmixed outgroup, and avoids windowing to identify introgressed segments. We collated introgressed variants for 20 non-African populations and filtered for those that matched the Altai Neanderthal at high-quality loci.

A handful of sequences in the hg19 reference genome are introgressed from archaic hominins. Therefore, we maximized the number of introgressed sites we could analyze by defining sites rather than variants as introgressed if either the reference or alternate allele for each SAV matched any Neanderthal base at a matching position. We ensured that SpliceAI predictions were similar for these allele pairs, regardless of which was the reference and alternate, by generating a custom hg19 sequence where introgressed reference alleles (N = 7,977) from Vernot et al., 2016 were replaced by the alternate allele using a custom script. We then applied SpliceAI to the introgressed reference alleles, now considered to be the alternate. We found that 24 of the 26 variants were classified as SAVs (**Table S10**). One of the remaining two variants was nearly identical in splicing probability (Δ max = 0.19 and Δ max = 0.2), whereas the other variant's predictions were different (Δ max = 0.16 and Δ max = 0.31) (**Table S10**). Given this overall similarity, we maintained the original predictions for introgressed Vernot et al., 2016 reference alleles in our dataframe but provide the predictions when these nucleotides are the alternate allele for all SAVs and non-SAVs in the project GitHub repository. We recalculated allele frequencies for all introgressed variants to account for sites where the reference sequence contained introgressed alleles, as the precomputed 1KG allele frequency would be incorrect. The Browning et al., 2018 metadata designate whether the reference or alternate allele is introgressed. Therefore, we used the 1KG allele frequency for sites with an introgressed alternate allele and subtracted the 1KG allele frequency from 1 for sites with an introgressed reference allele. For Vernot et al., 2016 introgressed variants, we calculated an average from the metadata, which included the allele frequencies in various populations for the

introgressed allele. We took the mean of the AFR, AMR, EAS, EUR, and SAS frequencies for all introgressed positions.

We categorized each variant's "origin" based on presence in 1KG and whether or not the variant was introgressed. Further, we classified each variant's allele origin based on introgressed variants identified by Vernot et al., 2016 "Vernot allele origin" and Browning et al., 2018 "Browning allele origin" due to the incomplete overlap among variants in those datasets. Variants that did not occur in 1KG were defined as "archaic-specific". Variants that were present in 1KG and introgressed were defined as "introgressed". Variants that were present in 1KG but not introgressed were considered "ancient" at two confidence levels. "High-confidence ancient" variants were present in at least two 1KG superpopulations at an allele frequency ≥ 0.05, while "low-confidence ancient" variants did not meet this threshold. We report analyses on the high-confident ancient set; this helps to remove cases of potential convergent mutation. We identified a small number of variants that were classified as introgressed by Vernot et al., 2016 and Browning et al., 2018 but absent in 1KG: 22 and 12, respectively. We maintained the "archaic-specific" category for these variants. Additionally, a handful of variants (N = 82) were absent in 1KG but present in GTEx. We reclassified these variants from "archaic-specific" to "low-confidence ancient".

4.5 Gene Characteristics, Mutation Tolerance, and Conservation

We used the SpliceAI annotation file for hg19 from GENCODE, Human Release 24 (Harrow et al., 2012), to count the number of exons per gene and calculate the length in bp of the gene body and the coding sequence. The number of isoforms per gene were retrieved from GENCODE, Human Release 40. We retrieved missense and loss-of-function (LoF) observed/expected ratios from gnomAD (Karczewski et al., 2020) to quantify each gene's tolerance to mutation. We also considered conservation at the variant level. We used the primate subset of the 46 way multi-species alignment (Pollard et al., 2010). Positive phyloP scores indicate conservation or slower evolution than expected, whereas negative phyloP scores indicate acceleration or faster evolution than expected based on a null hypothesis of neutral evolution.

4.6 Phenotype Enrichment

We followed the approach of McArthur et al., 2022 to assess enrichment for SAVs in genes implicated in different human phenotypes. Many gene enrichment analyses suffer from low power to detect enrichment because an entire genome is used as the null distribution. Relatedly, SAVs are unevenly distributed throughout archaic genomes. We addressed this issue by generating a null distribution from the observed data. We first retrieved phenotypes and the associated genes per phenotype from Enrichr (Chen et al., 2013; Kuleshov et al., 2016; Xie et al., 2021). We used both the 2019 GWAS Catalog and the Human Phenotype Ontology (HPO). The GWAS Catalog largely considers common disease annotations and has 1,737 terms with 19,378 genes annotated (Buniello et al., 2019), whereas HPO largely considers rare disease annotations and has 1,779 terms with 3,096 genes annotated (Köhler et al., 2021). All 3,516 terms were manually curated into one of 16 systems: behavioral, cardiovascular, digestive, endocrine, hematologic, immune, integumentary, lymphatic, metabolic, nervous, other, reproductive, respiratory, skeletal, skeletal muscle, and urinary.

We considered nine different gene sets, generated using SAVs with $\Delta \geq 0.2$, for our enrichment analyses: 1) genes with lineage-specific Altai SAVs (N = 310), 2) genes with lineage-specific Chagyrskaya SAVs (N = 172), 3) genes with lineage-specific Denisovan SAVs (N = 956), 4) genes with lineage-specific Vindija SAVs (N = 238), 5) genes with SAVs present in all three Neanderthals (N = 268), 6) genes with SAVs shared among all four archaics (N = 160), 7) genes with all archaic-specific SAVs (N = 2,252), 8) genes with introgressed SAVs per Vernot et al., 2016 (N = 237), and 9) genes with introgressed SAVs per Browning et al., 2018 (N = 373). The shared set only included variants present in all four archaics and excluded those that were inferred from parsimony. We retained duplicated gene names to reflect genes with multiple SAVs.

We identified which genes were present in both the GWAS Catalog and HPO per set using a boolean to calculate the observed gene counts per term per ontology. We then removed GWAS and HPO terms per set that did not include at least one gene from the set. This resulted in 713 Altai, 1,437 archaic-specific, 734 Browning et al., 2018 introgressed, 417 Chagyrskaya, 1,046 Denisovan, 553 Neanderthal, 420 shared, 614 Vernot et al., 2016 introgressed, and 519 Vindija terms for the 2019 GWAS Catalog and 638 Altai, 1,510 archaic-specific, 720 Browning et al., 2018 introgressed, 391 Chagyrskaya, 1,185 Denisovan, 571 Neanderthal, 389 shared, 591 Vernot et al., 2016 introgressed, and 533 Vindija terms for the Human Phenotype Ontology.

The max Δ was then shuffled across all 1,607,350 variants without modifying the annotation, allele origin, or distribution data. The distribution of genes for both ontologies was then recorded. We repeated this process 1×10^4 times per set and calculated enrichment as the number of observed genes divided by the mean empirical gene count per term. p-values were calculated as the proportion of empiric counts + 1 $\geq$ the observed counts + 1. We adjusted our significance level due to multiple testing by correcting for the false discovery rate (FDR). We used a subset (N = 1×10^3) of the empirical null observations and selected the highest p-value threshold that resulted in a $V/R < Q$ where V is the mean number of expected false discoveries and R is the observed discoveries (McArthur et al., 2022). We calculated adjusted significance levels for each set for Q at both 0.05 and 0.1.

4.7 Gene Expression, Tissue Specificity, and sQTL

We used TPM counts for each gene from GTEx, version 8, to analyze expression. We quantified tissue specificity as the relative entropy of each gene's expression profile across 34 tissues compared to the median across genes overall. Thus, a gene with expression only in a small number of tissues would have high relative entropy and a gene with expression across many tissues would have low relatively entropy to this background distribution. The 34 tissues were selected based on groupings from the Human Protein Atlas to minimize the amount of sharing between distinct tissues, e.g., since brain tissues are over-represented in GTEx. We used median expression across tissues as the null and calculated relative entropy using the entropy function from the SciPy statistics package (Virtanen et al., 2020). Based on the observed distribution of relative entropy scores (**Figure S28**), we designated genes with scores $\leq$ 0.1 as "low tissue-specificity", genes with scores > 0.1 and $\leq$ 0.1 as "medium tissue-specificity", and genes with scores > 0.5 as "high tissue-specificity". We compared both the number of SAVs per gene and the maximum Δ for SAVs among the three relative entropy categories.

We downloaded sQTL data from GTEx, version 8. We collated significant variant-gene

associations (N = 24,445,206) across all 49 tissues and intersected these with SAVs, using LiftOver (Hinrichs et al., 2006) to convert the SAVs to hg38 and then back to hg19 after intersecting.

4.8 Major Spliceosome Complex

We characterized differences in the major spliceosome complex between archaics and modern humans by identifying variants in the 246 genes associated with the complex. We identified 1,866 variants that did not occur in 1KG. We ran these variants through the Ensembl Variant Effect Predictor (McLaren et al., 2016) using the GRCh37.p13 assembly and all default options.

4.9 Analysis

All data analyses were performed using Bash and Python scripts, some of which were implemented in Jupyter notebooks. We employed non-parametric tests to analyze data including Fisher's exact test, Kruskal-Wallis tests, Mann-Whitney U tests, and Spearman correlation, implemented with SciPy (Virtanen et al., 2020). Partial correlations were run using the Pigouin package, version 0.5.2 (Vallat, 2018). Some additional metrics were calculated using custom functions. All reported p-values are two-tailed.

4.10 Visualization

Results were visualized using Inkscape, version 1.1 (Inkscape Project, 2020) and ggplot, version 3.3.5 (Wickham, 2016) implemented in R, version 4.1.2 (R Core Team, 2020). Additional packages used to generate figures include complexupset, version 1.3.3 (Krassowski, 2020); cowplot, version 1.1.1; eulerr, version 6.1.1 (Larsson, 2021); reshape, version 0.8.8 (Wickham, 2007); and tidyverse, version 1.3.1 (Wickham et al., 2019).

4.11 Data availability

We used publicly available data for all analyses. Archaic InDel data are from the following repository: http://ftp.eva.mpg.de/neandertal/Vindija/VCF/indels/. Archaic SNV data are from the following repositories: Altai Neanderthal (http://ftp.eva.mpg.de/neandertal/Vindija/VCF/Altai/), Chagyrskaya (http://ftp.eva.mpg.de/neandertal/Chagyrskaya/VCF/), Denisova (http://ftp.eva.mpg.de/neandertal/Vindija/VCF/Denisova/), and Vindija (http://ftp.eva.mpg.de/neandertal/Vindija/VCF/Vindija33.19/). Modern human data are from the Thousand Genomes Project (http://hgdownload.soe.ucsc.edu/gbdb/hg38/1000Genomes/). Introgressed tag SNPs from Vernot et al., 2016 were retrieved from: https://drive.google.com/drive/folders/0B9Pc7_zItMCVM05rUmhDc0hkWmc?resourcekey=0-zwKyJGRuooD9bWPRZ0vBzQ. Introgressed variants from Browning et al., 2018 were retrieved from: https://data.mendeley.com/datasets/y7hyt83vxr/1. gnomAD data were retrieved from: https://storage.googleapis.com/gcp-public-data--gnomad/release/2.1.1/constraint/gnomad.v2.1.1.lof_metrics.by_gene.txt.bgz. phyloP data for the primate subset were retrieved from: http://hgdownload.soe.ucsc.edu/goldenPath/hg19/phyloP46way/primates.phyloP46way.bw. ASE variants were retrieved from: https://drive.google.com/file/d/10ebWfA-sboAL1SDplmIrvH-xK4x9iohV/view. TPM data were

retrieved from the Human Protein Atlas (https://www.proteinatlas.org/download/rna_tissue_gtex.tsv.zip). sQTL data were retrieved from GTEx, version 8 (https://storage.googleapis.com/gtex_analysis_v8/single_tissue_qtl_data/GTEx_Analysis_v8_sQTL.tar). Genes associated with the major spliceosome complex were retrieved from the HUGO Gene Nomenclature Committee (https://www.genenames.org/data/genegroup/#!/group/1518). The compiled dataset used in our analyses is available on Dryad (DOI: 10.7272/Q6H993F9).

4.12 Code availability

All code used to conduct analyses and generate figures is publicly available on GitHub (https://github.com/brandcm/Archaic_Splicing).

4.13 Acknowledgements

We thank Mary Lauren Benton for kindly sharing data on tissue specificity. Evonne McArthur and David Rinker provided comments that improved this manuscript. We also thank members of the Capra Lab for feedback on figures. This research greatly benefited from access to the Wynton high-performance compute cluster at UCSF. L.L.C. was funded by National Institutes of Health grant T32HG009495 to the University of Pennsylvania. J.A.C. and C.M.B. were funded by National Institutes of Health grant R35GM127087.

4.14 Author Contributions

Conceptualization, C.M.B, L.L.C, and J.A.C.; Formal Analysis, C.M.B and L.L.C; Writing – Original Draft, C.M.B, L.L.C, and J.A.C.; Writing – Review & Editing, C.M.B, L.L.C, and J.A.C.

4.15 Competing interests

The authors declare no competing interests.

References

Abadi, M. et al. 2015. *TensorFlow: Large-scale Machine Learning on Heterogeneous Systems*.

Andrés, A. M. et al. 2010. Balancing Selection Maintains a Form of ERAP2 That Undergoes Nonsense-Mediated Decay and Affects Antigen Presentation. *PLOS Genetics* 6: e1001157. DOI: 10.1371/journal.pgen.1001157.

Aqeilan, R. I. et al. 2008. The WWOX Tumor Suppressor Is Essential for Postnatal Survival and Normal Bone Metabolism *. *Journal of Biological Chemistry* 283: 21629–21639. DOI: 10.1074/jbc.M800855200.

Baralle, F. E. and Giudice, J. 2017. Alternative Splicing as a Regulator of Development and Tissue Identity. *Nature Reviews Molecular Cell Biology* 18: 437–451. DOI: 10.1038/nrm.2017.27.

Barbosa-Morais, N. L. et al. 2012. The Evolutionary Landscape of Alternative Splicing in Vertebrate Species. *Science* 338: 1587–1593. DOI: 10.1126/science.1230612.

Black, D. L. 2003. Mechanisms of Alternative Pre-Messenger RNA Splicing. *Annual Review of Biochemistry* 72: 291–336. DOI: 10.1146/annurev.biochem.72.121801.161720.

Blekhman, R. et al. 2010. Sex-Specific and Lineage-Specific Alternative Splicing in Primates. *Genome Research* 20: 180–189. DOI: 10.1101/gr.099226.109.

Brand, C. M., Colbran, L. L., and Capra, J. A. 2022. Predicting Archaic Hominins Phenotypes from Genomic Data. *Annual Review of Genomics and Human Genetics* In press.

Browning, S. R. et al. 2018. Analysis of Human Sequence Data Reveals Two Pulses of Archaic Denisovan Admixture. *Cell* 173: 53–61.e9. DOI: 10.1016/j.cell.2018.02.031.

Buniello, A. et al. 2019. The NHGRI-EBI GWAS Catalog of Published Genome-Wide Association Studies, Targeted Arrays and Summary Statistics 2019. *Nucleic Acids Research* 47: D1005–D1012. DOI: 10.1093/nar/gky1120.

Cáceres, J. F. and Kornblihtt, A. R. 2002. Alternative Splicing: Multiple Control Mechanisms and Involvement in Human Disease. *Trends in Genetics* 18: 186–193. DOI: 10.1016/S0168-9525(01)02626-9.

Castellano, S. et al. 2014. Patterns of Coding Variation in the Complete Exomes of Three Neandertals. *Proceedings of the National Academy of Sciences* 111: 6666. DOI: 10.1073/pnas.1405138111.

Chen, E. Y. et al. 2013. Enrichr: Interactive and Collaborative HTML5 Gene List Enrichment Analysis Tool. *BMC Bioinformatics* 14: 128. DOI: 10.1186/1471-2105-14-128.

Chen, L. et al. 2020. Identifying and Interpreting Apparent Neanderthal Ancestry in African Individuals. *Cell* 180: 677–687.e16. DOI: 10.1016/j.cell.2020.01.012.

Cheng, J. et al. 2019. MMSplice: Modular Modeling Improves the Predictions of Genetic Variant Effects on Splicing. *Genome Biology* 20: 48. DOI: 10.1186/s13059-019-1653-z.

Chollet, F. et al. 2015. *Keras*. https://github.com/fchollet/keras.

Colbran, L. L. et al. 2019. Inferred Divergent Gene Regulation in Archaic Hominins Reveals Potential Phenotypic Differences. *Nature Ecology & Evolution* 3: 1598–1606. DOI: 10.1038/s41559-019-0996-x.

Collins, L. and Penny, D. 2005. Complex Spliceosomal Organization Ancestral to Extant Eukaryotes. *Molecular Biology and Evolution* 22: 1053–1066. DOI: 10.1093/molbev/msi091.

Danis, D. et al. 2021. Interpretable Prioritization of Splice Variants in Diagnostic Next-Generation Sequencing. *bioRxiv*: 2021.01.28.428499. DOI: 10.1101/2021.01.28.428499.

Dannemann, M., Andrés, A. M., and Kelso, J. 2016. Introgression of Neandertal- and Denisovan-like Haplotypes Contributes to Adaptive Variation in Human Toll-like Receptors. *The American Journal of Human Genetics* 98: 22–33. DOI: 10.1016/j.ajhg.2015.11.015.

Faustino, N. A. and Cooper, T. A. 2003. Pre-mRNA Splicing and Human Disease. *Genes & Development* 17: 419–437. DOI: 10.1101/gad.1048803.

Ge, Y. and Porse, B. T. 2014. The Functional Consequences of Intron Retention: Alternative Splicing Coupled to NMD as a Regulator of Gene Expression. *BioEssays* 36: 236–243. DOI: 10.1002/bies.201300156.

Gokhman, D. et al. 2019. Reconstructing Denisovan Anatomy Using DNA Methylation Maps. *Cell* 179: 180–192.e10. DOI: 10.1016/j.cell.2019.08.035.

Graveley, B. R. 2001. Alternative Splicing: Increasing Diversity in the Proteomic World. *Trends in Genetics* 17: 100–107. DOI: 10.1016/S0168-9525(00)02176-4.

Harrow, J. et al. 2012. GENCODE: The Reference Human Genome Annotation for The ENCODE Project. *Genome Research* 22: 1760–1774. DOI: 10.1101/gr.135350.111.

Hinrichs, A. S. et al. 2006. The UCSC Genome Browser Database: Update 2006. *Nucleic Acids Research* 34: D590–D598. DOI: 10.1093/nar/gkj144.

Huerta-Sánchez, E. et al. 2014. Altitude Adaptation in Tibetans Caused by Introgression of Denisovan-like DNA. *Nature* 512: 194–197. DOI: 10.1038/nature13408.

Inkscape Project. 2020. *Inkscape*.

Jagadeesh, K. A. et al. 2019. S-CAP Extends Pathogenicity Prediction to Genetic Variants That Affect RNA Splicing. *Nature Genetics* 51: 755–763. DOI: 10.1038/s41588-019-0348-4.

Jaganathan, K. et al. 2019. Predicting Splicing from Primary Sequence with Deep Learning. *Cell* 176: 535–548.e24. DOI: 10.1016/j.cell.2018.12.015.

Jenkinson, G. et al. 2020. LeafCutterMD: An Algorithm for Outlier Splicing Detection in Rare Diseases. *Bioinformatics* 36: 4609–4615. DOI: 10.1093/bioinformatics/btaa259.

Jeong, C. et al. 2018. Detecting Past and Ongoing Natural Selection among Ethnically Tibetan Women at High Altitude in Nepal. *PLOS Genetics* 14: e1007650. DOI: 10.1371/journal.pgen.1007650.

Karczewski, K. J. et al. 2020. The Mutational Constraint Spectrum Quantified from Variation in 141,456 Humans. *Nature* 581: 434–443. DOI: 10.1038/s41586-020-2308-7.

Karlebach, G. et al. 2020. The Impact of Biological Sex on Alternative Splicing. *bioRxiv*: 490904. DOI: 10.1101/490904.

Köhler, S. et al. 2021. The Human Phenotype Ontology in 2021. *Nucleic Acids Research* 49: D1207–D1217. DOI: 10.1093/nar/gkaa1043.

Krassowski, M. 2020. *ComplexUpset*. DOI: 10.5281/zenodo.3700590.

Krawczak, M., Reiss, J., and Cooper, D. N. 1992. The Mutational Spectrum of Single Base-Pair Substitutions in mRNA Splice Junctions of Human Genes: Causes and Consequences. *Human Genetics* 90: 41–54. DOI: 10.1007/BF00210743.

Kriventseva, E. V. et al. 2003. Increase of Functional Diversity by Alternative Splicing. *Trends in Genetics* 19: 124–128. DOI: 10.1016/S0168-9525(03)00023-4.

Kuleshov, M. V. et al. 2016. Enrichr: A Comprehensive Gene Set Enrichment Analysis Web Server 2016 Update. *Nucleic Acids Research* 44: W90–W97. DOI: 10.1093/nar/gkw377.

Larsson, J. 2021. *eulerr: Area-proportional Euler and Venn Diagrams with Ellipses*. Manual.

Li, H. 2011. A Statistical Framework for SNP Calling, Mutation Discovery, Association Mapping and Population Genetical Parameter Estimation from Sequencing Data. *Bioinformatics* 27: 2987–2993. DOI: 10.1093/bioinformatics/btr509.

Li, X. et al. 2017. The Impact of Rare Variation on Gene Expression across Tissues. *Nature* 550: 239–243. DOI: 10.1038/nature24267.

Li, Y. I. et al. 2016. RNA Splicing Is a Primary Link between Genetic Variation and Disease. *Science* 352: 600–604. DOI: 10.1126/science.aad9417.

Lopez, A. J. 1998. Alternative Slicing of Pre-mRNA: Developmental Consequences and Mechanisms of Regulation. *Annual Review of Genetics* 32: 279–305. DOI: 10.1146/annurev.genet.32.1.279.

Lowy-Gallego, E. et al. 2019. Variant Calling on the GRCh38 Assembly with the Data from Phase Three of the 1000 Genomes Project [Version 2; Peer Review: 2 Approved]. *Wellcome Open Research* 4. DOI: 10.12688/wellcomeopenres.15126.2.

Mafessoni, F. et al. 2020. A High-Coverage Neandertal Genome from Chagyrskaya Cave. *Proceedings of the National Academy of Sciences* 117: 15132. DOI: 10.1073/pnas.2004944117.

Martin, A. R. et al. 2019. Clinical Use of Current Polygenic Risk Scores May Exacerbate Health Disparities. *Nature Genetics* 51: 584–591. DOI: 10.1038/s41588-019-0379-x.

McArthur, E., Rinker, D. C., and Capra, J. A. 2021. Quantifying the Contribution of Neanderthal Introgression to the Heritability of Complex Traits. *Nature Communications* 12: 4481. DOI: 10.1038/s41467-021-24582-y.

McArthur, E. et al. 2022. Reconstructing the 3D Genome Organization of Neanderthals Reveals That Chromatin Folding Shaped Phenotypic and Sequence Divergence. *bioRxiv*: 2022.02.07.479462. DOI: 10.1101/2022.02.07.479462.

McCoy, R. C., Wakefield, J., and Akey, J. M. 2017. Impacts of Neanderthal-Introgressed Sequences on the Landscape of Human Gene Expression. *Cell* 168: 916–927.e12. DOI: 10.1016/j.cell.2017.01.038.

McLaren, W. et al. 2016. The Ensembl Variant Effect Predictor. *Genome Biology* 17: 122. DOI: 10.1186/s13059-016-0974-4.

Mendez, F. L., Watkins, J. C., and Hammer, M. F. 2012. Global Genetic Variation at OAS1 Provides Evidence of Archaic Admixture in Melanesian Populations. *Molecular Biology and Evolution* 29: 1513–1520. DOI: 10.1093/molbev/msr301.

Merkin, J. et al. 2012. Evolutionary Dynamics of Gene and Isoform Regulation in Mammalian Tissues. *Science* 338: 1593–1599. DOI: 10.1126/science.1228186.

Mertes, C. et al. 2021. Detection of Aberrant Splicing Events in RNA-seq Data Using FRASER. *Nature Communications* 12: 529. DOI: 10.1038/s41467-020-20573-7.

Meyer, M. et al. 2012. A High-Coverage Genome Sequence from an Archaic Denisovan Individual. *Science* 338: 222. DOI: 10.1126/science.1224344.

Nissim-Rafinia, M. and Kerem, B. 2002. Splicing Regulation as a Potential Genetic Modifier. *Trends in Genetics* 18: 123–127. DOI: 10.1016/S0168-9525(01)02619-1.

Peng, Y. et al. 2017. Down-Regulation of EPAS1 Transcription and Genetic Adaptation of Tibetans to High-Altitude Hypoxia. *Molecular Biology and Evolution* 34: 818–830. DOI: 10.1093/molbev/msw280.

Petr, M. et al. 2019. Limits of Long-Term Selection against Neandertal Introgression. *Proceedings of the National Academy of Sciences* 116: 1639. DOI: 10.1073/pnas.1814338116.

Plagnol, V. and Wall, J. D. 2006. Possible Ancestral Structure in Human Populations. *PLOS Genetics* 2: e105. DOI: 10.1371/journal.pgen.0020105.

Pollard, K. S. et al. 2010. Detection of Nonneutral Substitution Rates on Mammalian Phylogenies. *Genome Research* 20: 110–121. DOI: 10.1101/gr.097857.109.

Prüfer, K. et al. 2014. The Complete Genome Sequence of a Neanderthal from the Altai Mountains. *Nature* 505: 43–49. DOI: 10.1038/nature12886.

Prüfer, K. et al. 2017. A High-Coverage Neandertal Genome from Vindija Cave in Croatia. *Science* 358: 655–658. DOI: 10.1126/science.aao1887.

R Core Team. 2020. *R: A Language and Environment for Statistical Computing*. R Foundation for Statistical Computing. Vienna, Austria.

Rinker, D. C. et al. 2020. Neanderthal Introgression Reintroduced Functional Ancestral Alleles Lost in Eurasian Populations. *Nature Ecology & Evolution* 4: 1332–1341. DOI: 10.1038/s41559-020-1261-z.

Rodenas-Cuadrado, P., Ho, J., and Vernes, S. C. 2014. Shining a Light on CNTNAP2: Complex Functions to Complex Disorders. *European Journal of Human Genetics* 22: 171–178. DOI: 10.1038/ejhg.2013.100.

Rogers, A. R., Harris, N. S., and Achenbach, A. A. 2020. Neanderthal-Denisovan Ancestors Interbred with a Distantly Related Hominin. *Science Advances* 6: eaay5483. DOI: 10.1126/sciadv.aay5483.

Rogers, T. F., Palmer, D. H., and Wright, A. E. 2021. Sex-Specific Selection Drives the Evolution of Alternative Splicing in Birds. *Molecular Biology and Evolution* 38: 519–530. DOI: 10.1093/molbev/msaa242.

Sams, A. J. et al. 2016. Adaptively Introgressed Neandertal Haplotype at the OAS Locus Functionally Impacts Innate Immune Responses in Humans. *Genome Biology* 17: 246. DOI: 10.1186/s13059-016-1098-6.

Saudemont, B. et al. 2017. The Fitness Cost of Mis-Splicing Is the Main Determinant of Alternative Splicing Patterns. *Genome Biology* 18: 208. DOI: 10.1186/s13059-017-1344-6.

Scotti, M. M. and Swanson, M. S. 2016. RNA Mis-Splicing in Disease. *Nature Reviews Genetics* 17: 19–32. DOI: 10.1038/nrg.2015.3.

Shiina, T. et al. 2009. The HLA Genomic Loci Map: Expression, Interaction, Diversity and Disease. *Journal of Human Genetics* 54: 15–39. DOI: 10.1038/jhg.2008.5.

Sibley, C. R., Blazquez, L., and Ule, J. 2016. Lessons from Non-Canonical Splicing. *Nature Reviews Genetics* 17: 407–421. DOI: 10.1038/nrg.2016.46.

Singh, P. and Ahi, E. P. 2022. The Importance of Alternative Splicing in Adaptive Evolution. *Molecular Ecology* n/a. DOI: 10.1111/mec.16377.

Smith, J. E. and Baker, K. E. 2015. Nonsense-Mediated RNA Decay – a Switch and Dial for Regulating Gene Expression. *BioEssays* 37: 612–623. DOI: 10.1002/bies.201500007.

Telis, N., Aguilar, R., and Harris, K. 2020. Selection against Archaic Hominin Genetic Variation in Regulatory Regions. *Nature Ecology & Evolution* 4: 1558–1566. DOI: 10.1038/s41559-020-01284-0.

Tweedie, S. et al. 2021. Genenames.Org: The HGNC and VGNC Resources in 2021. *Nucleic Acids Research* 49: D939–D946. DOI: 10.1093/nar/gkaa980.

Vallat, R. 2018. Pingouin: Statistics in Python. *The Journal of Open Source Software* 3: 1026.

Vernot, B. and Akey, J. M. 2014. Resurrecting Surviving Neandertal Lineages from Modern Human Genomes. *Science* 343: 1017–1021. DOI: 10.1126/science.1245938.

Vernot, B. et al. 2016. Excavating Neandertal and Denisovan DNA from the Genomes of Melanesian Individuals. *Science* 352: 235–239. DOI: 10.1126/science.aad9416.

Verta, J.-P. and Jacobs, A. 2022. The Role of Alternative Splicing in Adaptation and Evolution. *Trends in Ecology & Evolution* 37: 299–308. DOI: 10.1016/j.tree.2021.11.010.

Virtanen, P. et al. 2020. SciPy 1.0: Fundamental Algorithms for Scientific Computing in Python. *Nature Methods* 17: 261–272. DOI: 10.1038/s41592-019-0686-2.

Wang, G.-S. and Cooper, T. A. 2007. Splicing in Disease: Disruption of the Splicing Code and the Decoding Machinery. *Nature Reviews Genetics* 8: 749–761. DOI: 10.1038/nrg2164.

Wickham, H. 2007. Reshaping Data with the Reshape Package. *Journal of Statistical Software* 21.

— 2016. *Ggplot2: Elegant Graphics for Data Analysis*. New York: Springer-Verlag. ISBN: 978-3-319-24277-4.

Wickham, H. et al. 2019. Welcome to the Tidyverse. *Journal of Open Source Software* 4: 1686. DOI: 10.21105/joss.01686.

Wright, C. J., Smith, C. W. J., and Jiggins, C. D. 2022. Alternative Splicing as a Source of Phenotypic Diversity. *Nature Reviews Genetics*. DOI: 10.1038/s41576-022-00514-4.

Xie, Z. et al. 2021. Gene Set Knowledge Discovery with Enrichr. *Current Protocols* 1: e90. DOI: 10.1002/cpz1.90.

Zeng, T. and Li, Y. I. 2022. Predicting RNA Splicing from DNA Sequence Using Pangolin. *Genome Biology* 23: 103. DOI: 10.1186/s13059-022-02664-4.

Zhang, Y. et al. 2018. Discerning Novel Splice Junctions Derived from RNA-seq Alignment: A Deep Learning Approach. *BMC Genomics* 19: 971. DOI: 10.1186/s12864-018-5350-1.

5 Supplementary Information

5.1 Supplementary Text

5.1.1 The major spliceosome complex is strongly conserved between archaic hominins and modern humans.

Alternative splicing occurs across nearly all eukaryotes and its molecular mechanisms are deeply conserved (Collins and Penny, 2005). Thus, we anticipated that the sequence patterns learned by SpliceAI in humans would generalize to archaic hominins. To test for any significant differences, we first compared the sequences of 246 genes associated with the major spliceosome complex (Tweedie et al., 2021) between archaic hominins and modern humans. Analyzing all archaic variants absent in the 1000 Genomes Project (1KG) (Lowy-Gallego et al., 2019), we identified 19 non-synonymous archaic-specific variants, only 8 of which were predicted to be deleterious by SIFT and 5 possibly or probably damaging by PolyPhen 2 (McLaren et al., 2016; **File S1**). Additionally, only two variants were predicted to disrupt protein function by both PolyPhen and SIFT (**File S1**). Furthermore, among these archaic-specific variants, none were shared among all four individuals and many were Denisovan-specific. Therefore, the major spliceosome complex is nearly identical between archaic hominins and modern humans, and there is no evidence that the sequence determinants of splicing have diverged.

5.1.2 Physical characteristics of a gene are associated with the number of SAVs.

Alternative splicing requires genes have at least one intron and the extent of splice altering variants may further be related to gene length. We considered the relationship between the the number of splicing variants (N = 0 - 11) in each gene and three gene traits: 1) number of exons, 2) length of gene body, and 3) length of coding sequence. These characteristics were positively associated at both Δ thresholds (**Table S4**) (**Figure S6**). We also considered the relationship between the number of known isoforms per gene and the number of SAVs. We found a significant, positive association at both thresholds (**Table S4**). However, this relationship is likely driven by the number of exons. When we conducted a partial correlation, controlling for the number of exons, both associations were non-significant with minimal effect size ($\Delta \geq 0.2$: partial Spearman, ρ = -0.003, P = 0.702, $\Delta \geq 0.5$: partial Spearman, ρ = 0.0008, P = 0.9174).

5.1.3 Sprime identifies more introgressed SAVs present in all five 1KG superpopulations.

Similarly to Vernot et al., 2016, most ancient SAVs occurred at ≥ 0.05 frequency in all five 1KG superpopulations (**Figure S18**). The next most frequent were SAVs that were present in all but east Asians. SAVs shared among non-Africans and those present in all but Europeans were also common.

There were some differences between the datasets for introgressed SAVs. We found that among those introgressed SAVs classified per Vernot et al., 2016, many were shared among non-Africans (**Figure 5D**). However, introgressed SAVs classified per Browning et al., 2018 were most commonly present in both Africans and non-Africans, followed by a smaller set of non-African SAVs (**Figure S20**). This difference likely reflects low frequency introgressed

variants that are allowed to occur in the reference population in Sprime. While introgression between modern humans and archaics occurred outside of Africa, many Africans have Neanderthal ancestry due to backflow from Eurasians into Africans (Chen et al., 2020). Among non-African subsets, both datasets were largely similar in their distribution (**Figure S20**, **Figure S21**).

5.2 Supplementary Files

File S1. This file is the variant effect predictor (VEP) output from Ensembl for 1,866 archaic-specific variants in genes associated with the major spliceosome complex.

File S2. This file contains the outputs from the gene ontology analysis for GWAS Catalog 2019 and Human Phenotype Ontology terms.

5.3 Supplemental Figures

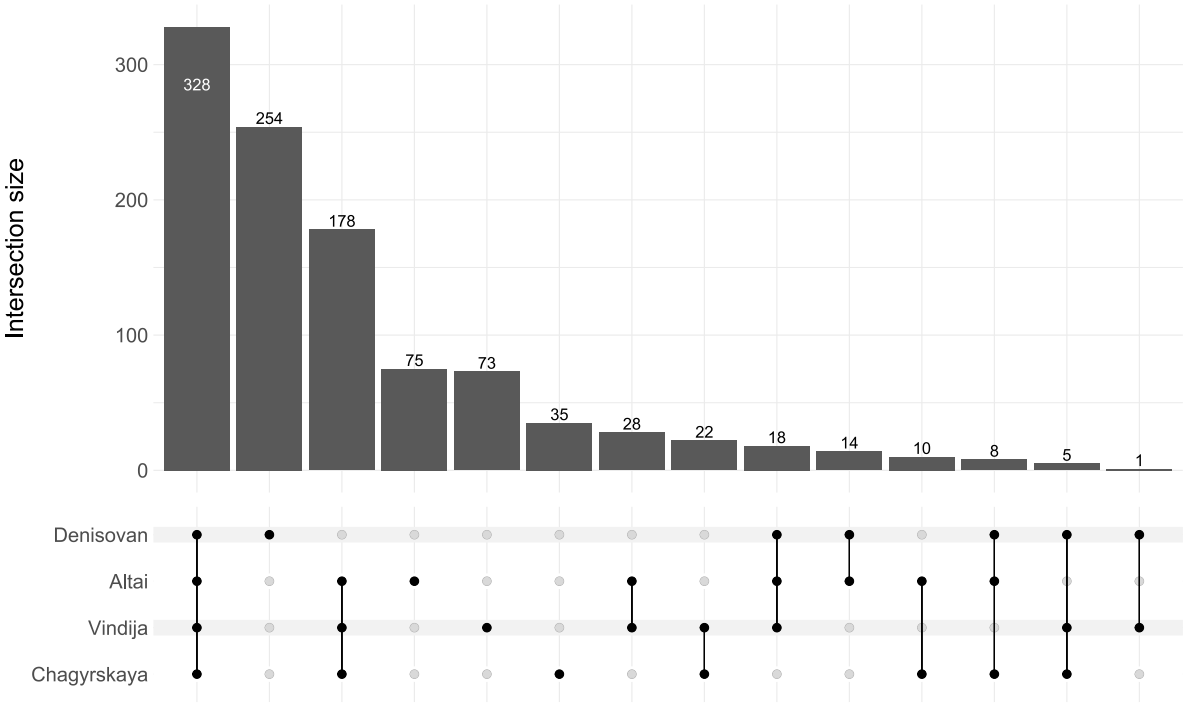

Figure S1: The distribution of SAVs is consistent with the archaic hominin phylogeny. Unique and shared SAVs at $\Delta \geq 0.5$.

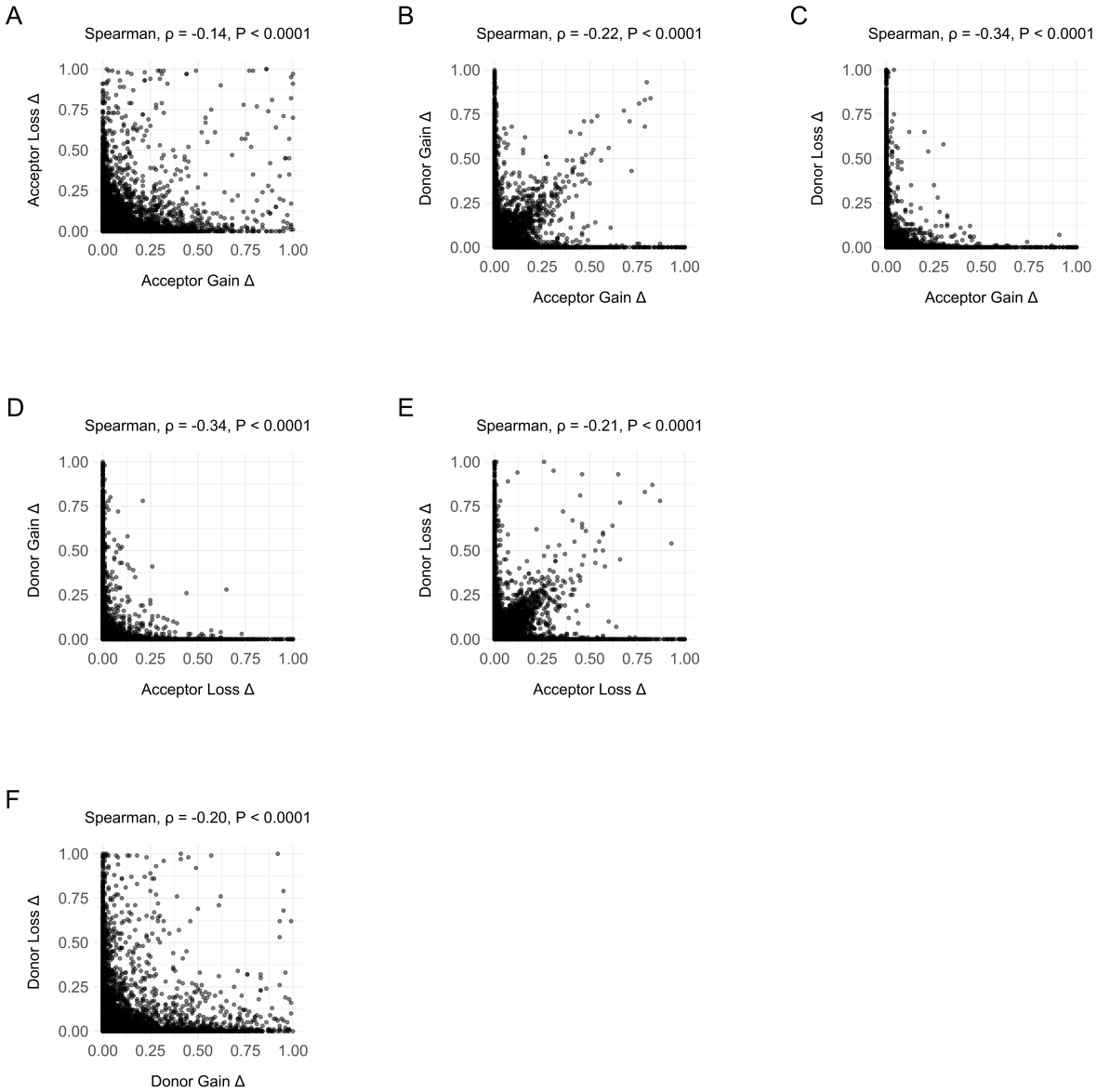

Figure S2: Delta scores between classes are negatively associated.
(A) Association between acceptor gain Δs and acceptor loss Δs for all variants with at least one $\Delta > 0$. **(B)** Association between acceptor gain Δs and donor gain Δs for all variants with at least one $\Delta > 0$. **(C)** Association between acceptor gain Δs and donor loss Δs for all variants with at least one $\Delta > 0$. **(D)** Association between acceptor loss Δs and donor gain Δs for all variants with at least one $\Delta > 0$. **(E)** Association between acceptor loss Δs and donor loss Δs for all variants with at least one $\Delta > 0$. **(F)** Association between donor gain Δs and donor loss Δs for all variants with at least one $\Delta > 0$.

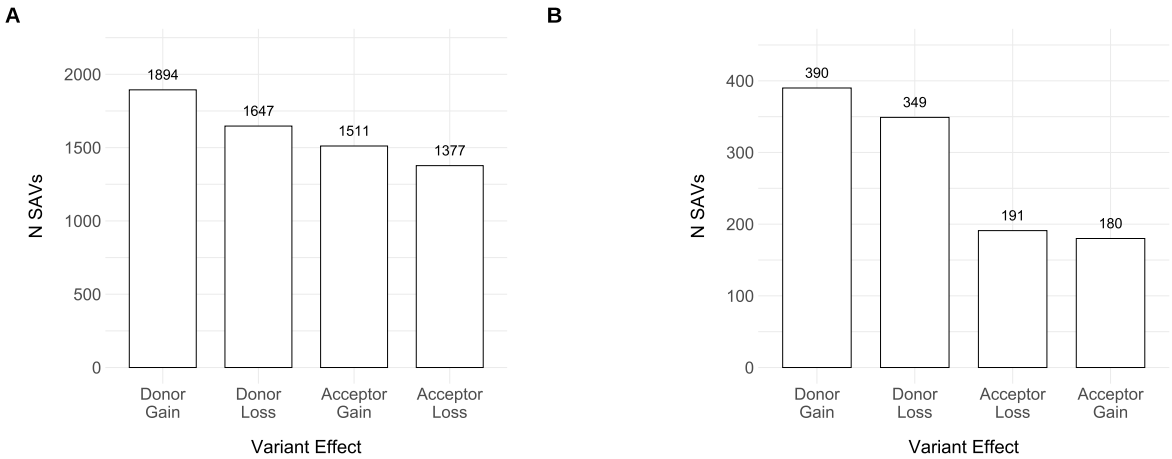

Figure S3: SAVs most commonly result in a donor gain.
(A) The distribution of variant effects for all variants at the $\Delta \geq 0.2$ threshold. Some variants result in multiple effects; therefore, the sum of these classes $\neq$ 5,950. **(B)** The distribution of variant effects for all variants at the $\Delta \geq 0.5$ threshold. Some variants result in multiple effects; therefore, the sum of these classes $\neq$ 1,049.

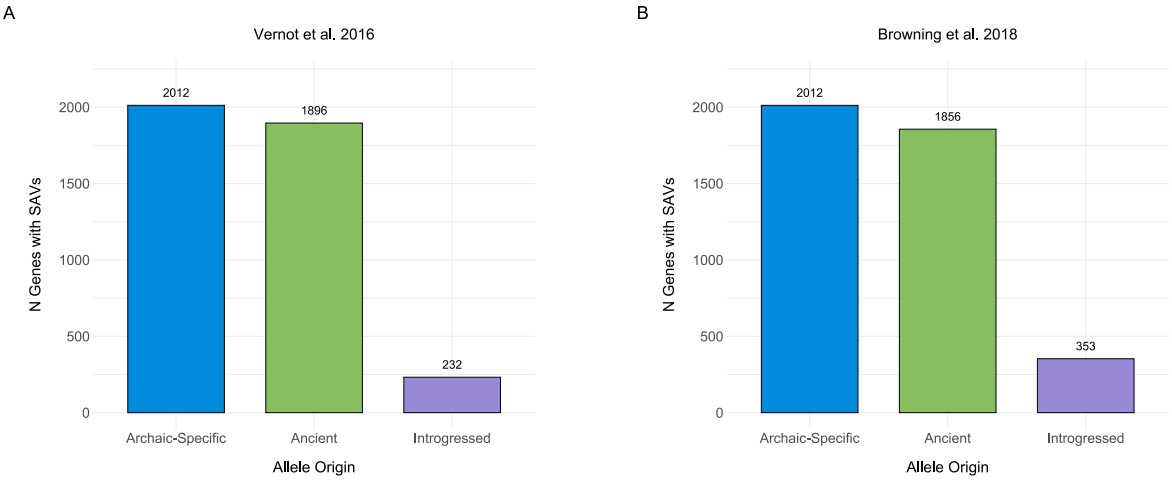

Figure S4: N genes with SAVs by allele origin.
(A) The number of genes encompassed by each SAV allele origin per Browning et al., 2018 at $\Delta \geq 0.2$. Some genes may occur in multiple categories **(B)** The number of genes encompassed by each SAV allele origin per Vernot et al., 2016 at $\Delta \geq 0.2$. Some genes may occur in multiple categories.

A

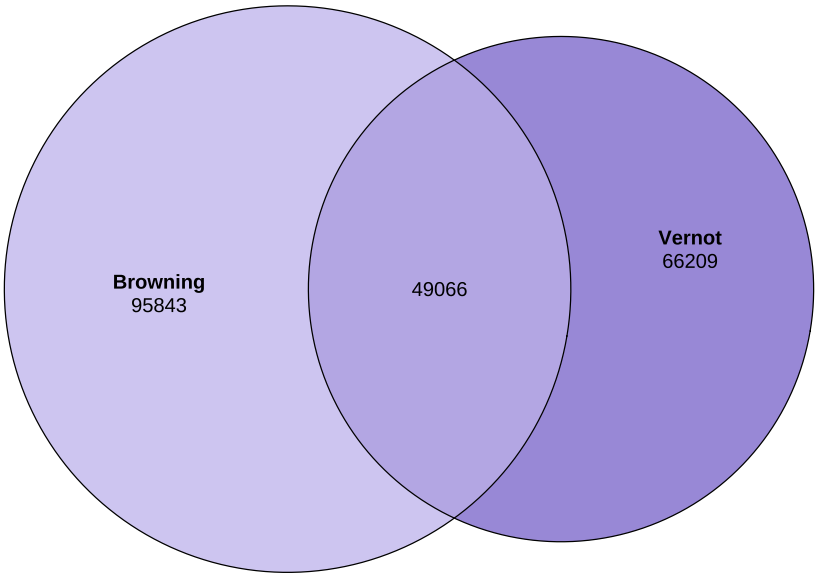

B

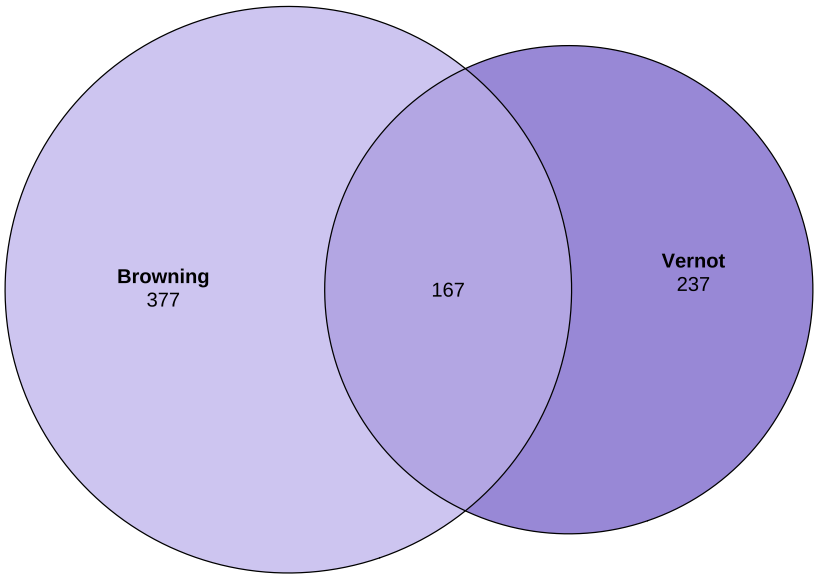

Figure S5: Two different sets of introgressed variants modestly overlap.
(A) The overlap between introgressed variants from Browning et al., 2018 and Vernot et al., 2016 that match a quality filtered locus in this study and are present in Thousand Genomes. **(B)** A subset of the overlap for variants with $\Delta \geq 0.2$.

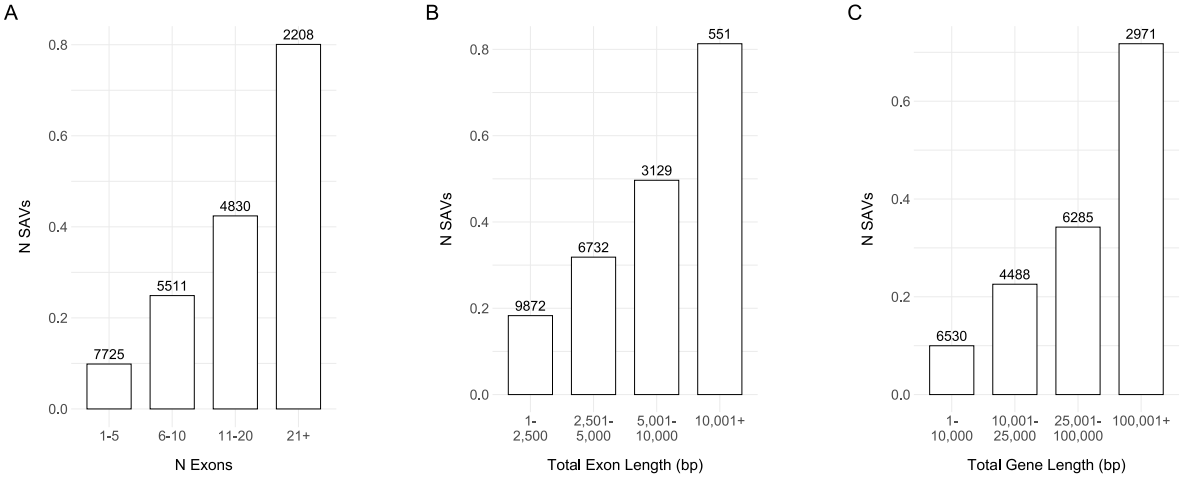

Figure S6: The number of exons and gene length are associated with more SAVs.
(A) Binned number of exons and the mean number of SAVs at $\Delta \geq 0.2$ per bin. N reflects the number of genes per bin. **(B)** Binned exon length in bp and the mean number of SAVs at $\Delta \geq 0.2$ per bin. N reflects the number of genes per bin. **(C)** Binned gene length in bp and the mean number of SAVs at $\Delta \geq 0.2$ per bin. N reflects the number of genes per bin.

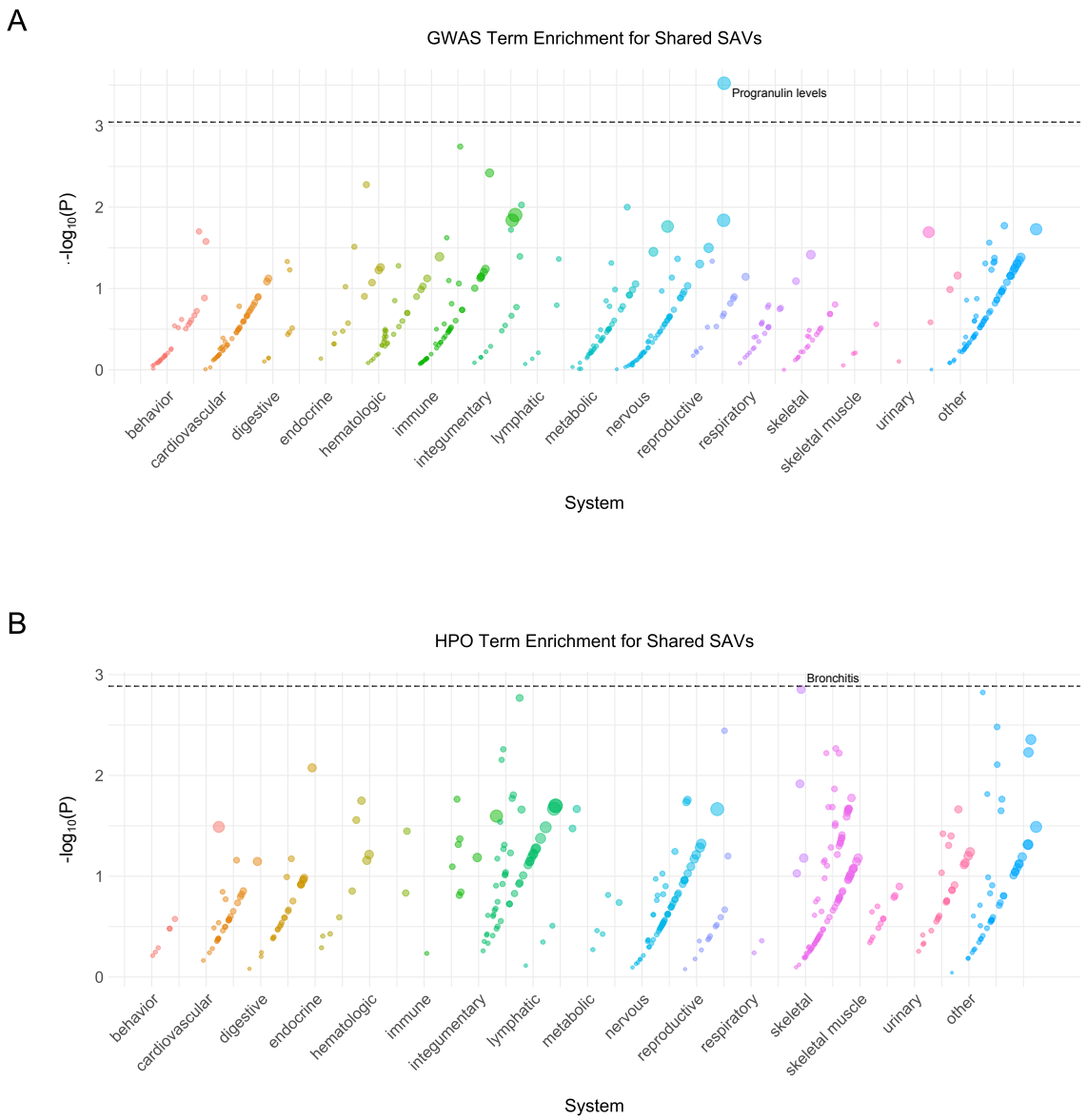

Figure S7: Shared phenotype enrichment.
(A) Phenotype associations enriched among genes with archaic-specific shared SAVs based on annotations the from GWAS Catalog. Phenotypes are ordered by increasing enrichment within manually curated systems. Circle size indicates enrichment magnitude. Enrichment and p-values were calculated from an empirical null distribution generated from 10,000 shuffles of maximum Δ across the entire dataset (Methods). Dotted and dashed lines represent false discovery rate (FDR) corrected p-value thresholds at FDR = 0.05 and 0.1, respectively. At least one example phenotype with a p-value $\leq$ the stricter FDR threshold (0.05) is annotated per system. **(B)** Phenotypes enriched among genes with archaic-specific shared SAVs based on annotations from the Human Phenotype Ontology (HPO). Data were generated and visualized as in **A**. See **File S2** for all phenotype enrichment results.

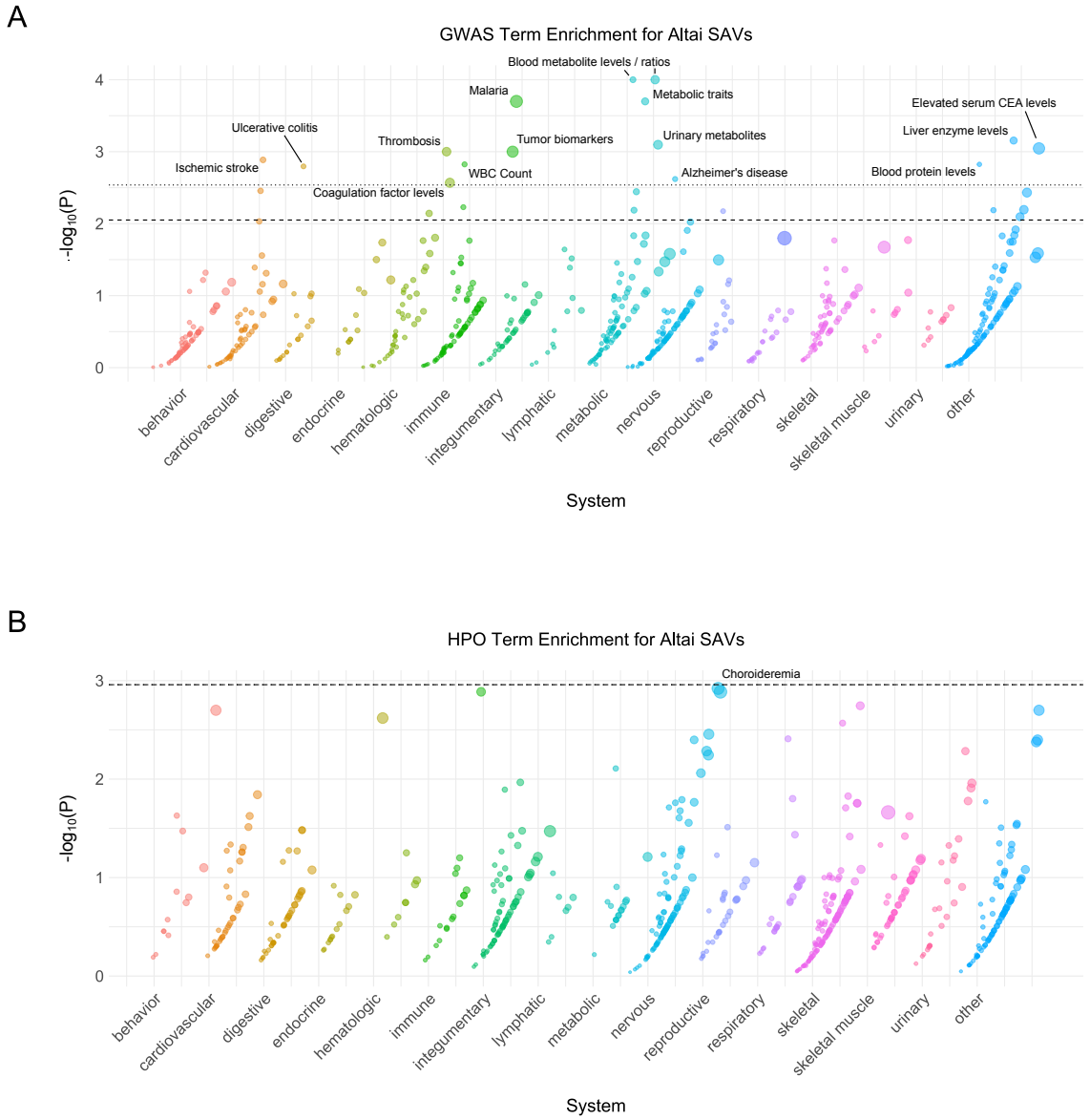

Figure S8: Altai phenotype enrichment.
(A) Phenotype associations enriched among genes with archaic-specific Altai SAVs based on annotations the from GWAS Catalog. Phenotypes are ordered by increasing enrichment within manually curated systems. Circle size indicates enrichment magnitude. Enrichment and p-values were calculated from an empirical null distribution generated from 10,000 shuffles of maximum Δ across the entire dataset (Methods). Dotted and dashed lines represent false discovery rate (FDR) corrected p-value thresholds at FDR = 0.05 and 0.1, respectively. At least one example phenotype with a p-value $\leq$ the stricter FDR threshold (0.05) is annotated per system. **(B)** Phenotypes enriched among genes with archaic-specific Altai SAVs based on annotations from the Human Phenotype Ontology (HPO). Data were generated and visualized as in **A**. See **File S2** for all phenotype enrichment results.

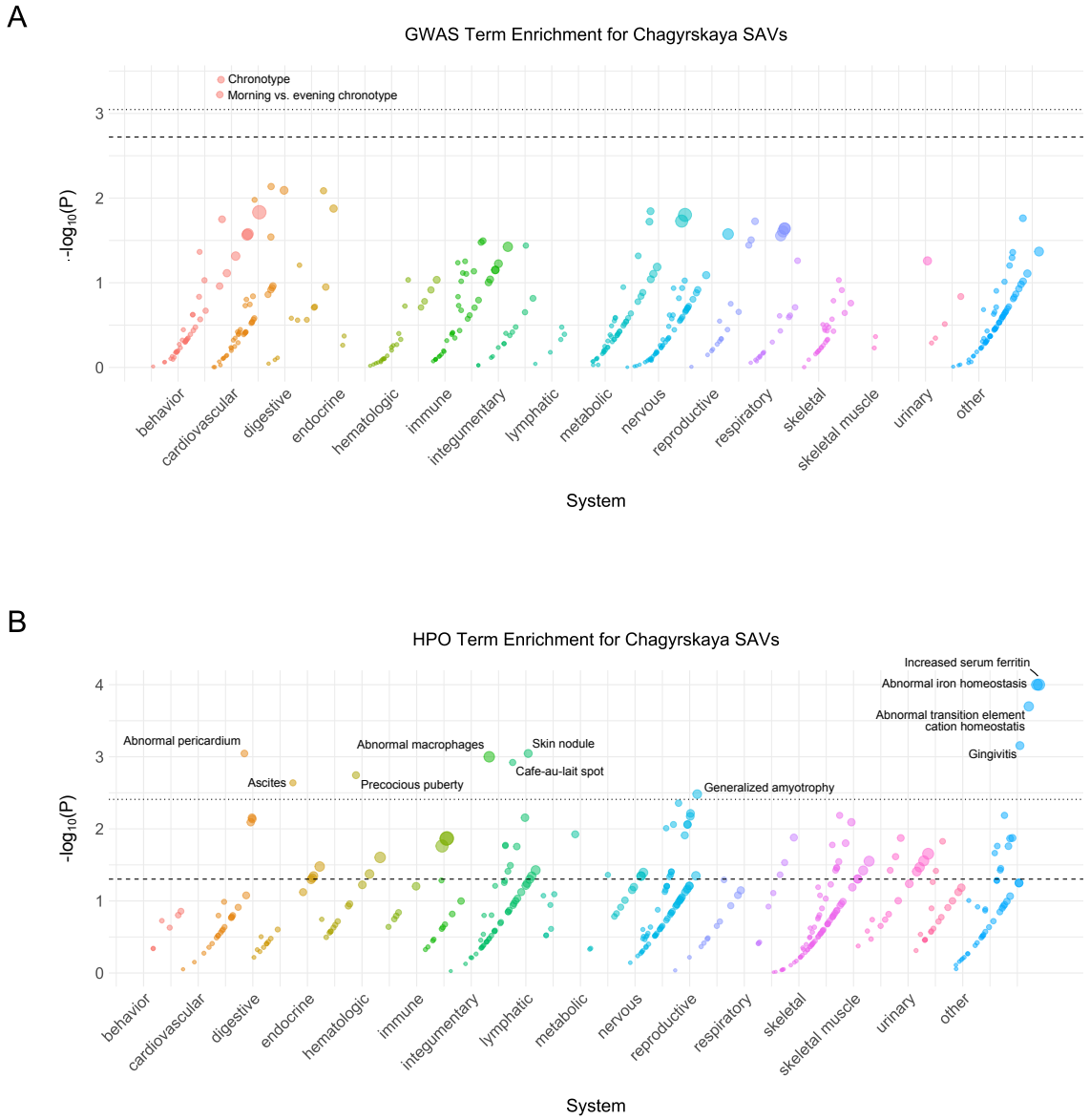

Figure S9: Chagyrskaya phenotype enrichment.
(A) Phenotype associations enriched among genes with archaic-specific Chagyrskaya SAVs based on annotations the from GWAS Catalog. Phenotypes are ordered by increasing enrichment within manually curated systems. Circle size indicates enrichment magnitude. Enrichment and p-values were calculated from an empirical null distribution generated from 10,000 shuffles of maximum Δ across the entire dataset (Methods). Dotted and dashed lines represent false discovery rate (FDR) corrected p-value thresholds at FDR = 0.05 and 0.1, respectively. At least one example phenotype with a p-value $\leq$ the stricter FDR threshold (0.05) is annotated per system. **(B)** Phenotypes enriched among genes with archaic-specific Chagyrskaya SAVs based on annotations from the Human Phenotype Ontology (HPO). Data were generated and visualized as in **A**. See **File S2** for all phenotype enrichment results.

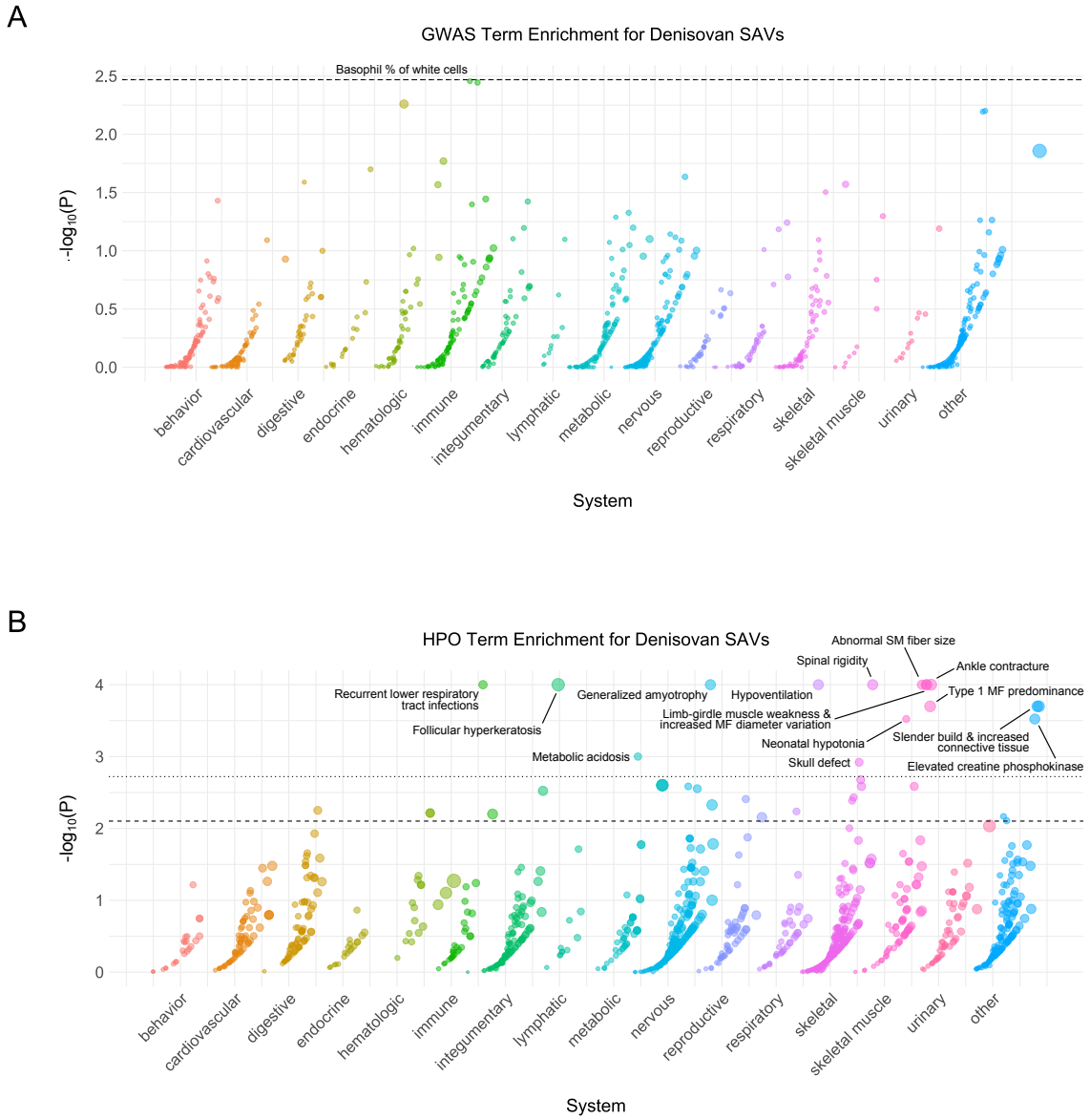

Figure S10: Denisovan phenotype enrichment.
(A) Phenotype associations enriched among genes with archaic-specific Denisovan SAVs based on annotations the from GWAS Catalog. Phenotypes are ordered by increasing enrichment within manually curated systems. Circle size indicates enrichment magnitude. Enrichment and p-values were calculated from an empirical null distribution generated from 10,000 shuffles of maximum Δ across the entire dataset (Methods). Dotted and dashed lines represent false discovery rate (FDR) corrected p-value thresholds at FDR = 0.05 and 0.1, respectively. At least one example phenotype with a p-value $\leq$ the stricter FDR threshold (0.05) is annotated per system. **(B)** Phenotypes enriched among genes with archaic-specific Denisovan SAVs based on annotations from the Human Phenotype Ontology (HPO). Data were generated and visualized as in **A**. See **File S2** for all phenotype enrichment results.

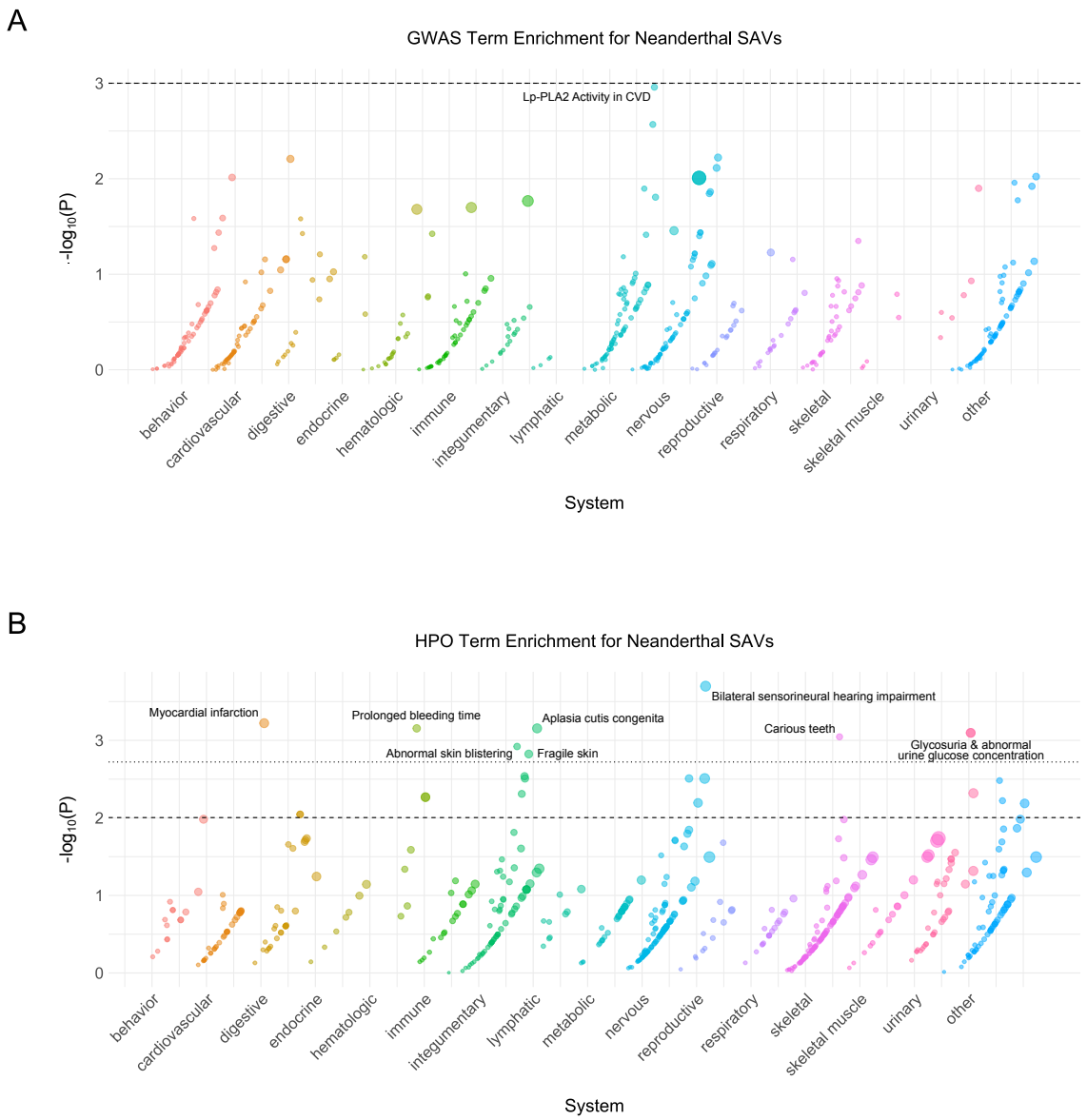

Figure S11: Neanderthal phenotype enrichment.
(A) Phenotype associations enriched among genes with archaic-specific Neanderthal SAVs based on annotations the from GWAS Catalog. Phenotypes are ordered by increasing enrichment within manually curated systems. Circle size indicates enrichment magnitude. Enrichment and p-values were calculated from an empirical null distribution generated from 10,000 shuffles of maximum Δ across the entire dataset (Methods). Dotted and dashed lines represent false discovery rate (FDR) corrected p-value thresholds at FDR = 0.05 and 0.1, respectively. At least one example phenotype with a p-value $\leq$ the stricter FDR threshold (0.05) is annotated per system. **(B)** Phenotypes enriched among genes with archaic-specific Neanderthal SAVs based on annotations from the Human Phenotype Ontology (HPO). Data were generated and visualized as in **A**. See **File S2** for all phenotype enrichment results.

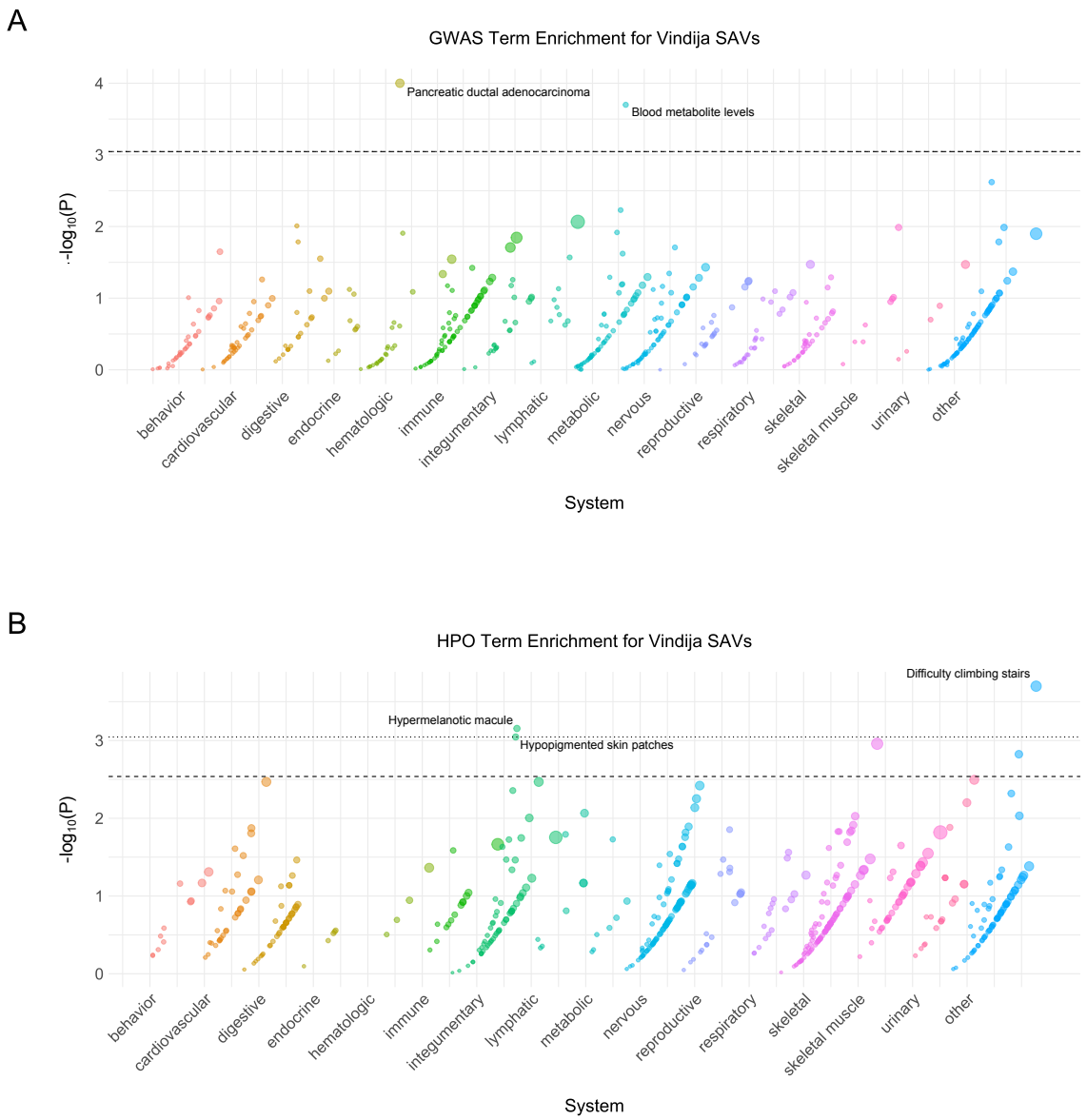

Figure S12: Vindija phenotype enrichment.
(A) Phenotype associations enriched among genes with archaic-specific Vindija SAVs based on annotations the from GWAS Catalog. Phenotypes are ordered by increasing enrichment within manually curated systems. Circle size indicates enrichment magnitude. Enrichment and p-values were calculated from an empirical null distribution generated from 10,000 shuffles of maximum Δ across the entire dataset (Methods). Dotted and dashed lines represent false discovery rate (FDR) corrected p-value thresholds at FDR = 0.05 and 0.1, respectively. At least one example phenotype with a p-value $\leq$ the stricter FDR threshold (0.05) is annotated per system. **(B)** Phenotypes enriched among genes with archaic-specific Vindija SAVs based on annotations from the Human Phenotype Ontology (HPO). Data were generated and visualized as in **A**. See **File S2** for all phenotype enrichment results.

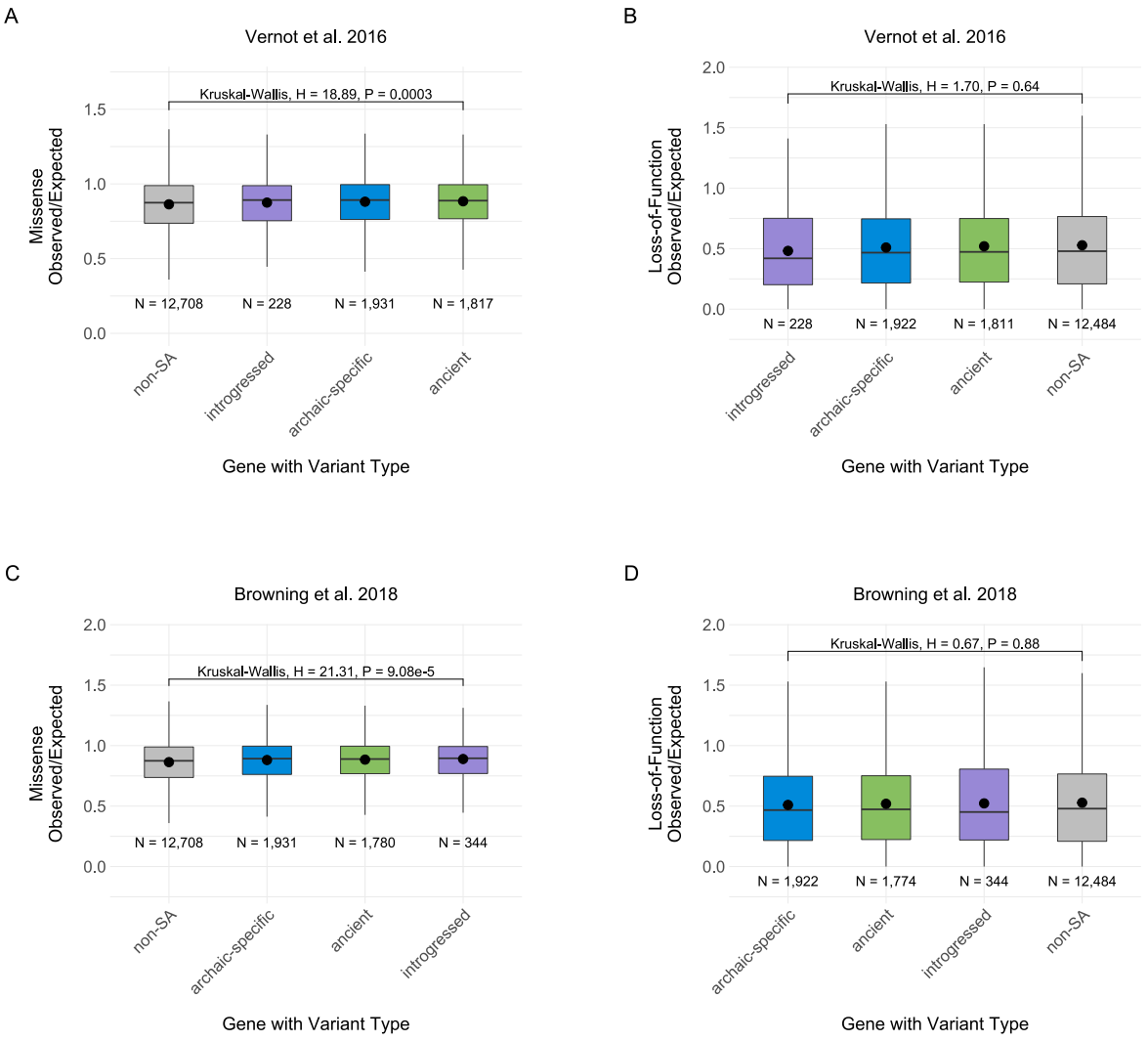

Figure S13: Gene mutational tolerance does not constrain the evolutionary history of SAVs.
(A) Observed over expected ratio for missense variants per gene from gnomAD among four different sets. The ancient, archaic-specific, and introgressed sets from Browning et al., 2018 include any gene that had $\geq$ 1 SAV at the $\Delta \geq 0.2$ threshold. Non-SA genes are all genes that do not occur in any of the other three sets. Boxplots indicate the first quantile, median, and third quantile and the mean is noted by the black point. Ns reflect the number of variants per set. **(B)** Observed over expected ratio for loss-of-function variants per gene from gnomAD among four different sets from Browning et al., 2018. The ancient, archaic-specific, and introgressed sets include any gene that had $\geq$ 1 SAV at the $\Delta \geq 0.2$ threshold. Non-SA genes are all genes that do not occur in any of the other three sets. Boxplots indicate the first quantile, median, and third quantile and the mean is noted by the black point. Ns reflect the number of variants per set. **(C)** Observed over expected ratio for missense variants per gene from gnomAD among four different sets from Vernot et al., 2016. **(D)** Observed over expected ratio for loss-of-function variants per gene from gnomAD among four different sets from Vernot et al., 2016.

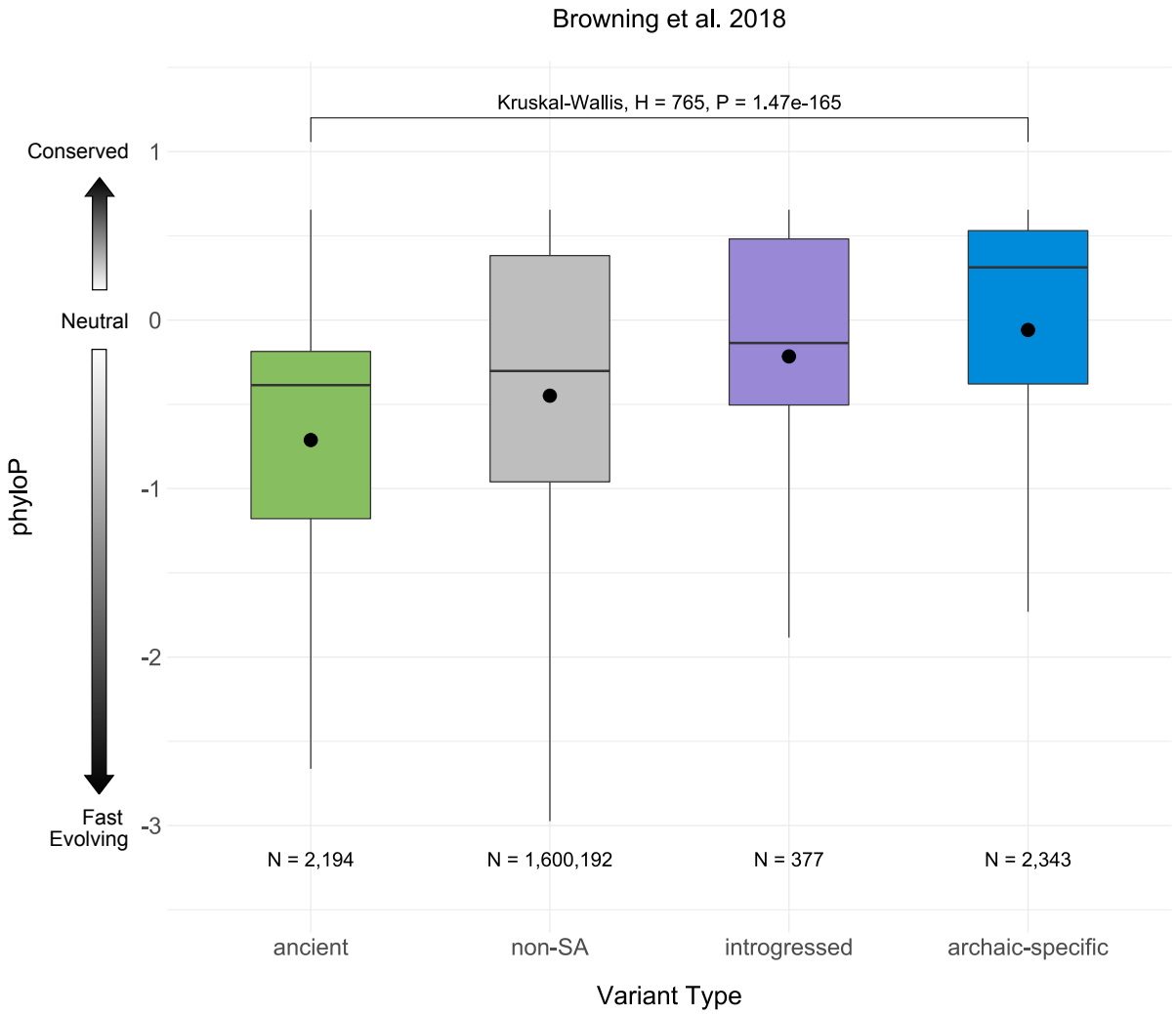

Figure S14: Site-level evolutionary conservation varies across SAVs with different origins. phyloP evolutionary conservation score distributions for archaic SAVs of different origins and non-SAVs. Positive scores indicate substitution rates slower than expected under neutral evolution (conservation), while negative scores indicate higher substitution rates than expected (fast evolution). The boxplots give the first quantile, median, and third quantile of the distributions, and the mean is noted by the black point. Ns are the number of variants per set. SAV classifications were based on Browning et al., 2018 introgression calls.

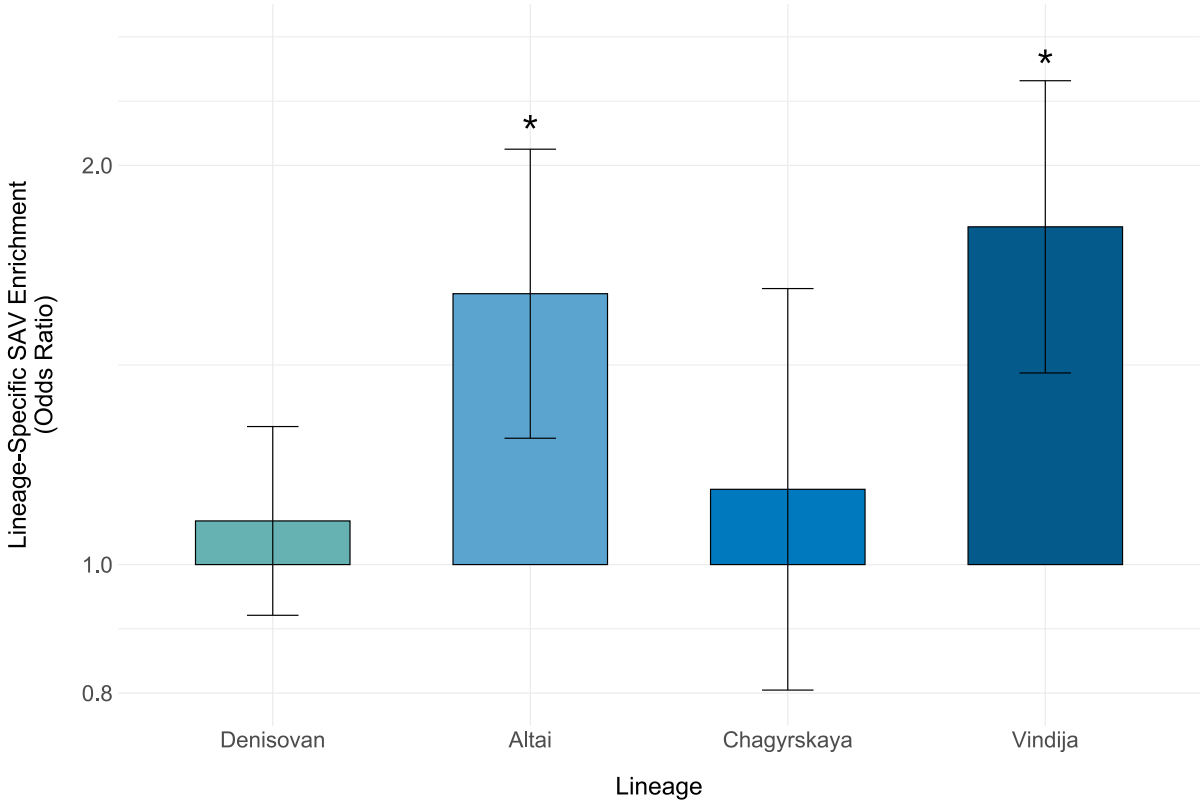

Figure S15: Lineage-specific high-confidence SAVs are enriched in two Neanderthals. Odds ratios from Fisher's exact test performed for each lineage's unique high confidence SAVs/non-SAVs compared to those shared among all four individuals. The number of variants used in each enrichment test are listed in **Table S6**. Asterisks reflect significance using a Bonferroni corrected α (0.0125). Error bars denote the 95% CI. Note the y-axis is $\log_{10}$ transformed.

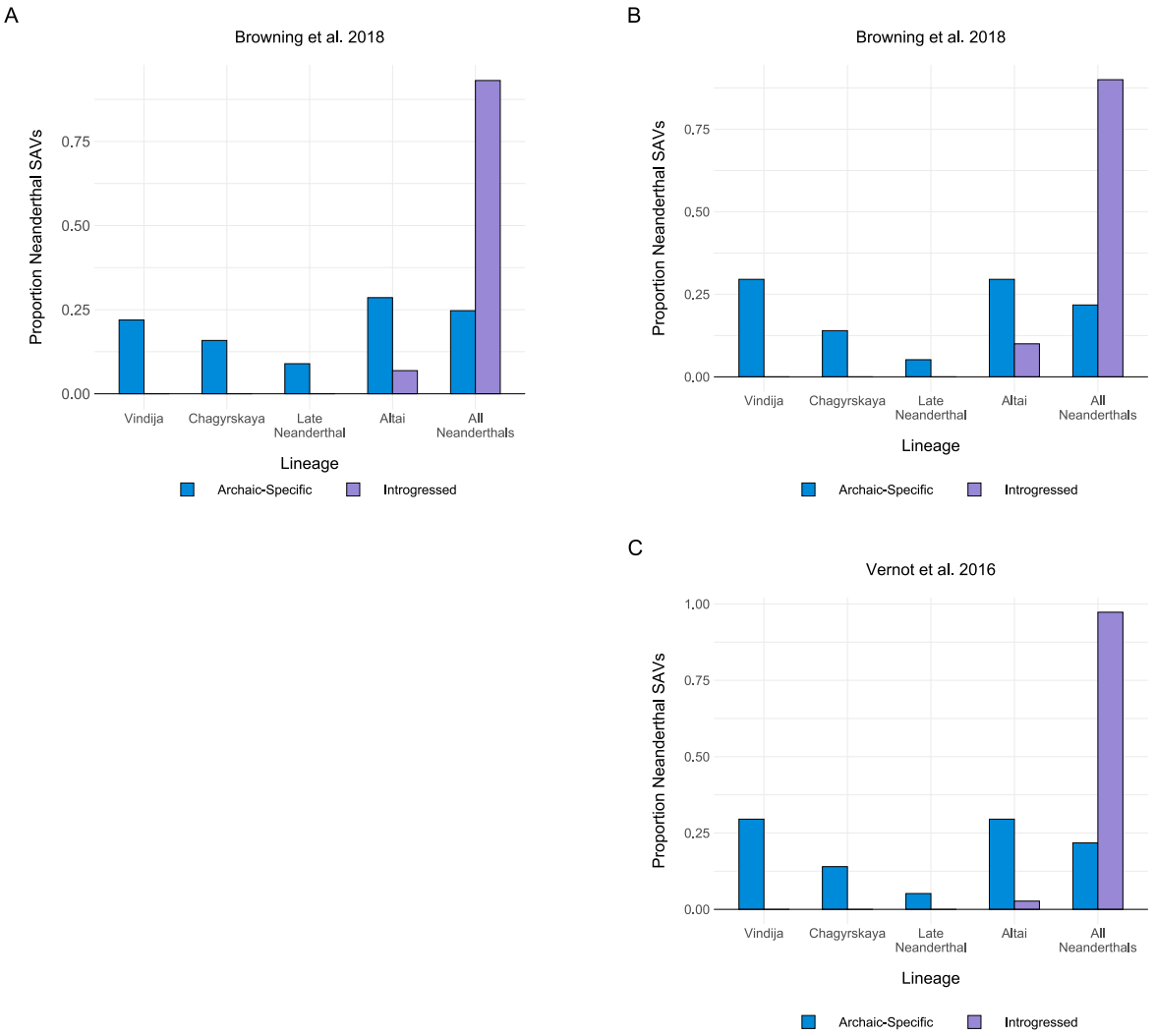

Figure S16: Introgressed SAVs are largely older variants.
(A) Proportion of SAVs at $\Delta \geq 0.2$ per Neanderthal lineage among archaic-specific SAVs (expected) and introgressed SAVs (observed) from Browning et al., 2018. Proportions were calculated from the sum of all Neanderthal lineages because power to detect introgressed Denisovan SAVs is low. All data are presented in **Table S7**. **(B)** Proportion of SAVs at $\Delta \geq 0.5$ using introgressed SAVs from Browning et al., 2018. **(C)** Proportion of SAVs at $\Delta \geq 0.5$ using introgressed SAVs from Vernot et al., 2016.

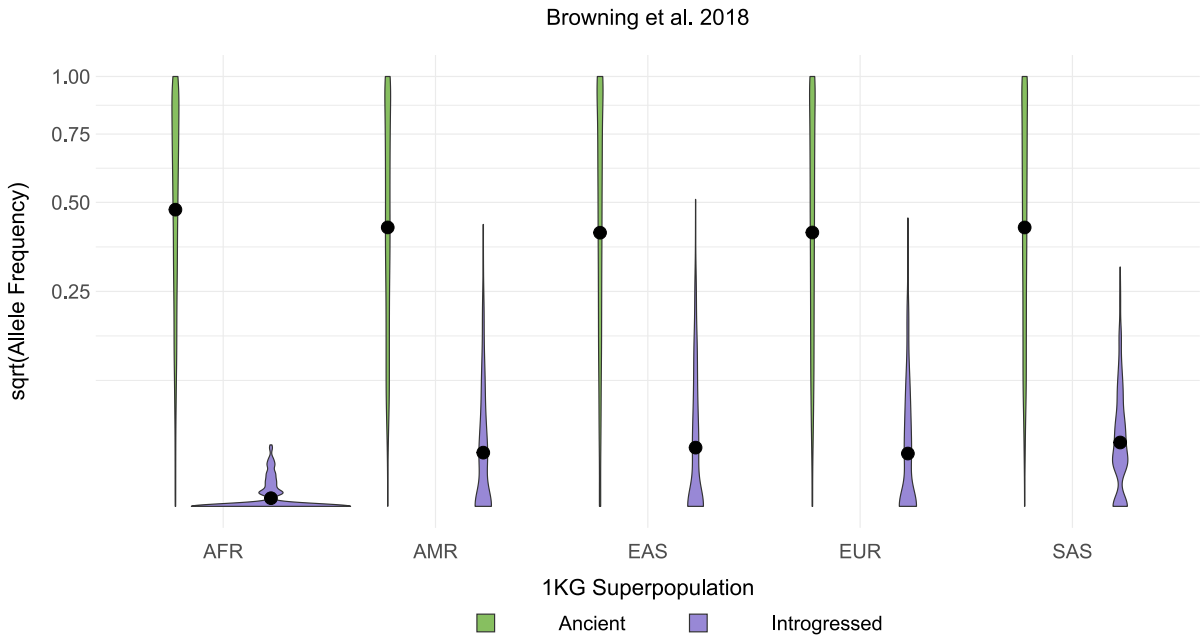

Figure S17: Ancient SAVs occur a moderate to high frequencies, whereas introgressed SAVs occur at lower frequencies. Allele frequency distributions for SAVs at $\Delta \geq 0.2$ per Browning et al., 2018 by 1KG superpopulation. Allele frequencies are from 1KG. If the introgressed allele was the reference allele, we subtracted the 1KG allele frequency from 1. The black dot represents the mean allele frequency. Note the y-axis is square root transformed.

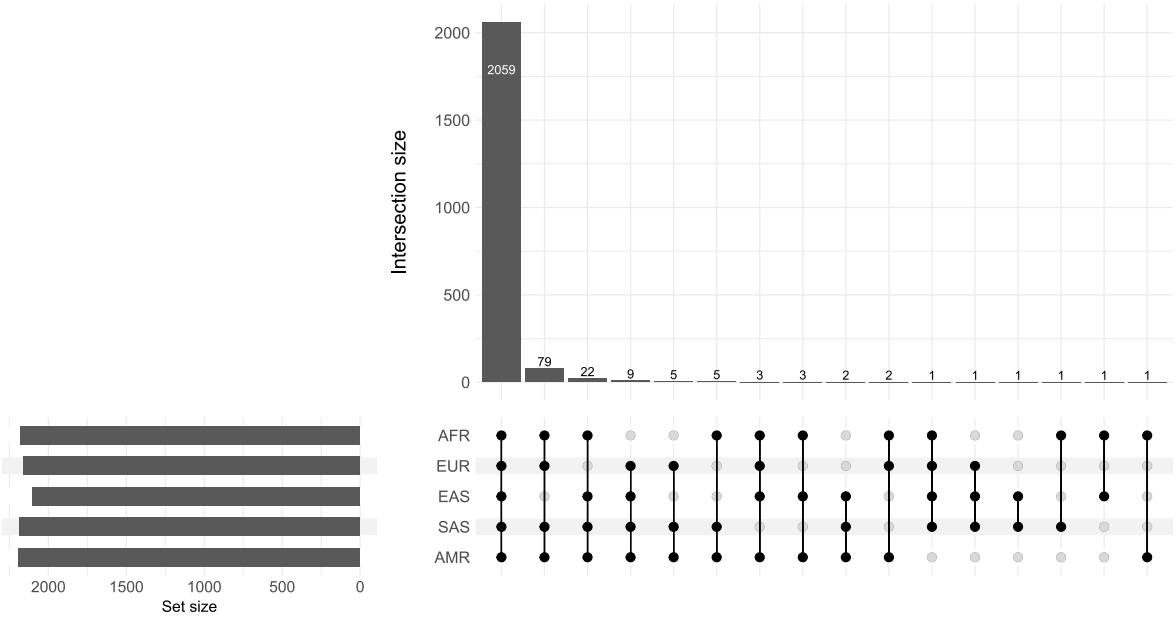

Figure S18: Most ancient SAVs occur in all 1KG superpopulations. Unique and shared ancient SAVs per Browning et al., 2018 at $\Delta \geq 0.2$. Allele frequencies are from 1KG. By definition, each ancient SAV was considered present in a population if the allele frequency was ≥ 0.05 for at least two superpopulations. AFR = African, AMR = American, EAS = East Asian, EUR = European, SAS = South Asian.

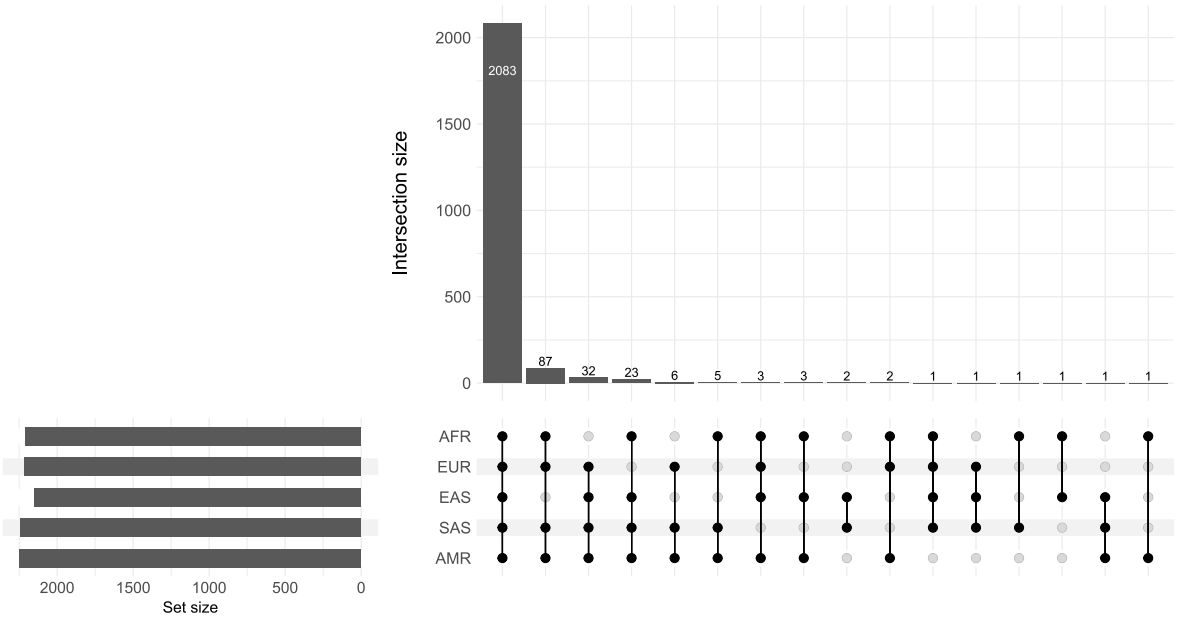

Figure S19: Most ancient SAVs occur in all 1KG superpopulations. Unique and shared ancient SAVs per Vernot et al., 2016 at $\Delta \geq 0.2$. Allele frequencies are from 1KG. By definition, each ancient SAV was considered present in a population if the allele frequency was ≥ 0.05 for at least two superpopulations. AFR = African, AMR = American, EAS = East Asian, EUR = European, SAS = South Asian.

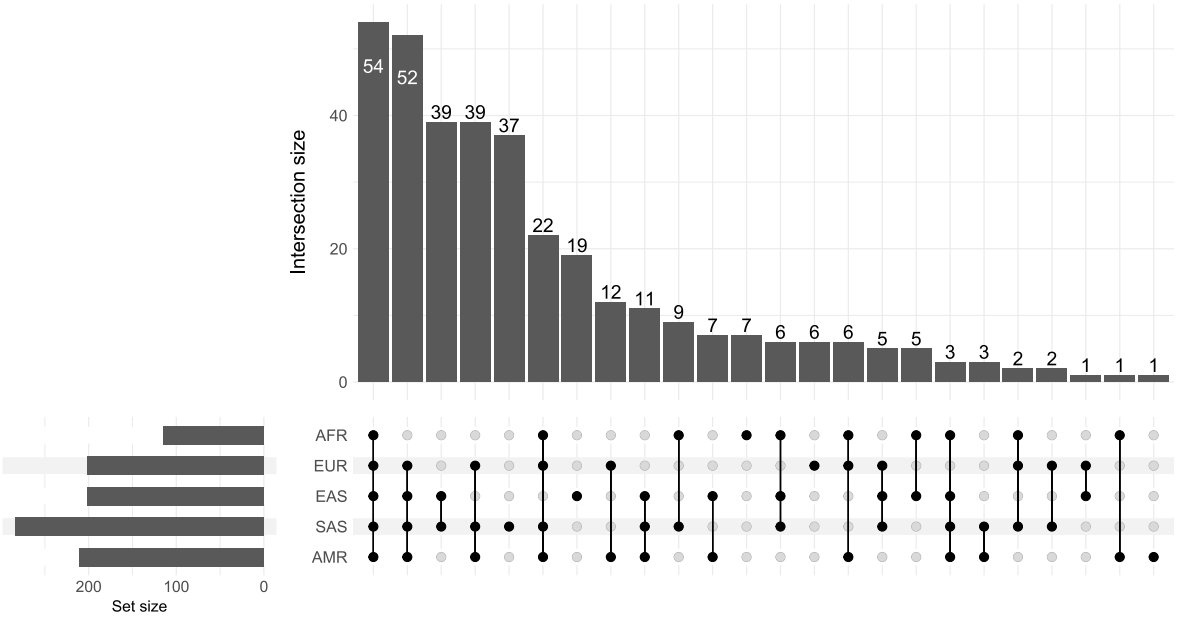

Figure S20: Many introgressed SAVs occur in multiple 1KG superpopulations. Unique and shared introgressed SAVs per Browning et al., 2018 at $\Delta \geq 0.2$. Allele frequencies are from 1KG. If the introgressed allele was the reference allele, we subtracted the 1KG allele frequency from 1. Each SAV was considered present in a population if the allele frequency was > 0.01 (N = 349). The remaining 28 variants occurred at ≤ 0.01 allele frequency. AFR = African, AMR = American, EAS = East Asian, EUR = European, SAS = South Asian.

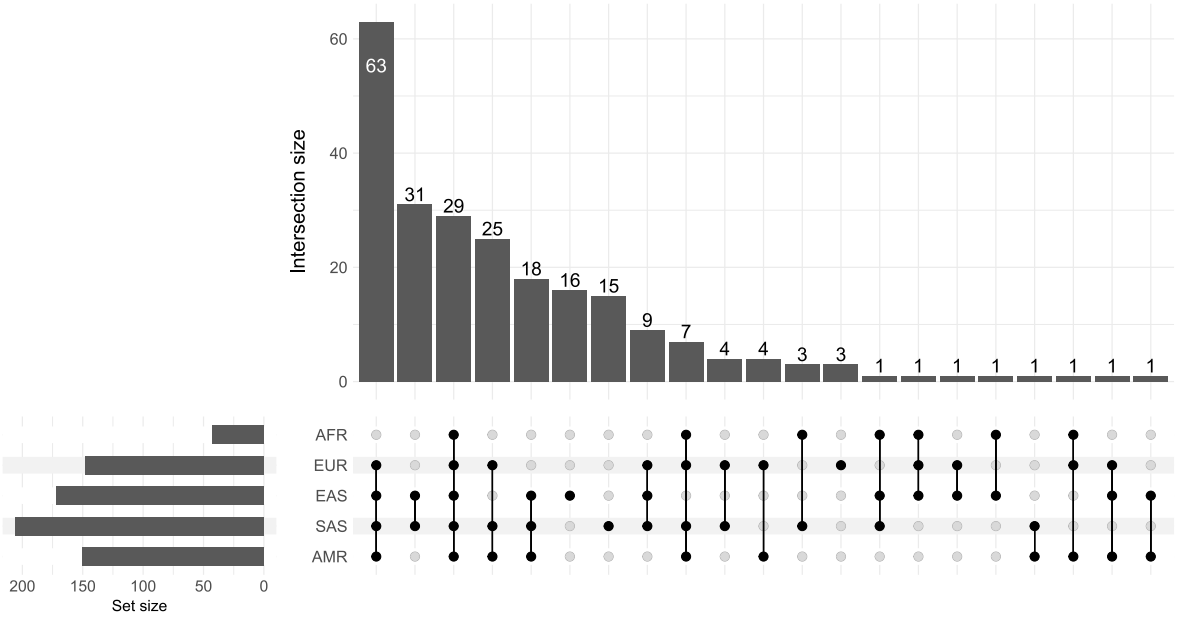

Figure S21: Many introgressed SAVs occur in multiple 1KG superpopulations. Unique and shared introgressed SAVs per Vernot et al., 2016 at $\Delta \geq 0.2$. Allele frequencies are from the Vernot et al., 2016 metadata. Each SAV was considered present in a population if the allele frequency was > 0.01 (N = 203). The remaining 34 variants occurred at ≤ 0.01 allele frequency. AFR = African, AMR = American, EAS = East Asian, EUR = European, SAS = South Asian.

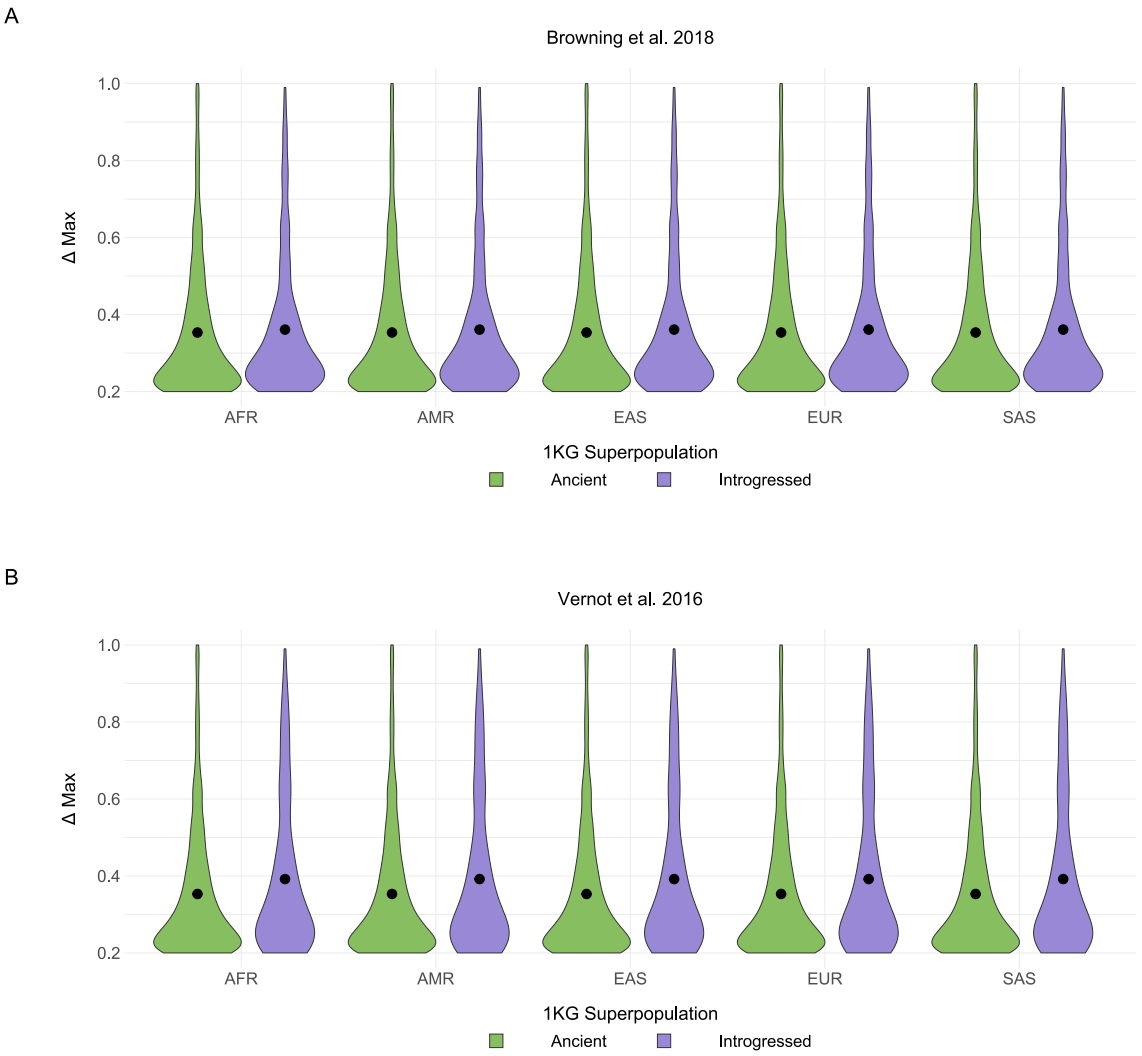

Figure S22: △ max does not differ between 1KG superpopulations.
(A) △ max for SAVs by 1KG superpopulation and allele origin per Browning et al., 2018. AFR = African, AMR = American, EAS = East Asian, EUR = European, SAS = South Asian. **(B)** △ max for SAVs by 1KG superpopulation and allele origin per Vernot et al., 2016.

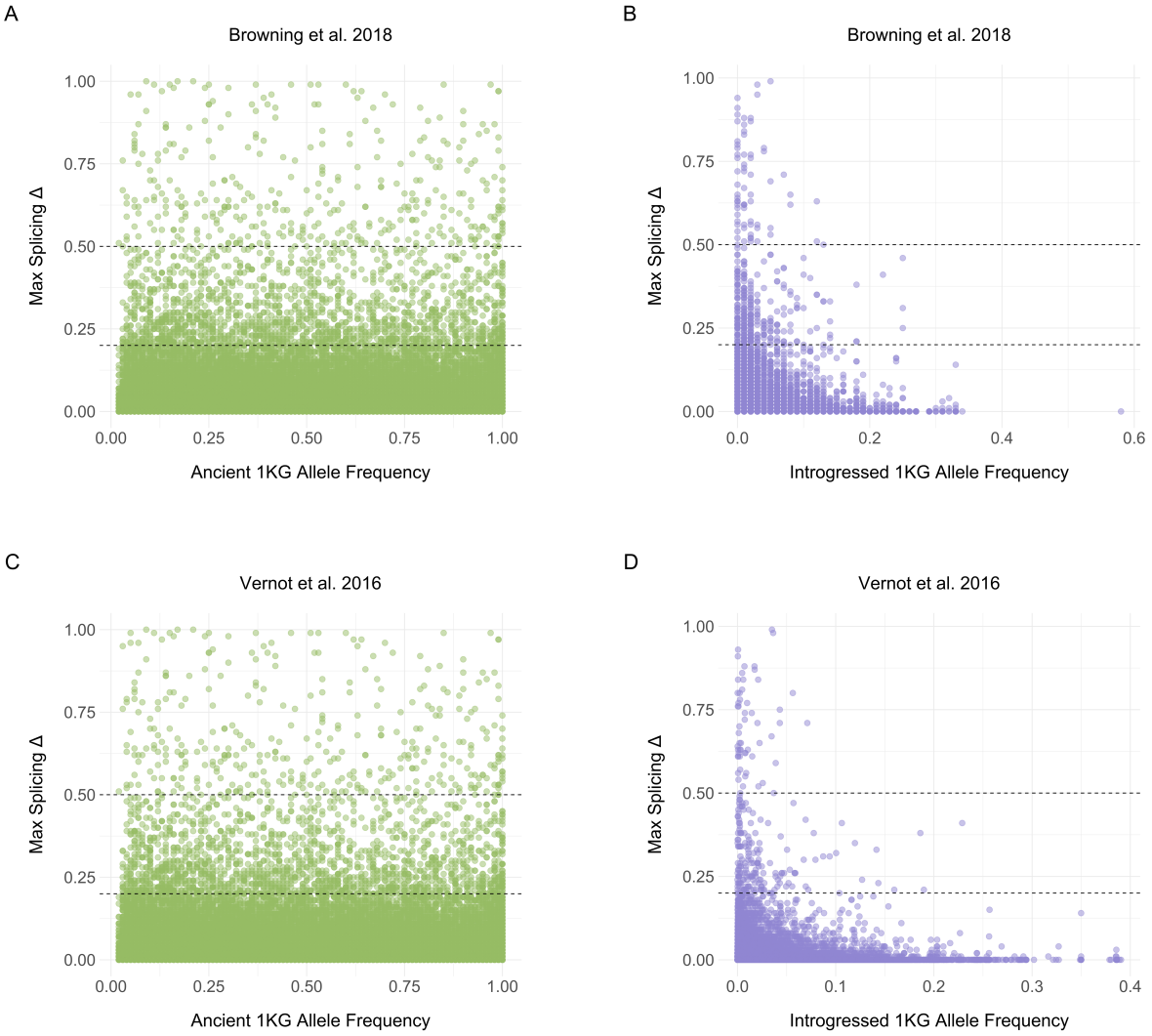

Figure S23: Δ max exhibits a variable relationship to 1KG allele frequency.
(A) 1KG allele frequency and Δ max for all ancient variants per Browning et al., 2018. Allele frequencies are from 1KG. Dashed lines reflect both Δ thresholds. **(B)** 1KG allele frequency and Δ max for all introgressed variants per Browning et al., 2018. Allele frequencies are from 1KG. If the introgressed allele was the reference allele, we subtracted the 1KG allele frequency from 1. **(C)** 1KG allele frequency and Δ max for all ancient variants per Vernot et al., 2016. Allele frequencies are from 1KG. **(D)** 1KG allele frequency and Δ max for all introgressed variants per Vernot et al., 2016. Allele frequencies represent the mean from the AFR, AMR, EAS, EUR, SAS frequencies from the Vernot et al., 2016 metadata.

A

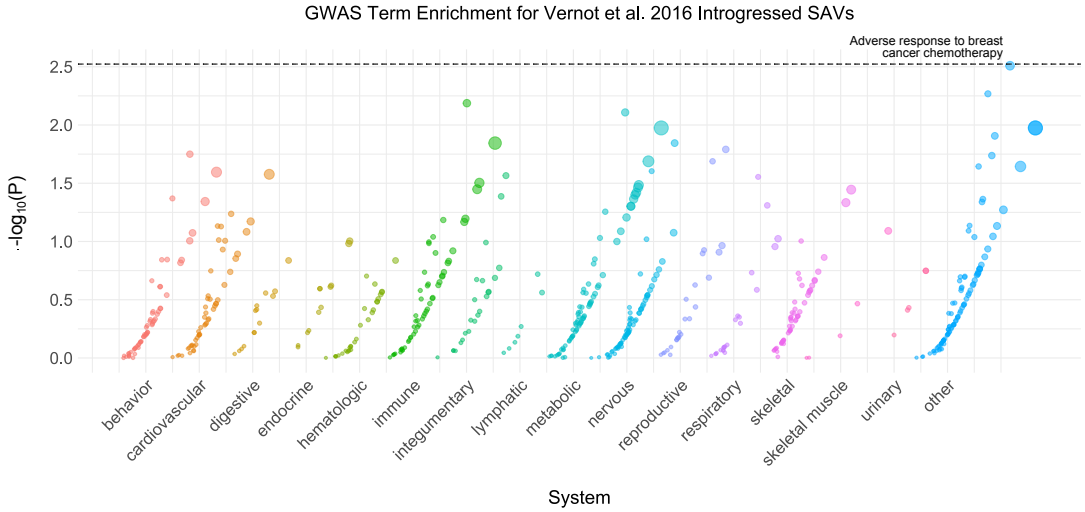

B

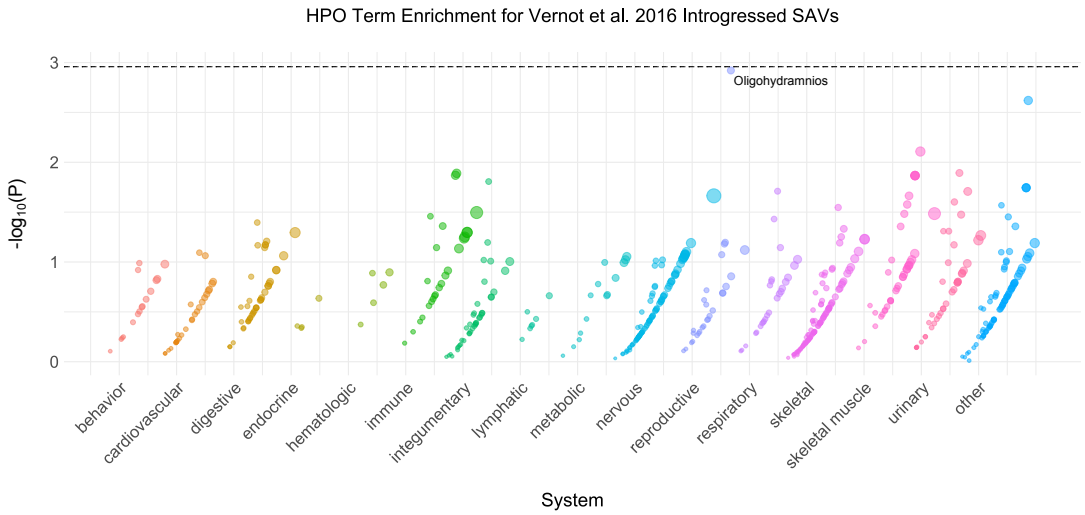

Figure S24: Vernot et al. 2016 introgressed phenotype enrichment.
(A) Phenotype associations enriched among genes with Vernot et al., 2016 introgressed SAVs based on annotations the from GWAS Catalog. Phenotypes are ordered by increasing enrichment within manually curated systems. Circle size indicates enrichment magnitude. Enrichment and p-values were calculated from an empirical null distribution generated from 10,000 shuffles of maximum Δ across the entire dataset (Methods). Dotted and dashed lines represent false discovery rate (FDR) corrected p-value thresholds at FDR = 0.05 and 0.1, respectively. At least one example phenotype with a p-value $\leq$ the stricter FDR threshold (0.05) is annotated per system. **(B)** Phenotypes enriched among genes with Vernot et al., 2016 introgressed SAVs based on annotations from the Human Phenotype Ontology (HPO). Data were generated and visualized as in **A**. See **File S2** for all phenotype enrichment results.

A

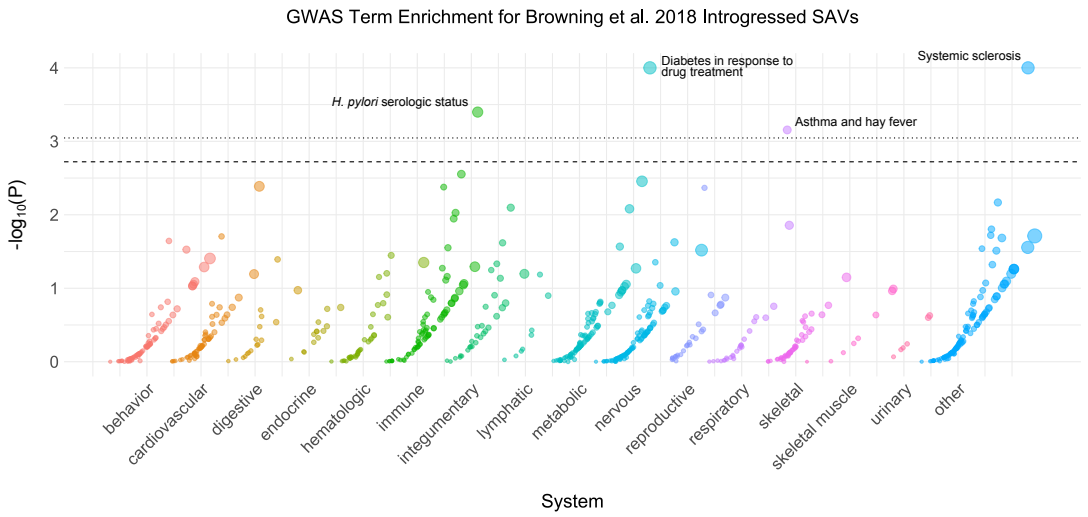

B

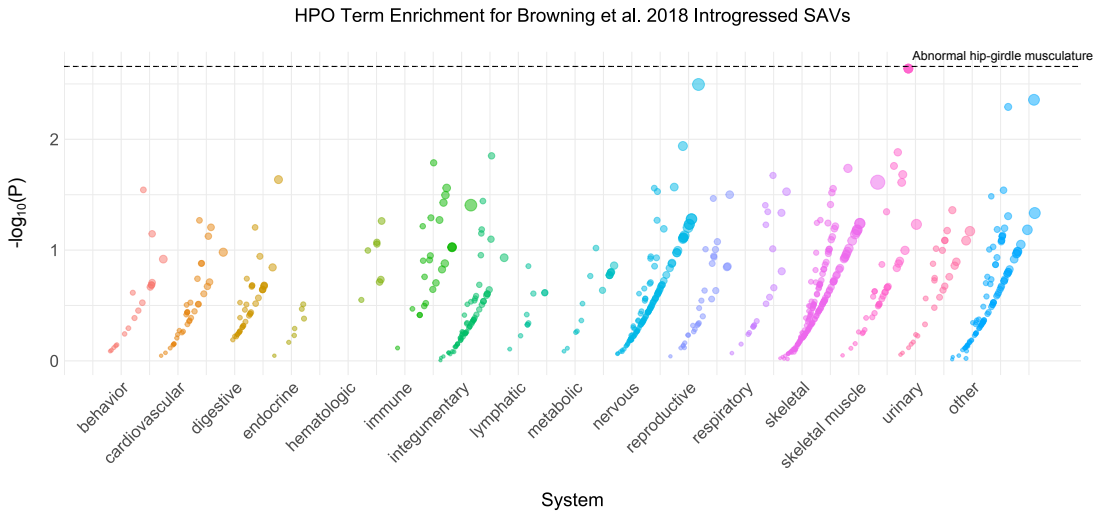

Figure S25: Browning et al. 2018 introgressed phenotype enrichment.
(A) Phenotype associations enriched among genes with Browning et al., 2018 introgressed SAVs based on annotations the from GWAS Catalog. Phenotypes are ordered by increasing enrichment within manually curated systems. Circle size indicates enrichment magnitude. Enrichment and p-values were calculated from an empirical null distribution generated from 10,000 shuffles of maximum Δ across the entire dataset (Methods). Dotted and dashed lines represent false discovery rate (FDR) corrected p-value thresholds at FDR = 0.05 and 0.1, respectively. At least one example phenotype with a p-value $\leq$ the stricter FDR threshold (0.05) is annotated per system. **(B)** Phenotypes enriched among genes with Browning et al., 2018 introgressed SAVs based on annotations from the Human Phenotype Ontology (HPO). Data were generated and visualized as in **A**. See **File S2** for all phenotype enrichment results.

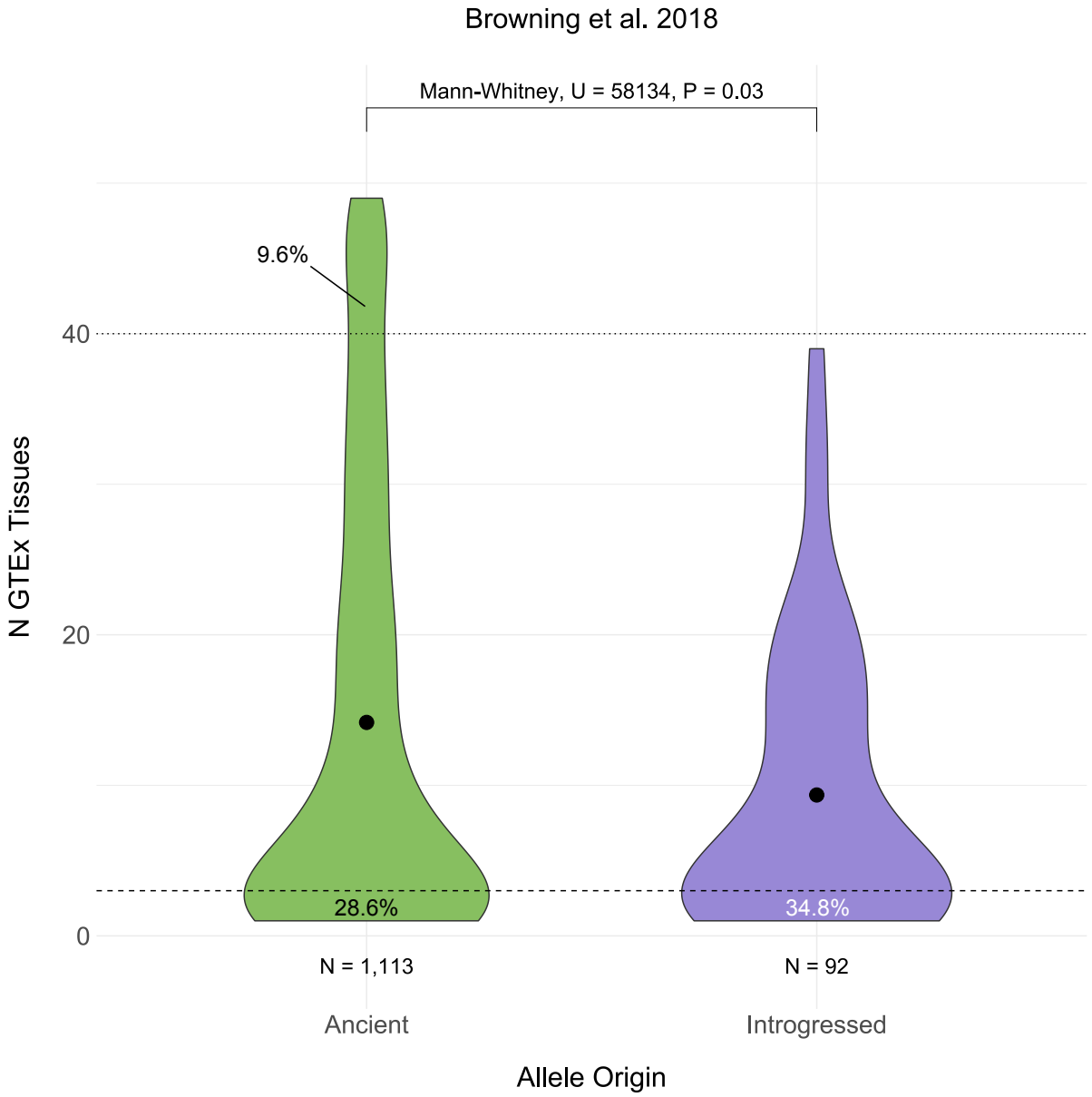

Figure S26: Introgressed SAV sQTLs are more tissue-specific than ancient variants. The distribution of GTEx tissues in which an ancient or introgressed SAV per Browning et al., 2018 was identified as an sQTL. We defined "tissue-specific" variants as those occurring in 1 or 2 tissues and "core" sQTLs as those occurring in > 40 of the 49 tissues. The dashed and dotted lines represent these definitions, respectively. The proportion of SAVs below and above these thresholds for both origins are annotated.

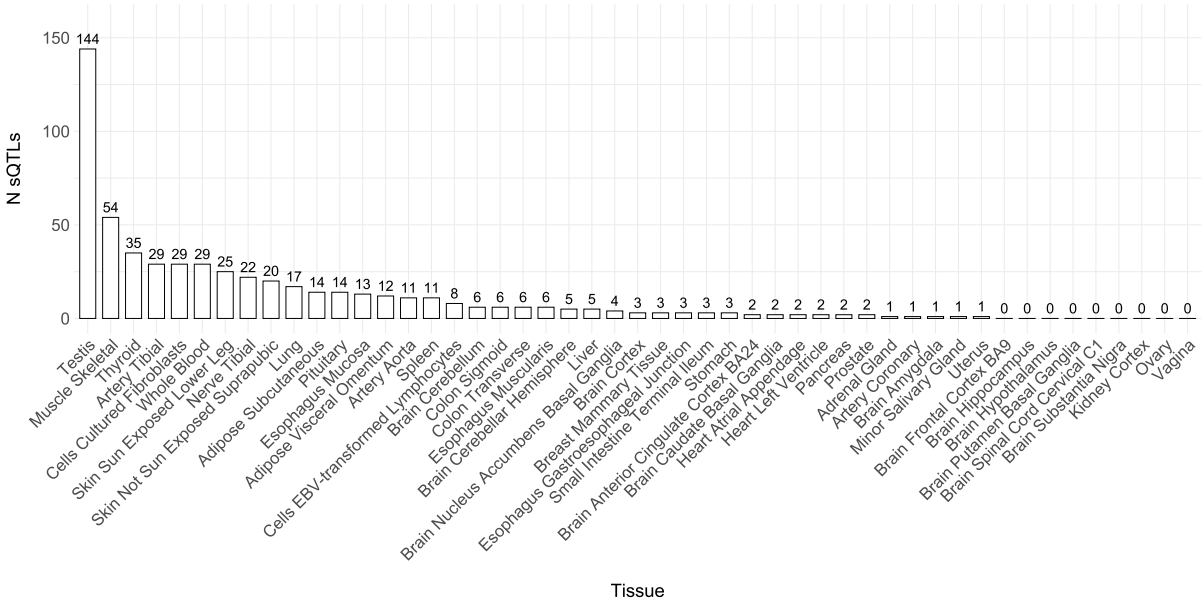

Figure S27: sQTL SAVs predominantly occur in testis, muscle skeletal, thyroid, tibial artery, fibroblasts, skin, and tibial nerve tissues. The number of tissue-specific (N GTEx tissues = 1 or 2) sQTL SAVs per GTEx tissue.

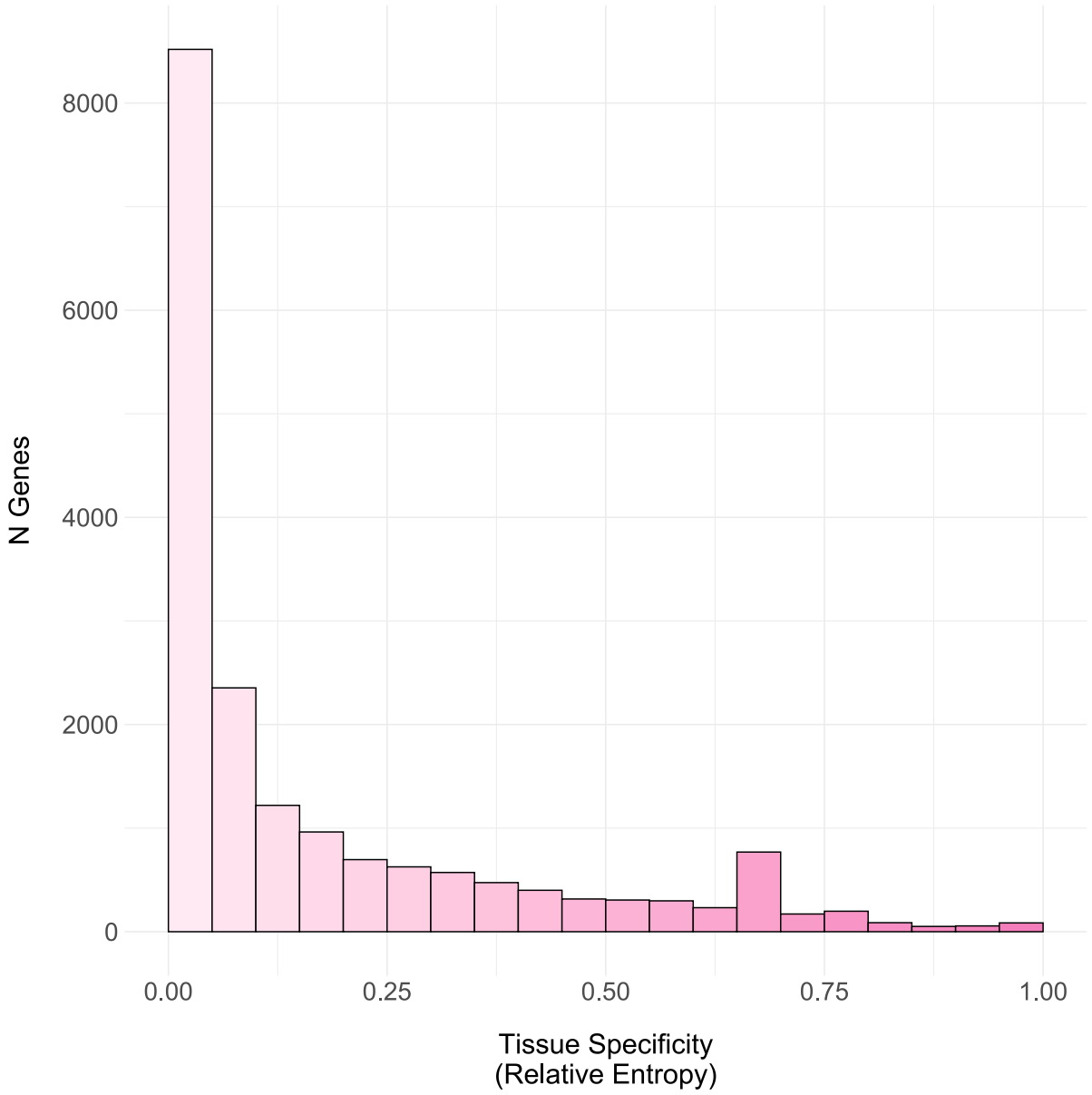

Figure S28: Most gene expression is not tissue-specific. The distribution of relative entropy in 0.05 bins calculated from GTEx TPM counts across 34 tissues for 18,392 genes.

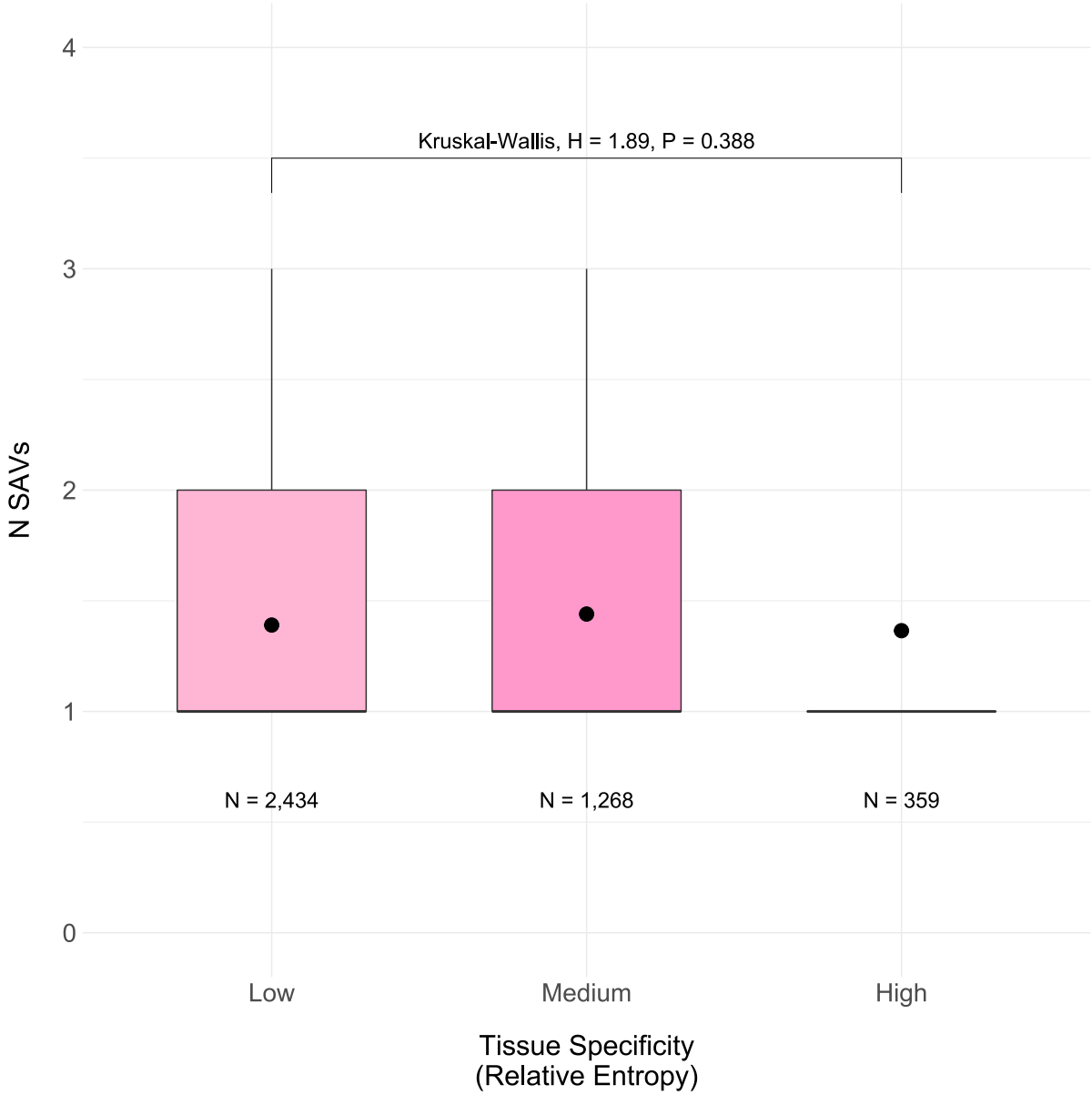

Figure S29: The number of SAVs is unrelated to tissue-specific gene expression. The number of SAVs by binned gene expression calculated from GTEx TPM counts across 34 tissues. We analyzed a total of 4,061 genes with SAVs. Low tissue specificity reflects relative entropy ≤ 0.1, medium tissue specificity reflects relative entropy > 0.1 and ≤ 0.5, and high tissue specificity reflects relative entropy > 0.5 (**Figure S28**).

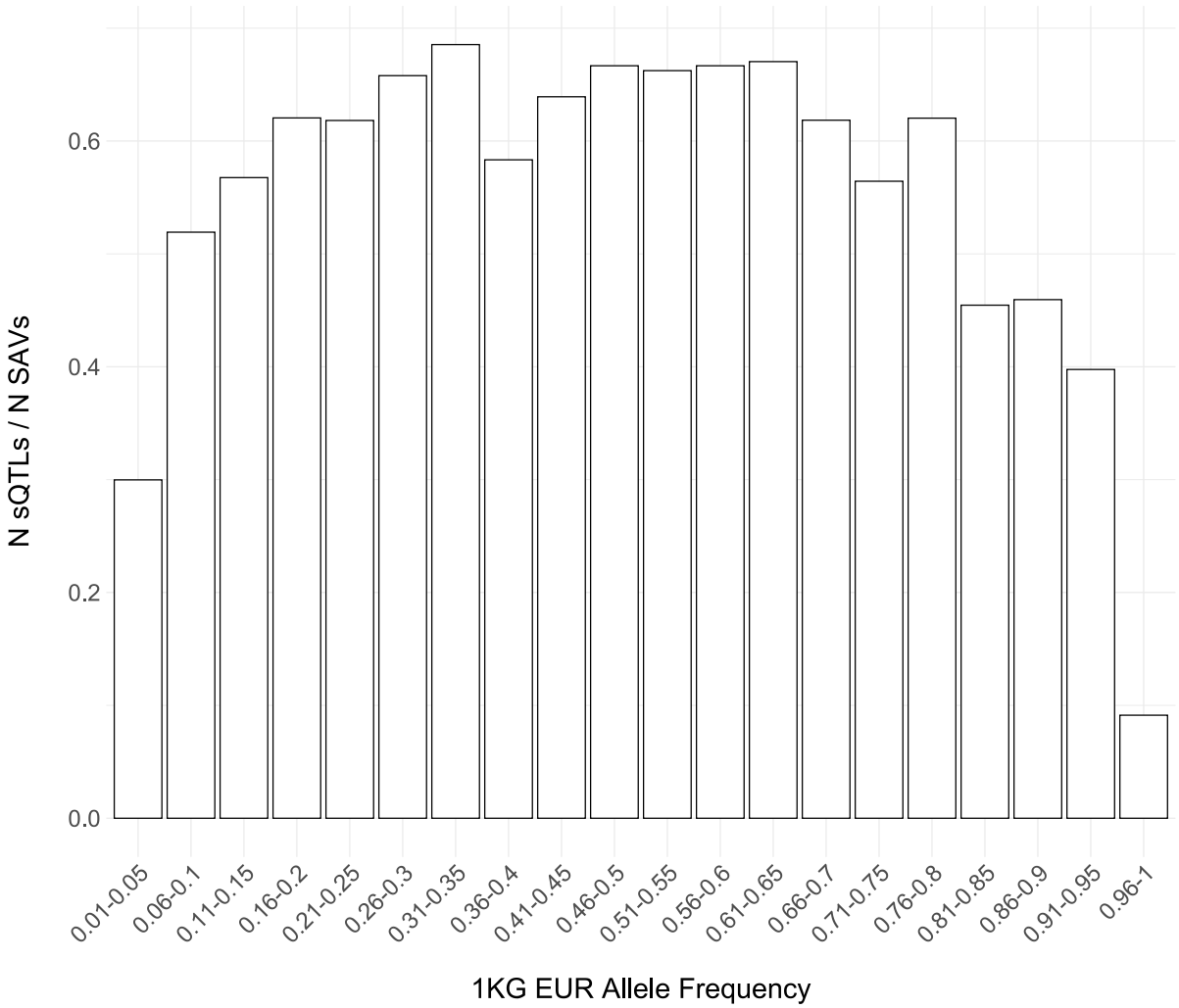

Figure S30: $>$ 50% of SAVs are sQTLs. The proportion of sQTLs also identified SAVs $\geq$ binned allele frequency thresholds among 1KG European individuals. We used the precalculated frequencies provided in the 1KG VCFs for this analysis.

5.4 Supplemental Tables

All Variants				
	./.	0/0	1/0	1/1
Altai	6,226	591,371	126,440	883,313
Chagyrskaya	37,156	583,787	98,076	888,331
Denisovan	21,574	546,792	139,774	899,210
Vindija	29,672	570,175	119,918	887,585
Variants with Δ Max $\geq$ 0.2				
	./.	0/0	1/0	1/1
Altai	18	2,227	538	3,167
Chagyrskaya	266	2,202	397	3,085
Denisovan	157	2,122	587	3,084
Vindija	163	2,160	496	3,131
Variath with Δ Max $\geq$ 0.5				
	./.	0/0	1/0	1/1
Altai	4	386	101	558
Chagyrskaya	69	394	61	525
Denisovan	45	376	107	521
Vindija	35	361	108	545

Table S1: Archaic genotype distribution. The number of genotypes per individual for all variants and both delta thresholds. "./." reflects a missing genotype. "0/0" reflects a homozygous site for the reference allele. "1/0" reflects a heterozygote. "1/1" reflects a homozygote for the alternate allele.

1KG Superpopulation	1KG Population	Sample Name	N SAVs
AFR	ESN	HG00137	3,266
	GWD	HG00338	3,344
	LWK	HG00619	3,320
	MSL	HG01198	3,514
	YRI	HG01281	3,493
AMR	CLM	HG01524	3,363
	MXL	HG01802	3,363
	PEL	HG02142	3,349
	PUR	HG02345	3,385
EAS	CDX	HG02629	4,120
	CHB	HG03060	4,160
	CHS	HG03190	4,142
	JPT	HG03708	3,368
	KHV	HG03711	3,379
EUR	CEU	HG03800	3,435
	FIN	HG04014	3,421
	GBR	NA11830	3,200
	GIH	NA18552	3,382
	IBS	NA18868	4,102
	TSI	NA19011	3,321
SAS	BEB	NA19452	4,078
	ITU	NA19741	3,284
	PJL	NA20537	3,168
	STU	NA21141	3,487

Table S2: The average number of SAVs per randomly sampled individual in 1KG. We randomly sampled one individual per 1KG population and ran SpliceAI on their combined variants. There were 4,582,422 total SpliceAI annotated variants among autosomal SNVs and 14,006 variants with a Δ max $\geq$ 0.2. These N SAVs reported here include any site where an individual had at least one alternate allele present (i.e., heterozygotes and homozygotes for the alternate allele).

N SAVs	N Genes	Genes
1	3,111	
2	769	
3	246	
4	71	
5	19	
6	14	
7	6	*CDH13*, *CDH23*, *CSMD1*, *DNAH17*, *HLA-DPA1*, *LAMA5*
8	1	*ADARB2*
9	2	*SDK1*, *WWOX*
10	1	*HLA-DPB1*
11	2	*CNTNAP2*, *SSPO*

Table S3: Distribution of SAVs per gene. The distribution of SAVs per gene with the specific genes listed for those with $\geq$ 7 SAVs.

Δ	Gene Characteristic	ρ	P Value
0.2	N Exons	0.3161	0
	CDS/Exon Length	0.1851	1.07E-135
	Gene Length	0.2920	0
	N Isoforms	0.1767	1.87E-113
0.5	N Exons	0.1330	2.20E-70
	CDS/Exon Length	0.0625	1.01E-16
	Gene Length	0.1017	8.99E-42
	N Isoforms	0.0769	1.24E-22

Table S4: Physical gene characteristic associations with N SAVs per gene. Spearman correlation between four variables: 1) the number of exons, 2) length of coding sequence in bp, 3) gene body length in bp, 4) the number of isoforms and the N SAVs per gene for both Δ thresholds.

Δ	N Unique SAVs	N Unique Non SAVs	N Shared SAVs	N Shared Non SAVs	OR	95% CI Lower Bound	95% CI Upper Bound	P Value	Bonferroni
0.2	2,416	615,666	1,933	571,264	1.160	1.092	1.231	0.000	Y
0.3	1,175	616,907	945	572,252	1.153	1.059	1.257	0.001	Y
0.4	685	617,397	533	572,664	1.192	1.064	1.335	0.002	Y
0.5	437	617,645	328	572,869	1.236	1.071	1.426	0.004	Y

Table S5: Enrichment tests for the sum of lineage-specific SAVs at different Δs. Input data for Fisher's exact tests. OR = odds ratio; 95% CI Lower Bound and 95% CI Upper Bound = the lower and upper bounds of the 95% confidence interval, respectively; P Value = unadjusted p-value.

Δ	Distribution	N Unique SAVs	N Unique Non SAVs	N Shared SAVs	N Shared Non SAVs	OR	95% CI Lower Bound	95% CI Upper Bound	P Value	Bonferroni
0.2	Altai	399	81,517	1,933	571,264	1.447	1.298	1.612	0.000	Y
	Chagyrskaya	218	53,457	1,933	571,264	1.205	1.047	1.387	0.011	Y
	Denisovan	1492	410,000	1,933	571,264	1.075	1.004	1.151	0.036	N
	Vindija	307	70,692	1,933	571,264	1.283	1.138	1.448	0.000	Y
	Total	2,416	615,666	1,933	571,264	1.160	1.092	1.231	0.000	NA
0.5	Altai	75	81,841	328	572,869	1.601	1.245	2.057	0.000	Y
	Chagyrskaya	35	53,640	328	572,869	1.140	0.804	1.615	0.452	N
	Denisovan	254	411,238	328	572,869	1.079	0.916	1.271	0.377	N
	Vindija	73	70,926	328	572,869	1.798	1.395	2.317	0.000	Y
	Total	437	617,645	328	572,869	1.236	1.071	1.426	0.004	NA

Table S6: Enrichment tests for lineage-specific SAVs. Input data for Fisher's exact tests. OR = odds ratio; 95% CI Lower Bound and 95% CI Upper Bound = the lower and upper bounds of the 95% confidence interval, respectively; P Value = unadjusted p-value.

Δ	≥ 0.2			≥ 0.5		
Distribution	Archaic-Specific N SAVs	Browning Introgressed N SAVs	Vernot Introgressed N SAVs	Archaic-Specific N SAVs	Browning Introgressed N SAVs	Vernot Introgressed N SAVs
Altai	312	15	7	57	4	1
Chagyrskaya	172	0	0	27	0	0
Denisovan	968	2	3	176	2	1
Late Neanderthal	97	0	0	10	0	0
Neanderthal	281	203	141	46	36	36
Other	154	37	20	31	4	4
Shared	203	120	66	43	23	14
Vindija	238	0	0	57	0	0

Table S7: Distribution of archaic-specific and introgressed SAVs. N SAVs for both Δ thresholds among archaic-specific and introgressed SAVs per Browning et al., 2018 and Vernot et al., 2016. Other denotes any combination of archaics not already listed.

Chromosome	Position	Reference Allele	Alternate Allele	Delta Max	Browning Allele Origin	Vernot Allele Origin	Annotation
chr1	22174518	G	T	0.98	introgressed	introgressed	*HSPG2*
chr1	55,537,474	C	G	0.33	low-confidence ancient	introgressed	*USP24*
chr1	161,681,848	C	T	0.20	introgressed	introgressed	*FCRLA*
chr1	212,985,592	G	A	0.52	introgressed	introgressed	*TATDN3*
chr11	86,159,859	G	A	0.26	ancient	introgressed	*ME3*
chr12	133,272,470	G	T	0.26	introgressed	introgressed	*PXMP2*
chr12	133,272,470	G	T	0.26	introgressed	introgressed	*RP13-672B3.2*
chr15	85,403,496	G	A	0.33	introgressed	introgressed	*ALPK3*
chr16	88,924,425	C	G	0.41	introgressed	introgressed	*TRAPPC2L*
chr19	40,913,595	G	A	0.23	introgressed	low-confidence ancient	*PRX*
chr22	50,684,852	G	C	0.25	introgressed	introgressed	*HDAC10*
chr4	170,990,750	G	A	0.22	introgressed	introgressed	*AADAT*
chr5	6,753,013	C	T	0.24	introgressed	introgressed	*PAPD7*
chr5	167,919,825	G	A	0.38	introgressed	introgressed	*RARS*
chr6	33,264,115	A	C	0.34	low-confidence ancient	introgressed	*RGL2*
chr8	130,763,783	C	T	0.87	introgressed	introgressed	*GSDMC*

Table S8: SAVs that exhibit allele-specific expression in modern humans. 16 SAVs from our dataset that matched variants from McCoy et al., 2017.

Distribution	N sQTLs
Altai	2
Chagyrskaya	3
Denisovan	8
Late Neanderthal	2
Neanderthal	9
Other	14
Shared	74

Table S9: Core sQTL SAV distribution among the archaics. The distribution of core sQTL SAVs (N = 1,145) among the archaics. Core sQTLs were defined as those variants detected in $>$ 40 tissues. All the variants represented here are either low or high-confidence ancient.

Chromosome	Position	Reference Allele	Alternate Allele	Delta Max Alternate Allele	Δ Max Reference as Alternate
chr1	52,820,680	C	T	0.23	0.23
chr1	152,944,501	A	T	0.23	0.23
chr1	183,750,131	C	A	0.26	0.26
chr1	**216,945,756**	**C**	**A**	**0.20**	**0.19**
chr10	17,373,518	T	C	0.22	0.22
chr11	84,191,111	T	C	0.40	0.40
chr11	99,345,359	C	G	0.67	0.67
chr17	14,109,360	T	G	0.20	0.21
chr18	60,003,587	G	A	0.31	0.30
chr19	33,410,289	T	C	0.71	0.71
chr20	62,224,595	G	A	0.41	0.41
chr3	52,486,376	T	C	0.34	0.35
chr4	38,805,942	G	C	0.38	0.37
chr4	100,460,531	A	G	0.35	0.35
chr4	135,122,662	G	A	0.80	0.80
chr5	118,669,326	G	C	0.22	0.22
chr5	126,989,007	A	G	0.91	0.91
chr5	148,430,560	A	C	0.32	0.32
chr6	51,889,358	T	C	0.42	0.42
chr6	52,138,226	C	G	0.21	0.21
chr7	119,524,266	C	T	0.30	0.30
chr7	126,797,408	T	A	0.43	0.43
chr7	140,801,296	T	C	0.25	0.25
chr7	140,958,656	A	G	0.26	0.26
chr7	**157,177,273**	**C**	**T**	**0.31**	**0.16**
chr7	158,543,832	C	A	0.21	0.22

Table S10: Maximum Δ for SAVs with an introgressed reference allele. Δ maximum for 26 SAVs whose reference allele rather than the alternate allele matched an introgressed tag SNP from Vernot et al., 2016. We switched the reference and alternate alleles for these (and non-SAV) loci and reran SpliceAI. "Delta Max Alternate Allele" indicates the originally predicted Δ where the reference allele is introgressed and "Delta Max Reference as Alternate" indicates the Δ when the reference and alternate alleles are switched. Bolded variants are those whose values did not pass the SAP threshold after switching alleles.

N Annotations	N
1	153,7451
2	30,448
3	1,154
4	75
5	36
6	15
7	25
8	22
9	36
10	20
11	20
12	15
13	58
14	70
15	34
16	6
17	6
18	32
19	6
20	3
21	24

Table S11: Distribution of multiple annotations. The number of variants with the given number of annotations from GENCODE, Human Release 24.